GEMINI
8-M Telescopes
Project

RPT-TE-G0039

Seeing Control Strategy for the Gemini 8m Enclosure

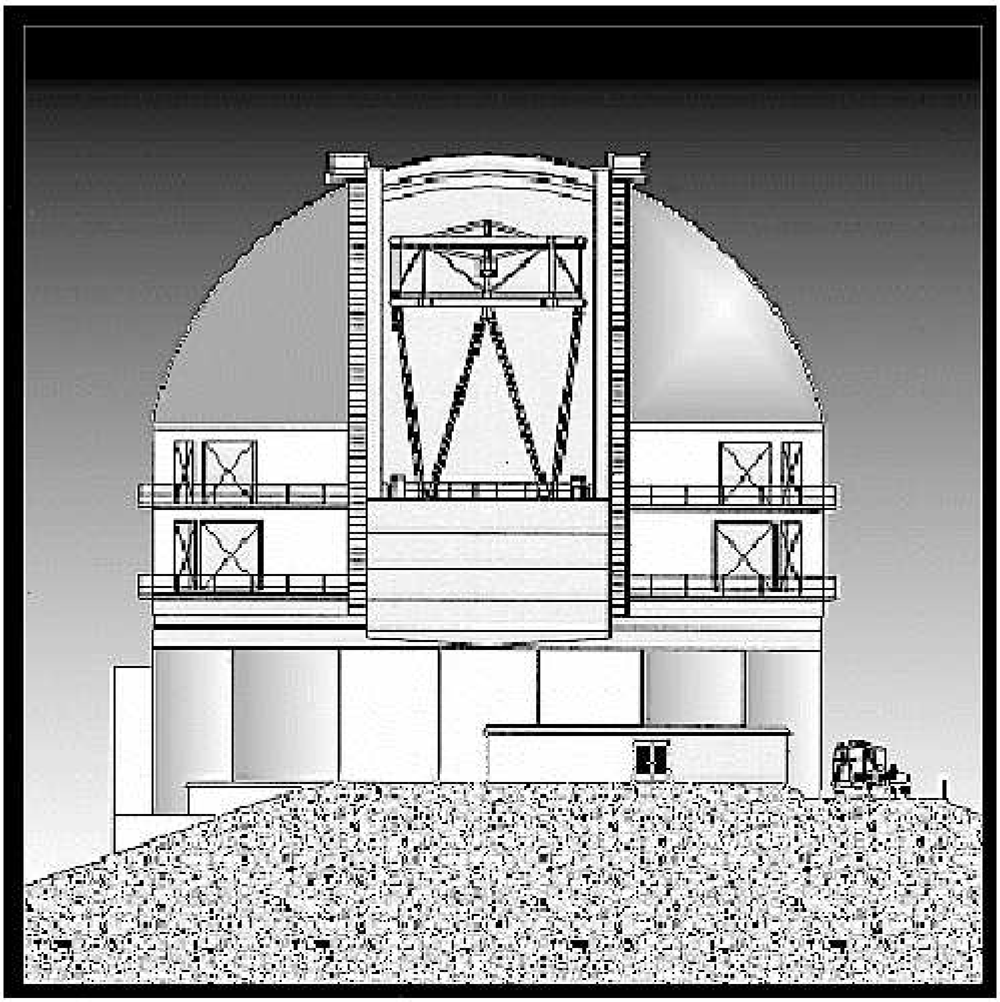

R. Ford
Telescope and Enclosure Group

December 14, 1993

GEMINI PROJECT OFFICE 950 N. Cherry Ave. Tucson, Arizona 85719
Phone: (520) 318-8545 Fax: (520) 318-8590

TABLE OF CONTENTS

LIST OF FIGURES

LIST OF TABLES

1. SUMMARY

1.1 ENCLOSURE SHELL SEEING CONTROL STRATEGY

The modeling has shown that:

- the shell seeing for all candidate coatings at the 5th percentile of the Mauna Kea windspeed (O m/s) is reduced with active flushing of the shell air space;
- a white coated shell will not meet the Gemini seeing requirements;
- a Lo-Mit coated shell should be used for the Gemini Enclosures;
- if the enclosure is operating in low ambient windspeeds, a flow rate equivalent to 10 chamber air volumes per hour of ambient air should be forced through the shell air space.

1.2 ENCLOSURE CHAMBER SEEING CONTROL STRATEGY

- High flushing rates will be required to minimize chamber seeing. The enclosure has been designed with large flushing vents to provide efficient passive flushing of the chamber regardless of the orientation of the enclosure with respect to the wind vector. During periods of low ambient windspeed, fans are provided to actively ventilate the chamber at flow rates not less than IO chamber volumes per hour;
- the level of active source power dissipation into the chamber air must be kept as low as possible; a level of 8.5 kW is acceptable. Active temperature control techniques must be utilized on certain sources (instrument packages) to maintain the power dissipation at this level;
- the use of high emissivity coatings (enamel paint) on surfaces inside the telescope chamber (except for the secondary support structure and top end ring) results in more energy transfer to the night sky via radiation (through the open flushing vents and shutters) and hence less energy transfer to the chamber air; the net result is lower values of chamber seeing;
- buoyant flows between the chamber floor and the chamber air, and between the basement air and the chamber air can be prevented by utilizing a low thermal capacity floor surface and providing an actively ventilated air volume below the floor;
- the chamber air should be conditioned during the daytime to obtain lower values of nighttime chamber seeing, and to minimize the convective power flow between the mount and the chamber air during the nighttime hours. Insulation is not required on the outer surface of the telescope mount if we adopt daytime air conditioning.

2. INTRODUCTION

Thermal modeling has been used to determine the best overall strategy for control of enclosure seeing for the Gemini 8m enclosure. Environmental conditions for Mauna Kea were used as boundary conditions in the modeling. Design drawings of the enclosure were used to create a thermal circuit network consisting of 130 elements and including more than 200 thermal linkages. The model was then used to duplicate the thermal response of several existing enclosures atop Mauna Kea by calibrating thermal links representing:

- the radiation to the night sky;
- the radiation to the earth;
- the volumetric flow rate of ambient air through the enclosure chamber.

The calibrated model was then used to show how the thermal performance of the enclosure was affected by changing other thermal links representing radiation, convection, and volumetric flow rates. Enclosure performance was evaluated by determination of the enclosure seeing. The enclosure seeing was determined by evaluating two separate effects: chamber seeing and shell seeing. The total seeing degradation (enclosure seeing) was taken as the square root of the sum of the squares of these two values. The model allowed determination of the best operational strategy to minimize enclosure seeing.

3. ENCLOSURE THERMAL DESIGN CONSIDERATIONS

3.1 COMPONENTS OF THE ENCLOSURE THERMAL CONTROL SYSTEM

Figure 1 presents an elevation view of the Gemini enclosure and support facility showing the principal components of the enclosure thermal control system. All underlined captions signify the important parts of this thermal control system:

- ventilation gates to allow wind to flush the chamber;
- a ring plenum to accept active flow from the ventilated shell, ventilated floor and ventilated mount floor;
- air conditioning for the enclosure chamber;
- shell air vents at the top of the ventilated shell to allow ambient air flow (fan forced) to enter the ventilated shell;
- passive flow valves in the enclosure base structure to allow (solar driven) buoyant flow to enter the bottom of the ventilated shell;
- an exhaust tunnel which connects the exhaust fans and dampers to the ring plenum, and within which is located the support facility chiller unit condensers.

3.2 PASSIVE FLUSHING AND VOLUMETRIC FLOW RATES

The principal aim (while the telescope is in the observing mode) is to maintain the temperature of the air volume through which the telescope is pointed to be equal to the ambient air temperature. This requirement must be met at all orientations of the enclosure shutter slit to the wind direction and when the ambient air temperature is changing. Water tunnel tests [Ford et al] have demonstrated that the most efficient method of achieving this aim is to provide high volumetric flushing rates, i.e. to exchange the air inside the enclosure with ambient air as rapidly as possible before it has a chance to change its temperature. The Gemini enclosure is designed such that the enclosure will provide efficient flushing in all enclosure slit/ wind orientations by using the ventilation gates shown on Figure 1. The thermal model has allowed us to investigate the temperature rise of the air as it passes through the enclosure with different volumetric flushing rates. Information from water tunnel tests (described in Section 5.3.3) has provided us with realistic flushing rates for different orientations of the enclosure shutters to the wind direction, and has been used as inputs for the modeling.

3.3 ACTIVE FLUSHING

Wind measurements taken on Mauna Kea [Cowley] indicate that for 5% of the time the wind velocity is zero. To achieve flushing of the chamber air during these periods of low ambient wind velocity we have incorporated active flushing. Fans, sited at both ends of an exhaust air duct adjacent to the plant room (see Figure I for the locations of the fans) draw ambient air into the enclosure chamber and exhaust the flow through an above grade tunnel. To provide this facility for just 5% of the time is an expensive proposition. However, we also use this system for actively controlling the temperature of the enclosure floor and shell, and for preventing warm air infiltrating into the enclosure chamber from below (the basement). To size the active flushing fans, the thermal model has been run with different volumetric flow rates.

3.4 CONTROL OF HEAT SOURCES IN THE ENCLOSURE CHAMBER

Heat generation in the enclosure chamber is undesirable as it directly changes the temperature of the air in the enclosure chamber. All heat sources that can be removed from the enclosure chamber have been located in the support facility. Examples include the hydraulic plant for the hydrostatic bearings. Remaining heat sources will be actively controlled if required. For example we plan to cool the hydrostatic oil before it reaches the telescope such that its exit temperature is at ambient air temperature. In the thermal model, we can change the beat generated directly in the enclosure chamber to determine how much heat we can release before we need to provide active management of the heat sources.

3.5 CONTROL OF HEAT SOURCES IN THE BASEMENT

If the air in the basement in warmer than the chamber air it can either conduct through the floor into the enclosure chamber or "leak" into the enclosure chamber.

We have incorporated several features to control this effect:

- We have sited only "cold structures" in the basement below the enclosure chamber. Top-ends and telescope spares are stored in the basement. The coating chamber and wash area are also sited here as they will not generate heat during normal telescope operation. The warm rooms, namely the control room, computer room, crew room, plant room, and instrument preparation room have all been located in the support building to the side of the enclosure. In addition, the support facility is sited partly underground;
- any "leakage" (infiltration) of air from the basement will be caught and extracted with the air that is used for cooling the space between the enclosure floor and the basement. This ventilated floor space can be seen in Figure 1. The thermal model will be used to determine the appropriate ventilation **rates** required for the ventilated floor.

3.6 CONTROL OF THE ENCLOSURE FLOOR TEMPERATURE

In addition to the floor space between the enclosure chamber and the basement roof being actively ventilated, the top surface of the enclosure floor will be designed to have a fast thermal time constant to allow it to track the ambient air temperature.

3.7 CONTROL OF ENCLOSURE OUTER SKIN TEMPERATURE

Many 4m-class enclosures have been painted with white titanium dioxide paint. This paint has a low solar absorptivity, and its function is to minimize heating of the enclosure skin during the daytime. This is important when considering the over thermal philosophy followed for the design of the 4m class telescope facilities where the enclosure volume is maintained at a steady temperature. The intent of using $Ti\text{-}O_2$ paint on the exterior of the enclosure was to minimize the influence of the daytime solar heating on the air inside the enclosure. However, the titanium oxide paint has a high thermal emissivity and during the night subcools by radiating to the cool sky. Air passing over the enclosure skin is cooled, then pockets of cool air have been observed to "fall" into the enclosure opening and increase "dome" seeing.

Our overall thermal design philosophy does not require a steady temperature environment inside the enclosure. The facility is being designed to provide flushing of the enclosure chamber air and to provide structures that are either actively cooled or have fast thermal time constants. To avoid the effect of sub-cooling of the enclosure skin we plan to use a low emissivity coating to reduce radiation to the sky. We have used the thermal model to investigate the performance of both Low-Mit and aluminized mylar tape. The results are detailed in Section 6.2. 1.

However, even when using these coatings, there was a problem during periods of low wind speeds. The skin would warm in the daytime and then slowly release the beat during the night. To avoid this problem, we have provided active ventilation of the space between the outer and inner skins. The results are presented in Section 6.2.2. The thermal model was used to determine the most appropriate time for starting this ventilation during the daytime.

3.8 DAYTIME AIR CONDITIONING

The thermal model has allowed us to investigate the requirement for air conditioning the enclosure during the daytime. Results are presented in Section 6.3.3.

3.9 TELESCOPE COOLING AND INSULATION

The thermal model includes the telescope mount, and is being used to determine the appropriate level of active ventilation required to cool the telescope structure and whether we require insulation on the telescope structural members. Results showing the telescope cooling are shown in Section 6.3.4.

4. RELATING THE TEMPERATURE OF THE AIR INSIDE THE ENCLOSURE CHAMBER AND POWER FLOW IN THE ENCLOSURE LIGHT PATH TO IMAGE DEGRADATION

The thermal behavior of the enclosure must be evaluated such that the image degradation caused by the enclosure will fall under a budgeted value during observing hours. The 2.2 micron error budget (50% encircled energy) for the F/16 telescope configuration is shown on Figure 2. This report shall use the more stringent low wind budget value (0.030 arcsecs) for the enclosure seeing.

The formula used to evaluate the chamber seeing relates the seeing due to the air inside the enclosure to the temperature differential between the air inside and outside the enclosure: [Racine et al]:

$$S_C = C_R\,(\Delta T)^{6/5} \qquad (1\text{-}1)$$

Where: S_C = chamber seeing, expressed as 50% encircled energy in arcsec (");
C_R = seeing coefficient (0.15"/°$C^{6/5}$);
ΔT = temperature difference between the air inside the enclosure and the ambient air (°C)

Thus to meet the error budget we have to maintain the absolute value of $\Delta T \leq 0.26$°C during the observing period.

A very similar relation is used to evaluate image degradation caused by a temperature difference between an air parcel located over the shutter slot and the ambient air. If the temperature of the outer shell of the enclosure is different than the ambient air, then power will be exchanged between the shell and the air. If the ambient air is moving, then power will flow into the air parcel above the shutter slot. The seeing is determined by first calculating the temperature of the air parcel that moves over the shutter, and then applying 1-1 using the temperature differential between this air parcel and the ambient air.

From boundary layer theory, the thickness of a boundary layer over a flat plate with turbulent flow conditions existing across the surface is [Incropera]:

$$\delta = 0.37 L Re_L^{-1/5} \quad \{\text{for } Re_L < 10^8\} \qquad (1\text{-}2)$$

$$\delta = 0.37 L (vL/\gamma)^{-1/5} \qquad (1\text{-}3)$$

where: δ = height of the boundary layer (m);
L = distance from the leading edge of the plate (m);
Re_L = Reynolds number;
v = velocity of the air (m/s);
γ = kinematic viscosity of the air (m^2/s).

The volume of the parcel of air over the shutter slot may now be determined as:

$$V = \delta A_O = \delta \pi D_O^2/4 \qquad (1\text{-}4)$$

where: V = volume of the air parcel (m^3);
A_O = area of the primary optic (m^2);
Do = diameter of the primary optic (m).

The volumetric flushing rate of ambient air through the air parcel is:

$$\dot{V} = \frac{Vv}{D_O} = \frac{\delta \pi D_O v}{4} \qquad (1\text{-}5)$$

where: $\dot{V}$ = volumetric flow through the parcel (m^3/s)-,
v = velocity of the ambient air (m/s);

Under steady state conditions, the power convected into the air parcel from the shell area upwind of the parcel plus the power in the ambient air infiltrated into the parcel must equal the power infiltrated out of the parcel. Applying an energy balance to control volume of air in the parcel:

$$\rho \dot{V} CT_O + hA_S (T_S - T_O) = \rho \dot{V} CT_P \qquad (1\text{-}6)$$

$$\rho \dot{V} CT_O + h(D_O L)(T_S - T_O) = \rho \dot{V} CT_P \qquad (1\text{-}7)$$

where: ρ = air density (kg/m^3);
C = air specific heat (J/kg-°C);
h = forced convection coefficient (W/m^2-°C);
A_S = shell area upwind of the shutter (m^2);
T_S = temperature of the shell (°C);
T_O = temperature of the ambient air (°C);
T_P = temperature of the air parcel over the shutter slot (°C);
L = length of the shell upwind of the shutter (m)

Substituting the expression for the volumetric flushing rate (1-5) through the air parcel into 1-6, the temperature of the air parcel over the shutter slot can be expressed as:

$$T_P = T_O + \frac{h4L}{\pi \rho C \delta v}\left(T_S - T_O\right) \qquad (1\text{-}8)$$

When the functional relations for the forced convection coefficient h (Section 5.3.1, Equation 1-28) and the boundary layer thickness δ (1-3) are substituted into 1-8, the expression becomes:

$$T_P = T_O + \left(\frac{13.8}{\rho C (v^{3/10})} \left(\frac{L}{\gamma} \right)^{1/5} \right) (T_S - T_O) \qquad (1\text{-}9)$$

Finally, when the expression for the temperature of the air parcel (1-9) is substituted into the seeing equation to evaluate shell seeing, we obtain:

$$S_S = C_R (T_P - T_O)^{6/5} \qquad (1\text{-}10)$$

where: Ss = shell seeing expressed as 50% encircled energy in arcsec(");
CR = seeing coefficient (0.15"/°$C^{6/5}$)

The thermal model solves for the shell temperature, and the ambient air temperature profile is an environmental boundary condition predefined as an input to the model. Thus the shell seeing can be calculated in a straightforward fashion with equations 1-9 and 1-10 for any particular thermal model run.

An alternate form of 1-10 involves the shell temperature T_S;

$$S_S = C_R \left[(T_S - T_O) \left(\frac{13.8}{\rho C (v^{3/10})} \right) \left(\frac{L}{\gamma} \right)^{1/5} \right]^{6/5} \qquad (1\text{-}11)$$

Equation 1-11 can be utilized to obtain shell to ambient air temperature bounds for defined value of shell seeing, given an ambient windspeed. For the Gemini enclosure, the arc length of the spherical cap of the enclosure upwind of the shutter slot is about 20 meters. If the density, kinematic viscosity, and the specific heat of the ambient air are assessed at 0°C for 4 km elevation, we can utilize 1-11 and plot ambient air velocity versus the shell to ambient air temperature differential that will give a shell seeing equal to the error budget value of 0.30 arcsec. This plot is shown on Figure 3.

- At the 70th percentile windspeed of 11 m/s, the shell can be 2◦C warmer or cooler than the ambient air for 0.03" seeing.

Assessment of the allowable temperature difference at the 5th percentile windspeed of 0 M/s is problematic, since the boundary layer thickness equation (1-3) is undefined for conditions of free convection. However, on all the subsequent seeing plots for the 5th percentile model runs, continuous free convective; linkages are defined to exist between the shell elements and the ambient air. Then 1-11 is applied assuming a sudden gust of wind at 1 m/s blows over the shutter.

- At the 5th percentile of the windspeed, the absolute value of the shell to ambient air temperature difference must not exceed 1°C.

5. THE THERMAL MODEL

The challenge of enclosure thermal design, given an enclosure structure which will survive worst case environmental boundary conditions, is depicted graphically on Figure 4, where every listed caption is a quantity which must be optimized in order to achieve the enclosure seeing error budget.

5.1 THERMAL MODELING METHODOLOGY

The methodology used in constructing a thermal model to evaluate enclosure thermal performance is listed as follows:

- site specific environmental parameters must be determined:
    1 an ambient air temperature profile (Section 5.2.1);
    2. wind velocity distribution (Section 5.2.2);
    3. solar loading (Section 5.2.3);
    4. sky irradiation (Section 5.2.4);
    5. earth irradiation (Section 5.2.5);
- construction drawings are used to define a thermal model which must represent every major structural component of the enclosure designed to survive the peak environmental boundary conditions at the site:
    1. thermophysical properties of prospective coatings, insulation and construction materials are defined (Section 5.3.4, 5.4);
- thermal linkages are then defined and applied to certain model elements:
    1. time constant convective links, radiative links, and flow links (Section 5.3.1);
    2. time variable convective links, radiative links, and flow links (Sections 5.3.2, 5.3.3, and 5.3.4);
- constant and time variable heat loads are applied to certain model elements:
    1. a data base is assembled to quantify the power that will be released from active sources (lights, drives, instruments, etc.) operating within the enclosure structure (Section 5.4);
- the model is calibrated against existing enclosures:
    1. calibration of radiative linkages to the earth and sky (Section 5.5.1);
    2. calibration of flow links and convective links (Section 5.5.2);
- the calibrated model parameters are held constant in subsequent transient runs, while the following parameters are varied (Section 5.6):
    1. surface coatings;
    2. ambient wind velocity;
    3. insulation thickness;
    4. fan forced flow rates;
    5. active source power dissipation;
- finally, the resultant temperature history output data for certain model elements are applied to seeing formulae to determine which combination of parameters will give superior enclosure seeing performance (Section 6.).

5.2 ENVIRONMENTAL BOUNDARY CONDITIONS

A first step towards determining the enclosure's thermal performance is establishing the site specific environmental boundary conditions. The boundary conditions are then used to establish the magnitude and time variation of the thermal links that are applied to the finite difference model which will be created to represent the enclosure.

5.2.1 Ambient Temperature Prorde

Knowledge of the ambient air temperature profile enables determination of the magnitude of two important sets of thermal linkages used in the modeling. Since convective heat transfer from a surface is proportional to the temperature difference between the surface and the ambient air, convective thermal links acting on the surface elements of the can be directly determined. The ambient air temperature profile is also required to determine the values of flow links acting between the ambient air and certain model air volume elements. The functional expressions for the convective and flow links are listed in Section 5.3.1.

Air temperature data was acquired for the month of August 1992, a period of peak annual daytime solar flux at Mauna Kea; because of the absence of ground cover daytime ambient air temperatures and diurnal temperature swings are at their greatest annual values. Raw and smoothed ambient temperature profiles are presented on Figures 5A and 5B. The curve labeled "R" on Figure 5A was obtained from UKIRT weather tower data, and represents a 30-day mean for August. The "R" curve was developed via a simple point averaging program written for use on a personal computer. The curve labeled "S" represents the smoothed profile used for the thermal modeling. The smoothed curve was developed via polynomial regression; a 50th order polynomial spline was fitted to the raw average data. Higher order splines did not significantly improve the fit. The nighttime air temperature profile, Figure 5B, shows the smoothed profile over the nighttime hours.

- The nighttime profile is essentially linear (-0.10 °C/hr) for an eight hour period commencing two hours after sundown (18:00);
- However, because there are relatively sudden changes in ambient air temperature during the night, we have investigated the enclosure response to a step change in ambient air temperature. The results are shown in Section 6.4.

Figure 6 presents an August mean temperature profile curve (for Mauna Kea) developed by Dr. William Weller of the Gemini Instrumentation Group subsequent to the completion of the Gemini enclosure thermal modeling. This profile utilized a CFHT database that was reduced with the rigorous statistical analysis packages of the IRAF software. The temperature values of Figure 6 compare well to those of Figures 5A and 5B, and substantiate their use as the ambient air temperature profile input to the thermal model.

5.2.2 Wind Velocity Distribution

The ambient wind speed is a predominant parameter affecting the nighttime thermal performance of the enclosure. Knowledge of the wind velocity distribution enables determination of forced convection coefficients and passive flushing volumetric flow rates through the enclosure chamber.

Figure 7 shows the site wind velocity distribution. This distribution was obtained from CFHT, and represents weather tower data sampled over the four years from 1987 to 1991.

- Five percent of the time, the wind velocity is zero, and free convection will exist on all surfaces not affected by active ventilation. Operation under conditions with quiescent wind speed places stringent demands on the thermal control system of the enclosure, since the resulting free convection conditions can create buoyancy driven flow off of the outer shell and also out of the chamber through the open shutter. To reduce the level of power flow moving through the light path of the telescope, we investigated a solution involving fan forced flows through both the chamber and through the air volume confined beneath the outer structural shell of the enclosure.
- 70 percent of the time, the wind velocity is under 11 m/s, and forced convection of varying magnitudes will exist on all surfaces in contact with the moving air mass. The 70th percentile has been defined in the Gemini Science Requirements as the wind velocity up to which the enclosure error budget of 0.030" must be met. [Osmer]

Model runs will be performed at both the 5th and 70th percentile wind velocity distribution values.

5.2.3 Solar Radiation

Solar loading values for the thermal model were developed via the use of handbook data and a personal computer.

The solar irradiation acting on the outer structural shell of the enclosure will be composed of both collimated and diffuse radiation. To be consistent with the August average ambient air temperature profile, solar irradiation must be determined for the middle of August. The first step is to calculate the collimated solar radiation, or the radiation incident upon a surface always oriented normal to the rays of the sun for the latitude and altitude of Mauna Kea. The collimated solar radiation is determined by the following expression [Kreider and Kreith]:

$$I_C = I_0 \tau_{atm} \qquad (1\text{-}12)$$

Where:
I_C = the collimated radiation **(**W/m^2**);**
I_0 **=** solar constant (1350 W/m^2);
τ_{atm}= atmospheric transmittance.

The atmospheric transmittance is calculated by the relation:

$$\tau_{atm} = 0.5(e^{0.65m(z,\alpha)} + e^{-0.095m(z,\alpha)}) \qquad (1\text{-}13)$$

where: α = the solar altitude angle;
z = altitude above sea level;
$m(z,\alpha)$ = air mass at altitude z and solar altitude cc.

The expression for determination of the air mass $m(z,\alpha)$ is:

$$m(z,\alpha) = m(0,\alpha)\frac{p(z)}{p(0)} \qquad (1\text{-}14)$$

where: $m(0,\alpha)$ = air mass at sea level (altitude 0);
$p(z)$, $p(0)$= atmospheric pressures at altitude z and sea level, respectively.

The sea level air mass can be determined from:

$$M(0,\alpha) = \sqrt{1230 + (614\sin\alpha)^2} - 614\sin\alpha \qquad (1\text{-}15)$$

At solar noon, 15 August, the sun is very nearly directly overhead at Mauna Kea, α=0, and the air mass is unity. If we assume an ambient air pressure of 650 mb, then the above equations give a collimated radiation value of 1100 W/m^2. The modeling described in this report neglects the effect of diffuse solar radiation acting on the outer shell of the enclosure.

Given the collimated radiation, the remaining step is to calculate its normal component onto surfaces of variable orientation with respect to the solar vector. This is easily achieved with the use of the following formula [Kreider and Kreith]:

$$I_N = I_C\left(\cos|z - \Psi| - \sin z \sin\Psi + \sin z \sin\Psi \cos|A - \beta|\right) \qquad (1\text{-}16)$$

where: I_N = normal component of the collimated radiation incident on the surface (W/m^2);
I_C = collimated radiation (W/m);
z = angle between the sun vector and the zenith, or the zenith angle;
Ψ = angle between the sun vector and surface normal;
β = angle between the horizontal plane projection of the surface normal and the local North- South meridian;
A = azimuth of the sun; $A=\sin^{-1}[\cos\delta_S \sin h/\cos(90-z)]$
δ_S = solar declination;
h = solar hour angle (degrees West from local solar noon)

Using solar declination and solar hour angle data from the Nautical Almanac for the latitude of Mauna Kea, solar flux curves are readily developed for surfaces of any orientation.

Figure 8 presents the normal solar flux (per m^2) on a horizontal surface ("H"), both sides of a North-South oriented planar vertical surface ("V"), and the collimated flux ("I"). We can observe the effect of large numbers of air mass on the collimated flux for low solar altitude angles: at 06:00 solar time the collimated flux is barely 10% of its peak value at solar noon.

The thermal model has three surface elements which receive solar radiation. Two of the elements represent the east and west sides of the enclosure basement. The other element represents the wall area of the enclosure above the chamber floor. A thermal link is not used to input solar flux into the model elements. Instead the power is input directly into the surface of the elements in the form of a time varying heat load. The absorbed solar radiation on the outer surface area of a model element is:

$$Qs = \alpha A I_N \tag{1-17}$$

where:
- Q_S = absorbed radiation (W);
- I_N = the normal incident solar radiation (W/m^2);
- α = the solar absorptance of the element surface;
- A = surface area of the element (m^2);

Figure 9 shows how much of the normal incident solar radiation will be absorbed for each of the three candidate coatings. The curves are for the *total projected surface area* of the enclosure (the spherical cap, and the cylindrical chamber and basement walls) and assume that the entire surface area is covered with one of the three candidate coatings listed. The curves have a characteristic "gull wing" shape because the projected surface area of the lower cylindrical walls of the enclosure rapidly decay away to nearly zero as the sun moves overhead, leaving only the projected area of the spherical cap to absorb the sun's rays.

Significant amounts of power are radiated onto the structural shell of the enclosure by the sun, regardless of the surface coating used, because of the large surface area. One goal of the modeling is to determine how much of this absorbed solar power is conducted into the walls of the structure and stored in the structural trusswork supporting the outer skin. Then the enclosure seeing caused by this stored heat as it discharges back out into the ambient air over the nighttime hours can be evaluated.

5.2.4 Sky Irradiation

The outer structural shell of the enclosure is continuously irradiated by the earth's atmosphere. At night, the inside of the enclosure will be irradiated as the atmospheric emission acts through the shutter and any open flushing vents.

Assuming the spectral distribution of atmospheric emission can be modeled as though the sky is a blackbody, then enclosure irradiation due to sky emission can be estimated with the Stephan-Boltzman Law:

$$I_{SKY} = \sigma T^4_{SKY} \tag{1-18}$$

where: I_{SKY} = sky irradiation (W/m^2);
σ = Stephan-Boltzman constant (5.67 E-8 W/m^2-°K);
T_{SKY}= effective sky temperature (°K)

The value used for the effective sky temperature at Mauna Kea is 243°K (-30°C) which is consistent with values used by others.[Kogure et al, Carrol et al] The thermal modeling assumed the effective sky temperature did not vary with time. Thus the value for the sky irradiation at Mauna Kea is 200 W/m^2.

5.2.5 Earth Irradiation

The basement walls of the enclosure and portions of the outer structural shell of the enclosure will be irradiated by the surface of the earth. The enclosure irradiation due to thermal emission from the earth's surface may also be evaluated with the Stephan-Boltzman Law:

$$I_{EARTH} = \sigma T^4_{EARTH} \tag{1-19}$$

where: I_{EARTH} = earth irradiation (W/m^2);
σ = Stephan-Boltzman constant (5.67 E-8 W/m^2-°K);
T_{EARTH} = effective earth temperature (°K)

There is no recorded data relating the variation of earth surface temperature with time at the locale of the summit ridge of Mauna Kea. The thermal model was used to determine this temperature variation.

Geophysical reconnaissance has shown that the wind has scoured all fine ash from the top layers of the cinder formations in the locale of the summit ridge [Harding Lawson Associates]. The bulk thermophysical properties listed in Table 1. I assume that the soil has a porosity of 50%, and that air fills all free voids. The thermal properties of red clay firebrick were used to model the solid soil particles representing the cinders.

Table 1.1 - Bulk Thermophysical Properties Used to Model the Soil at Mauna Kea

Density (kg/m^3)	Specific Heat (J/kg °C)	Thermal Conductivity (W/m °C)	Solar Absorp. (dimensionless)	Thermal Emiss. (dimensionless)
1,162	960	0.3	0.63	0.9

To be consistent with the August average ambient air temperature profile used in the modeling, the solar flux applied to the top of the group of elements used to model the soil was for the same time period. The soil top element also has a radiative link to the sky with a view factor of unity. The magnitude of the convective link between the soil and the ambient air depends on the wind velocity.

Figure 10 shows the simulated soil top temperature at the 5th percentile (0 m/s) of the windspeed and Figure 11 shows the same information at the 70th percentile (11 M/s) of the windspeed.

- At the 5th percentile of the wind velocity, the model predicts that the top surface of the soil will be 40 degrees warmer than the ambient air at solar noon, and that the soil top temperature will drop 10 degrees below ambient at night;
- at the 70th percentile of the wind velocity, the model predicts that the top surface of the soil will equal the ambient air at solar noon, and that the soil top temperature will subcool 5 degrees below ambient at night.

To form the earth element used in the modeling, a very large planar element is formed at the base of the enclosure. Depending on what percentile value of the ambient windspeed is used for a model run, the temperature profile of either Figure 10 or 11 is assigned to this element. The element is assigned the radiative properties of the soil. Radiative links are then defined between this earth element and elements representing the outer surface areas of the enclosure.

Since the sky and earth irradiation are of differing magnitudes, and since the view factors between the outer shell of the enclosure with respect to the earth and to the sky are different, we can predict that global temperature variations will exist for the shell even in the absence of solar radiation. This nighttime shell temperature variation is demonstrated in actual temperature data from the Keck enclosure, Section 5.5.1.

This completes the description of the environmental boundary conditions. We may now create a model to simulate the thermal behavior of the enclosure.

5.3 DESCRIPTION OF THE THERMAL MODEL

Ideas-TMG^{TM} modeling software is used to create a finite difference model representing all the principal structural elements of the baseline enclosure, as well as all the important air volume regions within the enclosure. The model has a total of 130 elements, consisting of solid "bricks", quadrilateral flat shells, beam elements, and non-geometric elements. The non-geometric elements are defined to represent model air volumes.

The energy equation for a finite difference control volume can be expressed as:

$$\int_A q_a dA + \int_V q_v dV = \int_V \rho C \frac{dT}{dt} dV \qquad (1\text{-}20)$$

which can be simplified to:

$$Q_A + Q_V = \frac{dU}{dt} \qquad (1\text{-}21)$$

where: Q_A = the net power flow across the control volume boundaries (W);
Q_V = power generated within the control volume (W);

$\frac{dU}{dt}$ = the rate of change of the volume's internal energy, or the power stored in the control volume (W).

The capacitance of the control volume representing an element m is defined assuming it has constant specific heat and constant density

$$C_m = \frac{dU_m}{dT_m} = \rho VC \qquad (1\text{-}22)$$

where:
C_m = the capacitance of the element m (W- hr/ °C);
ρ = density of the element (kg/m^2);
V = volume of the element (m^3);
C = specific heat of the element (W- hr/kg °C);

The magnitude of the power flow across the boundary area separating element m and an adjacent element n (The Q_A term of 1-21) can be characterized by a thermal linkage:

$$Q_{mn}=G_{mn}(T_m-T_n) \qquad (1\text{-}23)$$

where:
Q_{mn}= the power flow from element m to element n (W);
G_{mn}= the thermal link connecting m to n (W/°C);
T_m = temperature of element m (°C);
T_n = temperature of element n (°C)

A total of 200 thermal links are defined between various model elements. 90 are conductive, 40 are linear radiative, 40 are convective, and the remainder are either one or two way flow links. The one way flow links represent active ventilation processes, and the two-way flow links represent passive ventilation (flushing). When all the thermal links acting between the two elements are combined, 1-21 can be applied to the element m as:

$$Q_{V_m} + \sum Qmn = C_m \frac{dT_m}{dt} \qquad (1\text{-}24)$$

Q_{Vm}, C_m, and ΣQ_{mn} can all be functions of time. The thermal time constant of the element m is given by:

$$\tau_m(t) = \frac{C_m(t)}{\sum Q_{mn}(t)} \qquad (1\text{-}25)$$

where: τ_m = the time constant of the element m (hrs).

Thus the time constant of an element can change significantly over time.

Application of 1-24 on all the elements composing the thermal model yields a set of equations which are given initial temperature values and then simultaneously integrated over time to determine the transient response of the element temperatures. The lowest thermal time constant of the element set is used as the integration time step during the solution.

The next section is concerned with how the thermal links connecting the model elements are defined.

5.3.1 Conductive, Convective, Flow and Radiative Links

A conductive link acting between model elements is defined as:

$$G_K = k\ A/L \qquad (1\text{-}26)$$

where:
- G_K = the conductive link (W/ °C);
- k = the thermal conductivity (W/m °C);
- A = mean cross sectional area between the elements (m^2);
- L = distance between the elements (m);

In most instances, conductive links are defined implicitly within the modeling software simply by virtue of adjoining surfaces and do not require explicit definition.

A convective link between the surface area of a model element and the surrounding air is:

$$G_C = h\ A \qquad (1\text{-}27)$$

where:
- G_C = the convective link (W/°C);
- h = convection coefficient (W/m^2-°C);
- A = surface area of the model element (m^2)

The free and forced convection correlations suggested by Woolf [Woolf] were used for the modeling:

$$h_{FORCED} = 4\sqrt{v} \quad (\text{W/ m}^2\ \text{–°C}) \qquad (1\text{-}28)$$

$$h_{FREE} = 2(\Delta T)^{.25}\ (\text{W/ m}^2\ \text{–°C}) \qquad (1\text{-}29)$$

where:
- v = air velocity (m/s);
- ΔT = temperature difference between the surface of the object and the surrounding air.

These correlations have proven to be excellent design guidelines and can be rapidly programmed into "lookup" tables for the thermal model, where convective thermal linkages are varied with time due to increases in air velocity caused by fan operation and flushing.

Flow links between model air volume elements are defined as follows:

$$G_F = \rho \dot{V} C \tag{1-30}$$

where:
- G_F = the flow link (W/°C);
- ρ = air density (kg/ m^3);
- $\dot{V}$ = air volumetric flow rate between the elements (m^3/sec);
- C = air specific heat (J/kg-°C)

A radiative link between two model elements m and n is:

$$G_R=\sigma A_m \varepsilon VF_{BB}(T_m-T_n)(T^2_m-T^2_n) \tag{1-31}$$

where:
- G_R = linearized radiative link (W/ °C);
- σ = Stephan-Boltzman constant (5.67E-8 W/m^2-°K^4);
- A_m = surface area of element m (m^2);
- ε = emissivity of element m;
- VF_{BB} = view factor between the elements;
- T_m, T_n = temperatures of elements m and n, respectively (°K)

The magnitudes and time variations of the radiative, convective, and flow links acting between model elements must be defined explicitly and entered into the modeling software. To determine the value of these links, three factors must be known:

- the exact environmental boundary conditions which will act on the outside surface area of the model's outer shell. Some of these same conditions act to a lessor extent upon the areas and capacitances of model elements representing the inside the enclosure because of wind forced infiltration during the daytime hours;
- the surface areas of all model elements and the gray body view factors between them;
- at what times the shutter and flushing vents open and close, and for the case of fan forced active flow processes, the fan's flow rate and period of operation must be known.

5.3.2 Shutter Opening/Closing, Flushing Vent Opening/Closing, and Time Varying Power Fluxes

The model runs assume the shutter and flushing vents open concurrently at sun down (18:00 Hours Solar Time) and close at sun up the consecutive day (06:00 H.S.T.) While the shutter and vent apertures are open, the surfaces inside the enclosure (the mount, the floor, and the chamber wall) will radiate heat out to the night sky.

If the ambient wind velocity is at the 5th percentile values of zero m/s, free convection is defined to exist between all surfaces inside the enclosure and the chamber air. If the wind velocity is above the 5th percentile value, two other thermal linkages occur:

- a wind forced flow link will occur between the ambient air and the chamber air (via the open flushing vents) resulting in power being removed from the chamber air, since it is invariably warmer than the ambient air because both surfaces and active sources are releasing heat into the chamber air;
- the convective link between the surfaces inside the enclosure and the enclosure chamber air will change from free to forced because of the increase in chamber air velocity caused by the flushing. The result is more power will be transferred from the surfaces to the chamber air, and the objects inside the chamber will more rapidly equilibrate to the ambient air temperature profile.

Figures 12 and 13 present schematic representations of the time variation of the thermal linkages surrounding the chamber air element T_C. The thermal links are represented by symbols representing their inverse, or their thermal resistances (w/ units of °C/W). Time variable power fluxes are represented by wavy vectors acting on certain nodes, for example the solar flux vector P acting on the enclosure wall node T_W.

On Figure 12, the shutter and flushing vent switches are shown in daytime setting. Figure 13 shows the resultant resistance change when the switches are set on the nighttime, or observing position. The switches were timed to ramp from one position to another over a time period of three minutes, a value comparable with the time required to actuate the real devices.

For the sake of simplicity, the figures depict the principal structural elements around the chamber air element as single nodes. For instance, the wall element is depicted as a single node, whereas the actual network used for the thermal model consisted of a much more complex system of elements (outer shell, inner chamber wall, trusswork elements, weld contact elements, etc.) and included a shell air volume element. All categories of thermal links acted between these elements, including time variable links between the shell air and ambient air elements to represent fan forced flow, and resistance switches between the structural elements inside the wall and the shell air elements to represent the change in convective resistance during the forced flow.

5.3.3 Volumetric Flow Rates

This section describes how the air velocity and volumetric flow rates are determined for an enclosure being flushed with ambient air. Then the flow links and convective links that will be used in the modeling can be determined.

In order to obtain upper and lower bounds on enclosure performance, model runs were performed for two separate values of ambient wind velocity:

- the lower bound assumed the 5th percentile ambient wind speed of zero m/s for which quiescent conditions will exist and free convection is defined to exist on all element surfaces inside and outside the enclosure model, except where the air velocity term from active (fan forced) flow would result in greater power transfer than would result from free convection.

- the upper bound wind velocity term used for seeing evaluation assumed the 70th percentile wind speed of 11 m/s. Thus forced convection links are defined to exist over the surface areas of model elements representing the outside of the enclosure. For elements inside the enclosure, free or forced convection links are defined depending on whether the shutter and flushing vents are open.

Water tunnel flushing tests were conducted by the Department of Aeronautics and Astronautics at the University of Washington on a 1:177 scale model of the Gemini enclosure. The tests used a water tunnel velocity scaled to 14.5 m/s, and demonstrated that all visible liquid dye injected into the scale mockup of the enclosure would be removed by the water moving through the model via the flushing vents in 45 seconds, or 80 scale volumes/hour. Scaling the rate down to adjust for the 70th percentile wind velocity of 11 m/s, the flushing rate will be 60 volumes/hr for the global scale Gemini enclosure.

The following tables present the data used to determine the baseline modeling flow rates. Since the 5th percentile wind speed is zero, infiltration is not defined. Ventilation for these model runs is fan forced, except for buoyancy driven shell air volume flow rates. Model runs for the 70th percentile use both passive (infiltration and flushing) and fan forced ventilation.

Data from the UKIRT enclosure at Mauna Kea suggest that the buoyant flow between the ambient air and the shell air volume can approach 50 shell air volumes per hour during the peak solar event [Cavedoni]. At the CFHT, louvers (at the top of the enclosure structure) that allow passage of the shell air flow are closed at night to prevent warm air escaping into the telescope lightpath [Racine et al]. "Louver seeing" is thus prevented. This information is utilized in the following table.

Table 1.2 - 5th Percentile Baseline Ventilation Rates

Daytime	***Nighttime***
No Chamber Air Flow	10 chamber vol/hr = 150,000 m^3/hr (fan)
No Basement Air Flow	No Basement Air Flow
No Floor Air Flow	90 floor vol/hr = 150,000 m^3/hr (fan)
No Mount Air flow	100 Mount vol/hr = 1,800 m^3/hr
50 shell vol/hr = 81,250 m^3/hr (buoyancy)	No shell air flow (louvers closed)[1]

1. The first model runs demonstrated (Section 6.2.1) that at low ambient wind speeds, active ventilation of the shell air volume was required. Subsequent runs used a nighttime fan forced flow equivalent to 90 shell volumes (150,000 @) per hour; the results are presented in Section 6.2.2.

Table 1.3 - 70th Percentile Baseline Ventilation Rates

Daytime	***Nighttime***
1 Chamber vol/hr = 15,000 m^3/hr (infil)	60 Chamber vol/hr = 900,000 m^3/hr (infil)
1 Basement vol/hr = 9,100 m^3/hr (infil)	1 Basement vol/hr = 9,100 m^3/hr (infil)
1 floor vol/hr = 1,660 m^3/hr (infil)	90 floor vol/hr = 159,100 m^3/hr (fan)

No Mount air flow	100 Mount vol/hr = 1,800 m^3/hr (fan)
50 shell vol/hr = 81,250 m^3/hr (buoyancy)	No shell air flow (louvers closed)

The magnitudes of the flow links are determined by inserting the flow rate values into Equation 1-30.

5.3.4 Radiation to the Sky and Outer Skin Surface Emissivities

The magnitudes of the radiative link between the model element surface and the sky, sun, or another model element surface will depend on surface properties and view factors. The surface properties of the three candidate coatings used for the thermal modeling are presented in the following table.

Table 1.4 - Properties of Candidate Coatings

Coating Material	***Solar Absorptance***	***I.R. Emissivity***
White Ti-O_2 Paint	0.25	0.87
Lo-Mit^{TM} Paint	0.22	0.21
3M^{TM} Aluminized Mylar Tape	0.15	0.05

Lo-Mit^{TM} paint is a silicon based coating developed for use as a spray applied radiant barrier roof coating. In situ weathering tests were performed on the Lo-Mit paint atop the UKIRT enclosure on steel and aluminum sample specimens with various types of primer preparation. The weathered samples, together with unweathered control samples were then tested for 10 micron thermal emittance and solar absorptance. The tests demonstrated that the Lo-Mit paint can withstand the environmental conditions atop Mauna Kea. The methodology and results of these tests are presented in Appendix 1.

For modeling purposes, a sky enclosure element is formed by defining large geometric enclosure a large distance away from the model origin. This element is then defined as a sink at constant temperature of 243 ºK (The effective sky temperature). Since the sky radiation is concentrated in approximately the same spectral region as the surface emission of the enclosure, we elect to simplify the radiant power exchange between the sky and the enclosure by equating the sky absorptance of a model element surface to the emissivity of the surface. Then the power transfer from the sky enclosure element to the surface of the model element, Q_{SKY} (Watts) is:

$$Q_{SKY}=\sigma A_{ELEMENT}\varepsilon VF_{BB}T^4_{SKY} \tag{1-32}$$

where:

- σ = Stephan-Boltzman constant (5.67E-8 W/m^2-ºK^4);
- $A_{ELEMENT}$ = surface area of the element (m^2);
- ε = emissivity of the element surface;
- VF_{BB} = black body view factor of the element with respect to the sky;
- T^4_{SKY} = fourth power of the effective sky temperature (ºK^4)

The gray body view factor (VF_{GB}) of the sky element with respect to the surface area $A_{ELEMENT}$ of the model element is the black body view factor multiplied by the emissivity of the element surface:

$$VF_{GB} = \varepsilon VF_{BB} \tag{1-33}$$

Then the net radiative power transfer Q_R (Watts) between the sky element and the surface of the model element can then be expressed as:

$$Q_R=\sigma A_{ELEMENT}VF_{GB}(T^4_{ELEMENT}-T^4_{SKY}) \tag{1-34}$$

The net radiative power transfer expressed in 1-34 can be linearized for any particular instant in time for the transient analysis:

$$Q_R= G_R\, \Delta T \tag{1-35}$$

where: ΔT = temperature difference between the surface of the model element and the sky enclosure element (℃);

G_R = linearized radiative thermal link (W/C);

G_R = $\sigma A_{ELEMENT}\varepsilon VF_{GB}[T_{ELEMENT}-T_{SKY}]\ [T^2_{ELEMENT}-T^2_{SKY}]$ (1-36)

Linear radiative links are defined in a likewise fashion to exist between all model elements throughout the enclosure. A total of 40 radiative links are defined for the model. In addition, a element is defined to represent the enclosure shutter. To simulate radiant exchange between the inside of the enclosure and the sky, radiative links are defined to exist between the surface areas of all model elements inside the enclosure chamber and the sky through the shutter element during the time interval the shutter is open.

5.4 ADDITIONAL PARAMETERS USED IN THE THERMAL MODEL

The model is defined so that it is a full scale geometric representation of the baseline enclosure. Tables 1.5 1.6, and 1.7 list the values of surface areas, material types, surface coatings, volumes, and thermal capacitances used in the modeling. These values are used to determine conductive, radiative, convective, and flow links acting between the model elements. The 200 total links defined in the model will not be listed.

Table 1.5 - Baseline Enclosure Surface Areas and Coatings

Model Element	***Area (m^2)***	***Surface Coatings Modeled***
Outer Wall (Above floor)	2500	Lo-Mit, Ti-O_2, Mylar
Inner Wall (Chamber Wall)	2315	Lo-Mit, Enamel
Basement Wall (Outer)	1330	Lo-Mit, Ti-O_2, Mylar
Floor	900	Lo-Mit, Enamel

Outside of Mount	*500*	Lo-Mit, Enamel

Table 1.6 - Baseline Enclosure Air Volumes and Thermal C

Element	***Volume (m^3)***	***Capacitance (W-hr/°C)***
Chamber (Above floor)	15000	3,177
Basement	9100	1,930
Ventilated Floor Zone	1660	385
Shell Air (between walls)	1625	345
Inside of Mount	180	40

Table 1.7 - Baseline Enclosure Element Material Types, Volumes, and Thermal Capacitances

Element (Material)	***Volume (m^3)***	***Capacitance (W-hr/°C)***
Mount[1] (steel)	12.5	11,800
Outer Shell[2] (steel)	12.5	11,800
Trusswork[3] (steel)	11.2	10,555
Ventilated Floor[4] (steel)	4.5	4,560
Chamber Wall[5] (urethane)	185	3,760

Table 1.7 Notes:

1. Volume for outer mount boxwork and tube system only; does not include platework stiffeners inside mount thermal model. This platework system is linked to the outer mount elements with conductive links.
2. The outer shell is 5 nun thick, the minimum allowable value based on fabrication considerations.
3. Total volume of all trusswork elements. The trusswork is composed of a set of elements (representing the webs and chords of the trusses) connected to one another and to the shell and chamber wall with conductive links.
4. Volume of the floor top only. The floor top plate is 6 mm. The plate is lumped (single element). The floor top is coupled to the floor trusses with conductive links.
5. Volume for a total wall thickness of 80 mm. The model subdivides this wall into ten sub elements across the 80 mm thickness, and uses zero thickness coating elements.

Table 1.8 presents the thermophysical properties of the solid materials used in the modeling. Data from this table is used to determine conductive links and element capacitances.

Table 1.8 - Thermophysical Properties of Model Materials

Material	***Density (kg/m^3)***	***Conductivity (W/m °C)***	***Spec.Heat (Whr/kg°C)***
steel	7854	60.5	0.12
concrete	1900	1.0	0.22
plywood	500	0.12	0.35
urethane(foamed in)	70	0.03	0.29
glass wool (blanket)	30	0.03	0.23

A database assembled for all the devices dissipating power into the enclosure chamber (lights, drives, instruments) revealed that at no time would a nighttime value of 8.5 kW be exceeded. Table 1.9 presents a summary of the principal sources.

Table 1.9 - Niizhttime Enclosure Chamber Power Dissipation

Source	***Description***	***Diss. Power (kW)***
Telescope Azimuth Drives	15% of time slewing at max accel. rate,	4
Telescope Altitude Drives	85% time tracking; Wind drag at 5 M/s.	
Instrumentation (Cassegrain Electronics)	Total of 7 kW reduced 70% with active temperature control.	2
Control System Electronics	7 Crates at 500 W/each ; Assume no active temperature control.	2.5

Table 1.9 Notes

1 Shutter drives and enclosure drives are located outside the telescope chamber.

2. Daytime lighting load is approximately equal to nighttime telescope drive load.

The following are miscellaneous parameters used in the baseline modeling.

- All of the model runs used white ($Ti\text{-}O_2$) coated outer basement walls;
- The mount, chamber walls, and the floor are coated with enamel paint;
- The outer shell of the enclosure is 5mm steel plate, and is skip welded to the wall support structural steel such that the thermal contact ratios of the weld area relative to the shell is 0.00125 m^2/m^2 (derived from construction drawings);
- The chamber wall of the enclosure is 80 mm of urethane foam applied over a 7 mm plywood sheet;
- The outside of the telescope mount and the outside of the concrete mount support pier are not insulated;
- The roof of the basement has 50 mm of glass wool insulation, and the walls of the basement have 80 mm of sprayed in urethane foam insulation. (Subsequent analysis has determined that insulation in the basement roof and walls is not required: Gemini Project Document No. RPT-TE-G0033, "The Effect of Insulation on the Thermal Response of the Floor and Walls of the Gemini Enclosure")

5.5 Calibration of the Thermal Model

5.5.1 Keck Data

The black body view factor for a small convex object (in this instance, the model's outer shell) residing in a large cavity (the sky element) forming an enclosure is unity. From Equation 1-33, the gray body view factor for such a geometry then becomes equal to the emissivity of the surface. However, portions of the real enclosure surface are being irradiated by the surface of the earth. In addition, the sky temperature decreases with zenith angle, whereas the modeling utilizes a sky element at the constant effective temperature of 243 °K. The effect of earth irradiation and zenith angle dependent sky temperature were accounted for in the modeling by calibrating the model to duplicate the known performance of an existing enclosure.

Figure 14 presents temperature data for the outer surface of the Keck enclosure, and shows how the zenith angle dependent sky temperature affects the surface temperature of a white painted enclosure at night. In Figure 14:

"A" = The ambient air temperature;
"S" = The surface temperature at or below the dripline of the dome;
"M" = The surface temperature at approximately 45° from zenith;
"T" = The surface temperature at the very top of the dome.

Wind velocity data from the same database indicated that the mean velocity of the wind the same night was about 13 m/s.

From Figure 14 we note that:

- The nighttime dome surface temperature increases by about 4°C from zenith to horizon in linear fashion;
- The dome temperature near the dripline corresponds to the ambient air temperature.

The temperature of the skin at 45° from zenith is important because it represents the average skin temperature. This temperature value can be used to calculate the average amount of power transfer between the skin and the air passing over the open shutter.

For a gray body view factor of 0.32 to a constant temperature sky of 243 °K, a white coated outer model shell with a forced convection coefficient corresponding to the 70th percentile wind speed of 11 m/s will equilibrate to about -2 °C below ambient nighttime air temperature. Since the emissivity of white $Ti\text{-}O_2$ pigmented paint is 0.87, the black body view factor of the model element to the constant temperature effective sky will be 0.36. The model is thereby calibrated for radiant exchange to the earth and sky, and gray body view factors for the other candidate coatings can now be determined with Equation 1-33 to evaluate the radiative links between the outer shell element and the sky element for subsequent model runs.

Figure 26 presents the shell temperature profiles (over the nighttime hours) for the three candidate coatings at the 70th percentile of the ambient windspeed.

5.5.2 **UKIRT** Data

Data from the UKIRT enclosure were used to calibrate model flow links and other thermal links acting on the model chamber air element.

Figure 15 presents some real time temperature data from the 20-meter diameter UKIRT enclosure. The square box symbols identified as "Dome_Temp" indicate the air temperature inside the enclosure, and the "X" symbols labeled "Air_Temp" are from a sensor on the weather tower outside the enclosure and indicate the ambient air temperature.

- The temperature difference averages about 1.5 °K over the nighttime hours.

Figure 16 presents one of the simulations used to check flow links in the model. Here, 15 kW is being dissipated inside the enclosure, and at the same time the enclosure is being flushed with five enclosure volumes per hour of ambient air, a value derived from water tunnel tests performed on unventilated spherical enclosures where the flushing flow occurs through the open shutter. (Wong &Forbes] The curves labeled C and A are the chamber air and the ambient air, respectively. The curves are in good agreement with the real time UKIRT profiles of Figure 15.

5.6 MODEL SOLUTION

The model is solved by simultaneous integration of the energy equations for the 130 total finite difference elements over very small time steps until the maximum time value for the transient analysis is reached. As an example, the energy equation for the chamber air element is presented below. Only one flow link and three convective links act on this element, and as a result the energy balance can be expressed with a minimum of expressions:

$$\rho VC\frac{dT_i}{dt} = \rho\dot{V}C(T_o - T_i) + h_w A_w (T_w - T_i) + h_f A_f (T_f - T_i) + h_m A_m (T_m - T_i) + \dot{E} \quad (1\text{-}38)$$

where:
T_i = temperature of the chamber air volume element (°C);
T_o = ambient air element temperature (°C);
T_w = surface temperature of the chamber wall element (°C);
T_f = surface temperature of the floor element (°C);
T_m = surface temperature of the mount element (°C);
ρ = air density (0.8 kg/m^3 at T=0°C for 4 km Elevation);
V = volume of the chamber air element (m^3);
C = specific heat of the chamber air (0.278 W-hr/kg-°C);
$\dot{V}$ = volumetric flow rate through the chamber air element (m^3/hr);
A_w, A_f, A_m = surface areas of the chamber wall, floor, and mount elements (m^2);
H_w, h_f, h_m = convective heat transfer coefficients between the wall, floor, and mount element surfaces, respectively, and the chamber air element (W/m^2-°C);
$\dot{E}$ = power generated within the chamber air volume element by active sources; (W)

The surface area elements are all linked to one another and to the night sky (only when the shutter opens) with time varying radiative linkages. The volumetric flow rate and all convective heat transfer coefficients are also time variant, as defined by the values of flow links and convective links used during a particular integration time step. The values of the radiative, flow, and convective thermal linkages depend on the orientation of the vent and shutter switches, as described in Section 5.3.2. The power generation term may also vary with time.

6. MODEL RESULTS

Numerous model runs were performed to develop the thermal design strategy for the Gemini baseline enclosure. Temperature response data for all 130 model elements were obtained, but only the data for the mount, the floor, the chamber wall, the outer shell, the chamber air, and various other air volume elements will be presented. The model was used to determine how the thermal performance of the Gemini enclosure was affected by the following parameters:

- different surface coatings;
- different levels of ambient wind speed;
- variation of passive and active ventilation flow rates acting on the chamber air;
- variable levels of power generation representing active sources operating in the chamber air and the basement air;
- active temperature control of the chamber air during daytime hours (air conditioning);
- active ventilation through the air volume between the chamber wall and the outer shell.

The enclosure seeing was determined by evaluating two separate effects: Chamber seeing and shell seeing. If these effects are independent, total seeing degradation (enclosure seeing) will be the square root of the sum of the squares of these two values.

- Chamber seeing is determined from the temperature difference between the chamber air and the ambient air. Equation 1-1 from Section 1.3 is used to evaluate chamber seeing:

$$S_C = C_R\,(\Delta T)^{6/5} \qquad (1\text{-}1)$$

Where:
- S_C = chamber seeing (");
- C_R = seeing coefficient (0.15"/°$C^{6/5}$);
- ΔT = temperature difference between the air inside the enclosure and the ambient air (°C)

- The shell seeing of the enclosure is determined by evaluating the temperature difference between the air over the shutter slot and the ambient air with Equation 1-11:

$$S_C = C_R\,(\Delta T)^{6/5} \qquad (1\text{-}11)$$

Where:
- S_C = shell seeing (");
- C_R = seeing coefficient (0.15"/°$C^{6/5}$);
- K = dimensionless parameter;
- ΔT = temperature difference between the parcel of air over the shutter slot and the ambient air (°C)

6.1 PERFORMANCE OF A WHITE COATED GEMINI ENCLOSURE AT THE 5TH AND 70TH PERCENTILE VALUES OF THE AMBIENT WINDSPEED

Figure 17 summarizes the model input parameters for a white coated Gemini baseline enclosure operating at the 5th percentile wind speed. (The final baseline configuration is not white coated; subsequent model runs (Section 6.2.1) have demonstrated that a white coating will result in inferior performance.) For this model run, 8.5 kW is input to the chamber air to represent active sources (Section 5.4), and the ventilation rates of Table 1.2 are used. Figure 18 shows the 48 hour temperature response of the chamber air volume and all principal structural elements.

Figure 19 shows the same information over the nighttime hours. Refer to Figure 19:

- the floor and wall subcool below the ambient air (because of radiant exchange with the night sky out through the shutter);
- the chamber air and ambient air are almost equal over the nighttime hours (because of the 10 vol/hour of ambient air moving through the chamber);
- the mount temperature averages about I degree warmer than the ambient air for the nighttime hours (because it has a greater thermal time constant than the wall and floor);
- the outer shell dips below the ambient profile about two hours after sundown and falls to 6 degrees below ambient by the end of the night.

Figure 20 lists the model input parameters for a white coated Gemini baseline enclosure now operating at the 70th percentile wind speed (11 m/s). 8.5 kW is input to the chamber air, and the ventilation rates of Table 1.3 are used. Figure 21 presents the temperature profiles over 48 hours:

- the shell temperature is driven much closer to the ambient air temperature (Compare to Figure 18) because of the greater convective heat transfer between the shell and the air.

Figure 22 shows the same profiles over the nighttime hours:

- the outer shell begins to equilibrate with the ambient air temperature at sundown and subcools by two degrees below ambient over the nighttime hours;
- because of the high chamber flushing rate and the increased convective heat transfer in the chamber over the nighttime hours, the temperatures of the mount, wall, and floor are driven closer to the ambient air temperature profile.

Figure 23 and 24 present the enclosure seeing over the nighttime hours for the white coated enclosure at the 5th and 70th windspeed percentiles, respectively.

<u>Conclusions:</u>

- enclosure seeing at the 5th percentile windspeed can be an order of magnitude greater than enclosure seeing at the 70 percentile windspeed;
- enclosure seeing is dominated by shell seeing: white painted enclosures will not meet the Gemini error budget requirements (0.030 arcsec).

6.2 ENCLOSURE SHELL SEEING

6.2.1 The Effect of the Candidate Coatings on Shell Seeing

Figure 25 shows the shell temperature profiles for white, Lo-Mit, and Mylar coated shells at the 5th percentile of the ambient windspeed.

- The white coated shell drops below the ambient air temperature profile two hours after sundown and falls as low as six degrees below ambient by sunrise the next day;
- The Lo-Mit and Mylar coated shell temperatures are about equal over the nighttime hours and never fall below the ambient air profile.

Figure 26 presents the shell temperatures at the 70th percentile-of the wind speed.

- The shell temperatures for all three coatings begin to equilibrate with the ambient profile two hours after sundown;
- The performance of the Lo-Mit and Mylar coatings are virtually indistinguishable and their temperatures are virtually equal to the ambient air temperature after midnight;
- The white coated shell is 2 ℃ below the ambient air for most of the night.

Once we know the temperature of the shell surface, shell seeing can be determined with Equation 1-11. Figure 27 shows the shell seeing for candidate coatings on the baseline enclosure at the 5th percentile of the windspeed. Figure 28 presents the shell seeing profiles for the same coatings at the 70th percentile of the windspeed.

- Shells coated with Lo-Mit and Mylar result in less shell seeing over the nighttime hours;
- Nighttime shell seeing at the 5th percentile windspeed is an order of magnitude greater than nighttime shell seeing at the 70th percentile windspeed.

Conclusion:

- Lo-Mit or aluminized Mylar should be used to coat the outer surface of the enclosure's shell.

6.2.2 The Use of Forced Ventilation to Reduce SheU Seeing

To reduce nighttime shell seeing at the 5th percentile windspeed, the use of fan forced flow in the air space between the shell and the chamber wall was investigated. Figure 29 shows the effect of such ventilation for shells covered with the candidate coatings at the 5th percentile of the ambient windspeed. A nighttime flow rate of 150,000 m^3/hr (10 baseline enclosure chamber volumes per hour) was used to flush the shell air space for these model runs. Comparing this figure to Figure 25, it can be seen that the forced flushing drives the shell temperatures closer to the ambient temperature. Figure 30 shows the shell seeing resulting from the forced flushing.

Conclusion:

Comparing the seeing profiles on Figure 30 to those on Figure 27 (no fan ventilation) it can be concluded that:

- forced ventilation of the shell air cavity significantly reduces shell seeing at the 5th percentile of the ambient wind velocity.

6.3 ENCLOSURE CHAMBER SEEING

6.3.1 The Effect of the Candidate Coatings on Chamber Seeing

Figures 31 and 32 show how the candidate coatings influence the chamber seeing for the 5th and 70th percentile values of the windspeed, respectively. These profiles are obtained by applying Equation 1-1 to the chamber air to ambient air temperature differential. The plots are shown over the total 48-hour period of analysis to show the "spikes" occurring just before the shutter is opened.

- The "spikes" occur because of a buildup in the chamber air temperature over the day. Several hours before sundown the seeing goes to zero because the chamber air temperature equals the ambient air temperature; the chamber air temperature then goes on to exceed the ambient air temperature resulting in higher seeing values;
- Once the shutter and flushing vents are opened and flushing begins, the chamber to ambient temperature differential (and hence the chamber seeing) becomes smaller over the nighttime hours.

Conclusion:

- the effect of shell surface coatings on the nighttime chamber seeing is insignificant.

We have previously demonstrated (Section 6.2) that Lo-Mit or aluminized mylar coatings will reduce shell seeing. For the Gemini enclosure, Lo-Mit paint (or equivalent) should be used, based upon considerations of:

- initial Cost: Lo-Mit is an order of magnitude cheaper than Mylar, per applied square meter;
- applicability: The Lo-Mit coating can be spray applied to the enclosure shell, the mylar coating relies on a pressure sensitive adhesive bonding system;
- maintainability: A re-spraying operation will take much less time than a re-taping operation, especially if the previous application of tape has to be stripped off the shell surface.

6.3.2 The Effect of Variable Heat Loads in the Chamber air on Chamber Seeing

To investigate the chamber seeing caused by an increase in active source power on the chamber air, model runs were performed using 0, 10, 20, and 30 kW sources dissipating power directly into the chamber air element of the baseline enclosure. The nighttime flushing flow rates used for the model runs were (Tables 1.2 and 1.3) 10 chamber volumes per hour of fan forced flow for the 5th percentile windspeed, and 60 chamber volumes per hour of passive flushing at the 70th percentile. Figure 33 and 34 show the results for the model runs at the 5th and 70th percentiles, respectively.

Conclusion:

- the nighttime chamber seeing is directly proportional to the rate of energy dissipation in the chamber air and inversely proportional to the chamber flushing rate.

A database (summarized in Table 1.9) assembled to quantify the active sources dissipating power into the chamber air of the baseline enclosure reveals that at no time would a value of 8.5 kW be exceeded; all subsequent modeling assumes constant 8.5 kW dissipation to the chamber air element.

6.3.3 Daytime Air Conditioning

Figure 35 shows the 48-hour temperature response curves for a Lo-Mit coated baseline enclosure operating at the 5th percentile wind speed but with daytime air conditioning. During the day the chamber air temperature was conditioned so that at the shutter open event (sundown) it would be one degree warmer than the minimum nighttime ambient air temperature. Figure 36 shows the same information over the nighttime hours. The temperature response of an object subjected to a sudden change in its thermal environment is proportional to its time constant:

- the chamber wall rapidly equilibrates after the shutter is opened and ventilation commences and by the end of the night it has subcooled 1 degree below ambient;
- the floor equilibrates next, followed by the mount; the temperatures of these objects are within 0.5 degrees of the ambient air the last 10 hours of the night;
- comparing the shell temperature response to the Lo-mit coated shell temperature profile on Figure 25, we see that the nighttime behavior of the shell temperature is unaffected by the daytime air conditioning, and thus the enclosure shell seeing will be unaffected.

The chamber seeing for the model run with air conditioning is shown on Figure 37 (caption "1") and compared to the chamber seeing for a model run with no A.C. (caption "2").

Conclusion:

- daytime air conditioning reduces nighttime chamber seeing.

6.3.4 Thermal Control of the Telescope Mount

The mount is in close proximity to the telescope lightpath. If the mount is at a different temperature than the chamber air over the nighttime hours, then power will flow into the telescope lightpath.

Figure 38 shows the convective power flow between the mount and chamber air element for the 5th percentile model run with daytime air conditioning (caption "I"). Also included on the plot is the power flow when the model was re-run with the air conditioning turned off (caption "2").

Conclusion:

- conditioning the chamber air during the day results in much less net power flow from the mount into the chamber air at night.

6.4 The Effect of Sudden Drops in Ambient Air Temperature on Enclosure Seeing

To investigate degradation of enclosure seeing caused by a rapid fluctuation in the ambient air temperature, a step of -1 degree C was input to the ambient air temperature profile at midnight. Figure 39 and 40 show the temperature response of the chamber air and of the shell for the 5th and 70th percentile values of the wind velocity, respectively. The 1-(1/e) temperature value (63% of the initial temperature step) is indicated on the plots. Because it has a lower thermal capacitance, the chamber air responds much quicker than the shell:

- at the 5th percentile windspeed, the temperature time constant (1-(1/e)) of the chamber air is 4 minutes, and the time constant of the shell is 24 minutes;
- at the 70th percentile windspeed, the temperature time constant of the chamber air is less than one minute and the time constant of the shell is 9 minutes.

Figure 41 and 42 show the chamber seeing, the shell seeing, and the (total) enclosure seeing response caused by the -1 degree step in the ambient air temperature for the 5th and 70tb percentile values of the wind velocity, respectively. The 0.030 arcsec enclosure seeing error budget value is indicated on the plots.

- At the 5th percentile windspeed, 24 minutes must elapse before the enclosure seeing meets the 0.030 " error budget value;
- At the 70th percentile windspeed, 2 minutes must elapse for the enclosure seeing to meet the error budget value.

Conclusions:

A sudden downward change in ambient air temperature will produce:

- chamber seeing that is inversely proprtional to time;
- enclosure seeing that is dominated by chamber seeing;
- shell seeing that is proportional to time;
- shell seeing that is always below the 0.030 arcsec error budget.

7. ACKNOWLEDGMENTS

I would like to thank Keith Raybould (Manager of the Gemini Telescope Structure, Building, and Enclosure Group) for proofreading this report. I would like to thank Dr. Matt Mountain (Gemini project scientist) and Dr. Fred Gillett (K.P.N.O. staff scientist) for discussions relating the enclosure performance to image degradations. Thanks must also be extended to Kevin Duffy, Christian Ruel, and Marc Hammel (MAYA Heat Transfer Technologies Ltd. in Montreal) for providing user support for their extremely powerful I-DEAS TMG (Thermal Model Generator) software. Thanks to Perigrine McGehee (Gemini Controls Group) and Dr. Bill Weller (Gemini Instrumentation Group) for showing me data reduction subroutines to quickly post process the vast amount of output a TMG run can produce. Also many thanks to Naomi Libby and Ruth Kneale of the Gemini Project Enclosure Group for their efforts in producing this report.

8. REFERENCES

- W.L. Carrol, C. Conner, K. Whitley, "BLAST Parametric Analyses for Keck Observatory Thermal Design", Keck Observatory Technical Note 152, October 1985.

- Cavedoni, C., U.K.I.R.T., personal communication, August 1993.

- Cowley, D., C.F.H.T., personal cormnunication, December 1992.

- R. Ford, P. Gillett, S. Hardash, G. Pentland, K. Raybould, "Gemini 8M Enclosure, Support Facility and Site Plan Preliminary Design Review", Gemini Project Document No. RPT-TE-G0015, May 1993.

- Harding Lawson Associates, "Preliminary Geotechnical Recommendations, Proposed Gemini 8-Meter Telescope, Mauna Kea, Island of Hawaii.", January 18, 1993.

- Incropera, F.P., Dewitt, D.P., *Fundamentals of Heat and Mass Transfer,* Wiley, New York, 1990.

- Kogure, T., Tokunaga, A.T., "Japanese National Large Telescope and Related Engineering Developments", *Astrophysics and Space Science*, Vol. 160, 1989.

- Kreider, J.F. Kreith, F., *Solar Heating and Cooling,* McGraw-Hill, New York, 1977.

- Osmer, P.S., "Gemini Science Requirements", Gemini Project Document SPE-PS-G0001, November 1992.

- R. Racine, D. Salmon, D. Cowley, and J. Sovka, "Mirror, Dome, and Natural Seeing at *CFHT", Publications of the Astronomical Society of the Pacific,* No. 667, September, 1991.

- W.Y. Wong and F.F. Forbes, "The Gemini 8m Telescope, Technical Report No. 1, Water Tunnel Tests on Enclosure Concepts", Proc. SPIE 1532-15, July 1991.
- N. Woolf, "Dome Seeing", *Publications of the Astronomical Society of the Pacific*, No. 91, 1979.

APPENDIX I - LO-MIT PAINT TESTING

A total of four plates of dimensions 0.20 m by 0.25 m were sheared from 10 gauge (3 mm) hot rolled low carbon steel plate. The plates were cleaned of all oil and grease with lacquer thinner. The plates were then primer painted with a single thin coat of Sinclairs No. 14 "Corroprime" paint. Painting operations were performed inside a ventilated painting booth. The day the plates were painted it was cold (Air temp = 7 °C) and raining; thus an accelerator (5% by volume of "Japanese drier") was used to force the primer coat to dry faster and allow the plates to be coated with the Lo-Mit the same day. Four hours after the primer coat application, a "tack coat" of Lo-Mit was applied, straight from the one liter sample provided by the manufacturer. The final “wet coat" (again with no thinner included) was applied 30 minutes later, and the plates were allowed to dry in the booth for three days before being packed in Styrofoam. Two of the plates were then shipped to Mauna Kea and fixed to the top of the UKIRT support facility roof. These test plates remained in position for a seven month period from January to July 1993. The two remaining control plates were left in their packages and stored atop a shelf inside the Gemini offices in Tucson. A visual inspection of the weathered plates showed evidence of pitting; a half dozen pits perforated the Lo-Mit coating but did not penetrate the primer coat, and thus no corrosion was evident. It is not obvious whether this pitting was the result of wind blown particulates or rough handling.

A weathered plate and a control plate were then sent to the National Solar Thermal Test Facility at Sandia National Laboratories in Albuquerque, New Mexico. Each plate was measured at 15 different locations. The following table summarizes the results.

Sample	*Thermal Reflectance {10 micron, 20°C} (Mean, Std Dev)*	*Thermal Emittance {10 micron, 20°C} (Mean, Std Dev)*	*Solar Reflectance (Mean, Std Dev)*	*Solar Absorptance (Mean, Std Dev)*
Weathered	0.789, 0.007	0.211, 0.007	0.778, 0.022	0.224, 0.022
Control	0.767, 0.004	0.234, 0.004	0.794, 0.005	0.206, 0.005

The mean thermal emittance of the weathered plate has decreased by 10% relative to the mean emittance of the control plate.

The mean solar absorptance of the weathered plate has increased by 9% relative to the mean absorptance of the control plate.

FIGURES

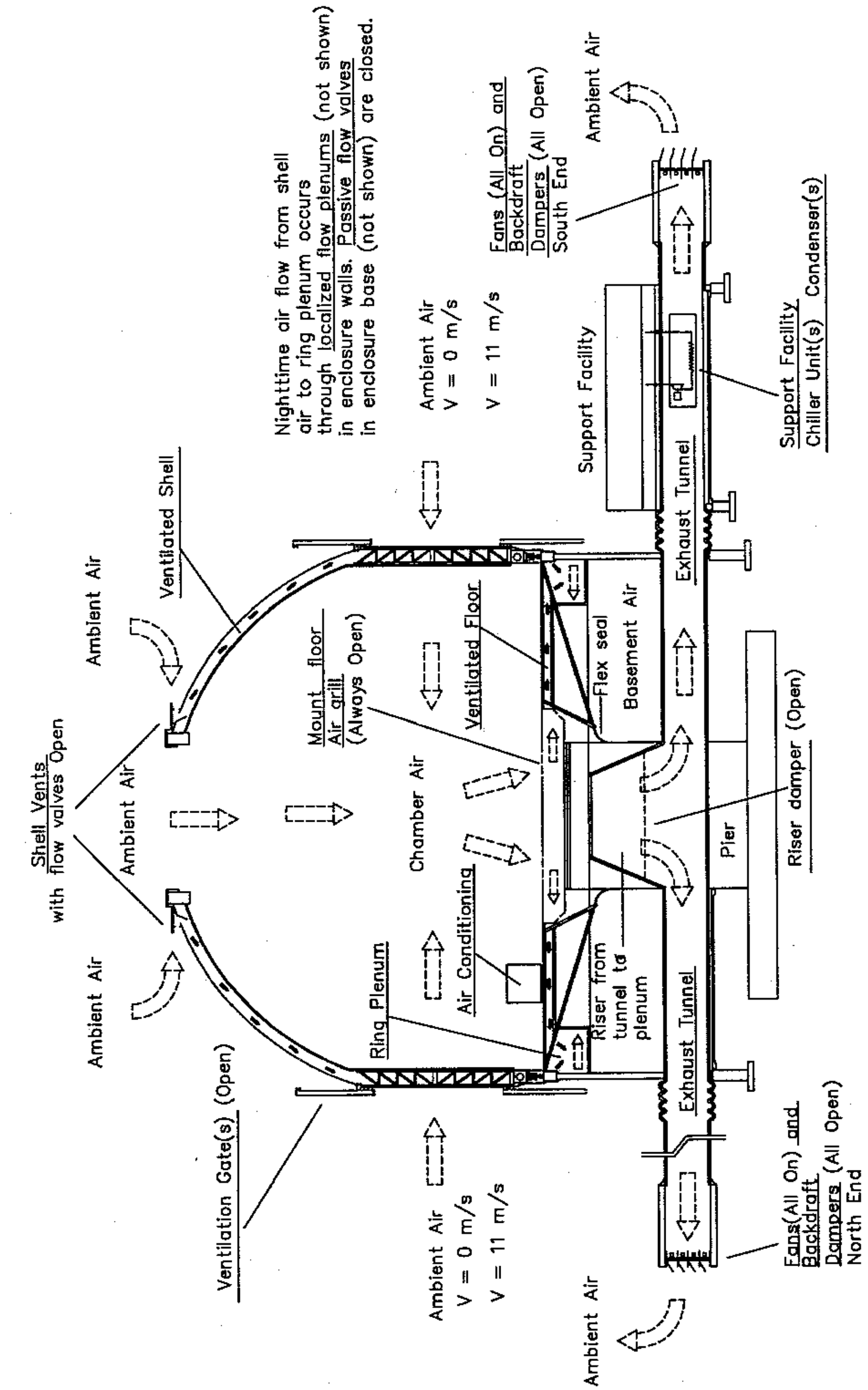

Shell Vents
with flow valves Open
Ambient Air
Ambient Air
Ambient Air
Ventilated Shell
Ventilation Gate(s) (Open)
Ring Plenum
Air Conditioning
Chamber Air
Mount floor
Air grill
(Always Open)
Ventilated Floor
Flex seal
Basement Air
Riser from
tunnel to
plenum
Riser damper (Open)
Pier
Exhaust Tunnel
Exhaust Tunnel
Support Facility
Support Facility
Chiller Unit(s) Condenser(s)
Nighttime air flow from shell
air to ring plenum occurs
through localized flow plenums (not shown)
in enclosure walls. Passive flow valves
in enclosure base (not shown) are closed.
Ambient Air
V = 0 m/s
V = 11 m/s
Ambient Air
V = 0 m/s
V = 11 m/s
Fans (All On) and
Backdraft
Dampers (All Open)
South End
Fans(All On) and
Backdraft
Dampers (All Open)
North End
Ambient Air
Ambient Air

Figure 1.

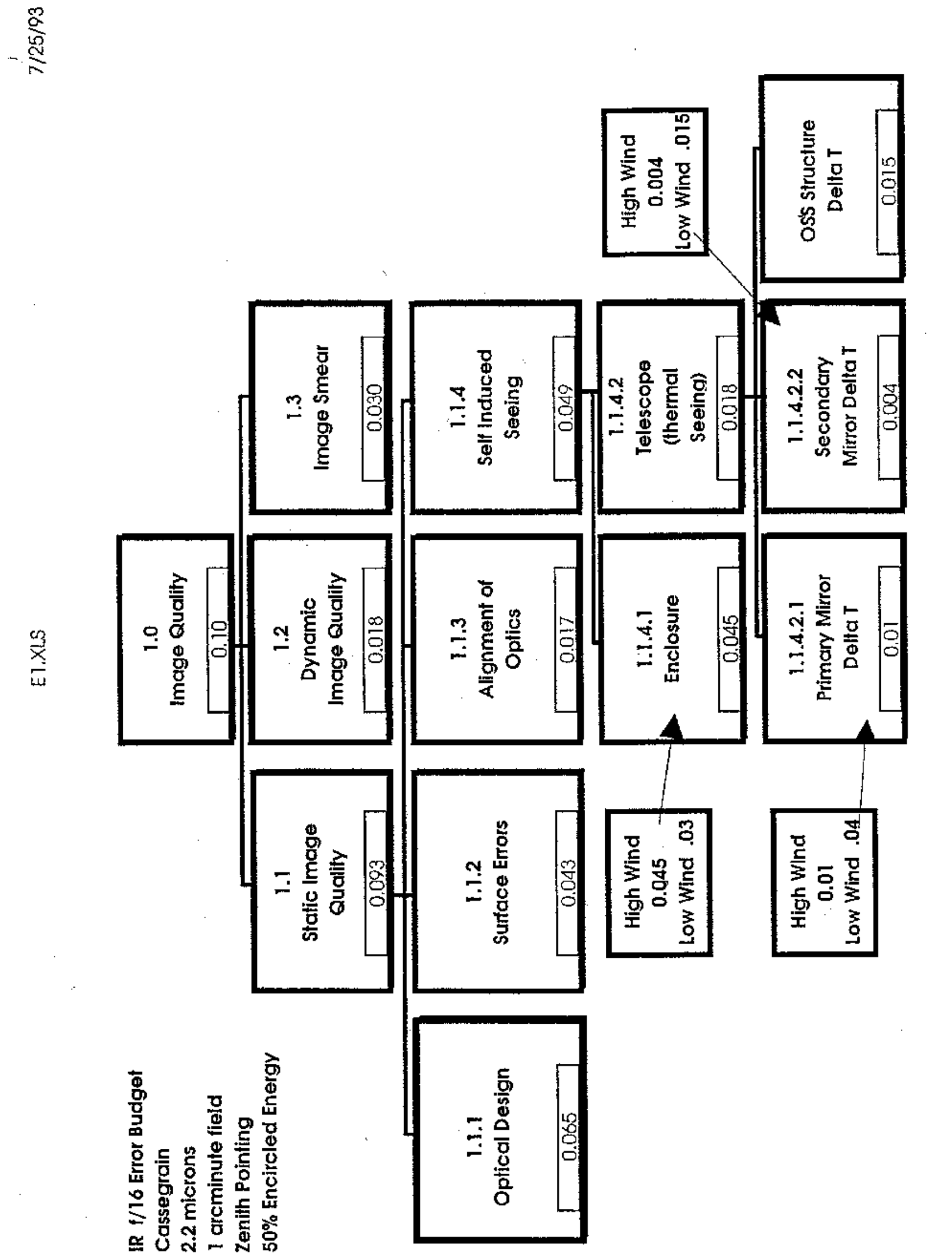
7/25/93
E1.XLS
IR f/16 Error Budget
Cassegrain
2.2 microns
1 arcminute field
Zenith Pointing
50% Encircled Energy
1.0 Image Quality 0.10
1.1 Static Image Quality 0.093
1.2 Dynamic Image Quality 0.018
1.3 Image Smear 0.030
1.1.1 Optical Design 0.065
1.1.2 Surface Errors 0.043
1.1.3 Alignment of Optics 0.017
1.1.4 Self Induced Seeing 0.049
1.1.4.1 Enclosure 0.045
1.1.4.2 Telescope (thermal Seeing) 0.018
1.1.4.2.1 Primary Mirror Delta T 0.01
1.1.4.2.2 Secondary Mirror Delta T 0.004
OSS Structure Delta T 0.015
High Wind 0.045 Low Wind .03
High Wind 0.01 Low Wind .04
High Wind 0.004 Low Wind .015

Figure 2

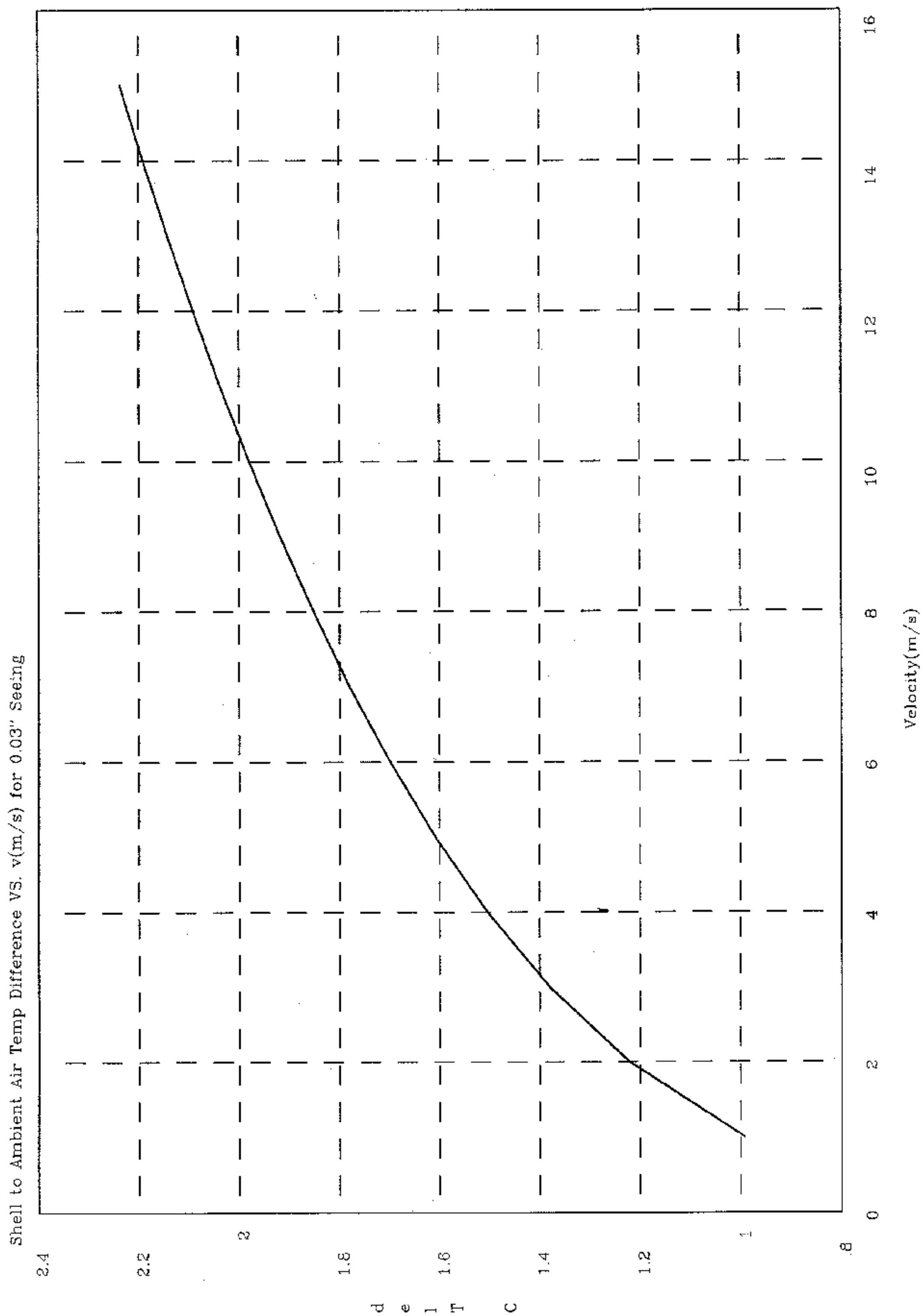
Shell to Ambient Air Temp Difference VS. v(m/s) for 0.03" Seeing
Velocity(m/s)
delT C
0
2
4
6
8
10
12
14
16
.8
1
1.2
1.4
1.6
1.8
2
2.2
2.4

Figure 3.

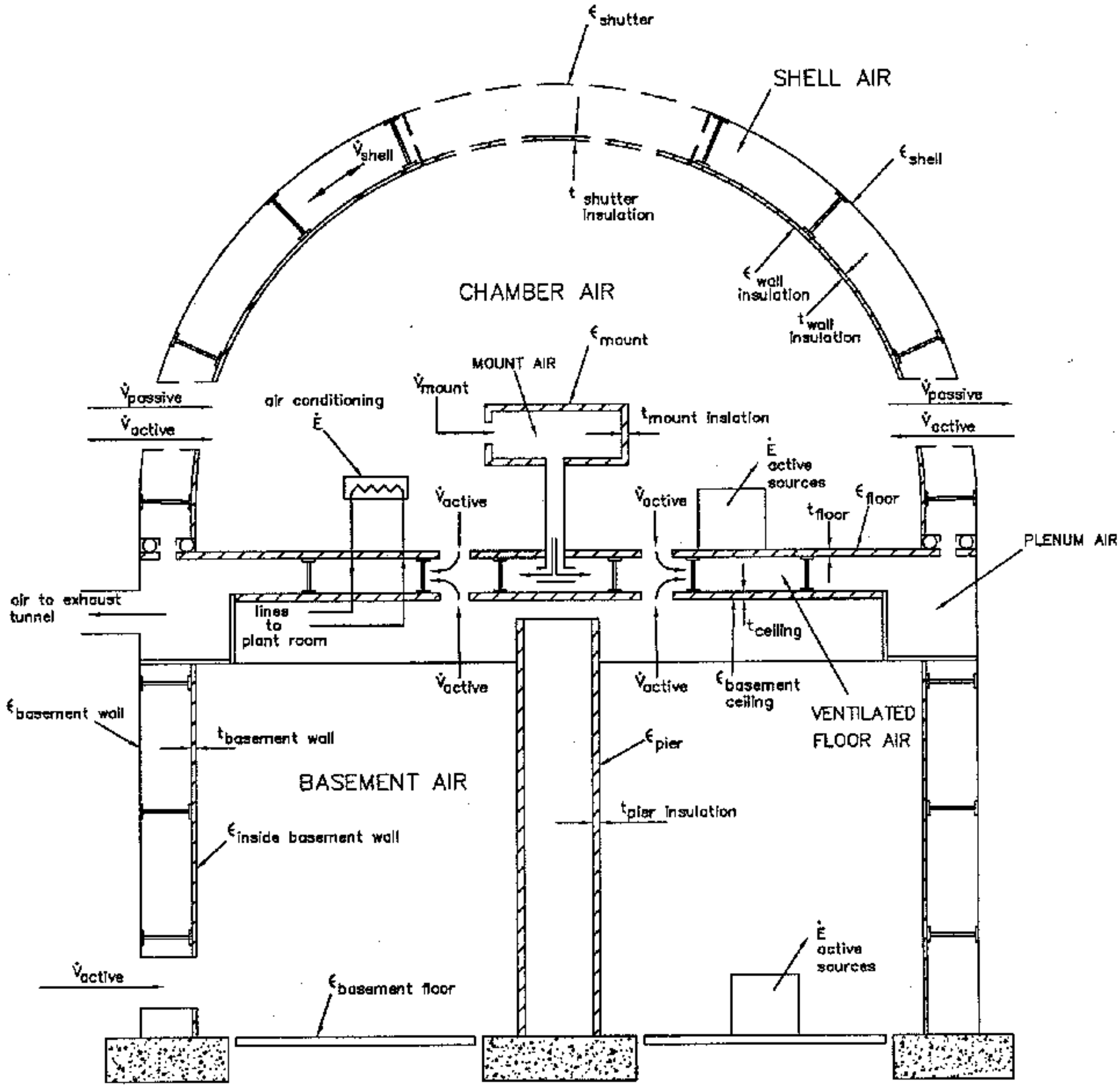

Not to scale for illustration only

Figure 4.

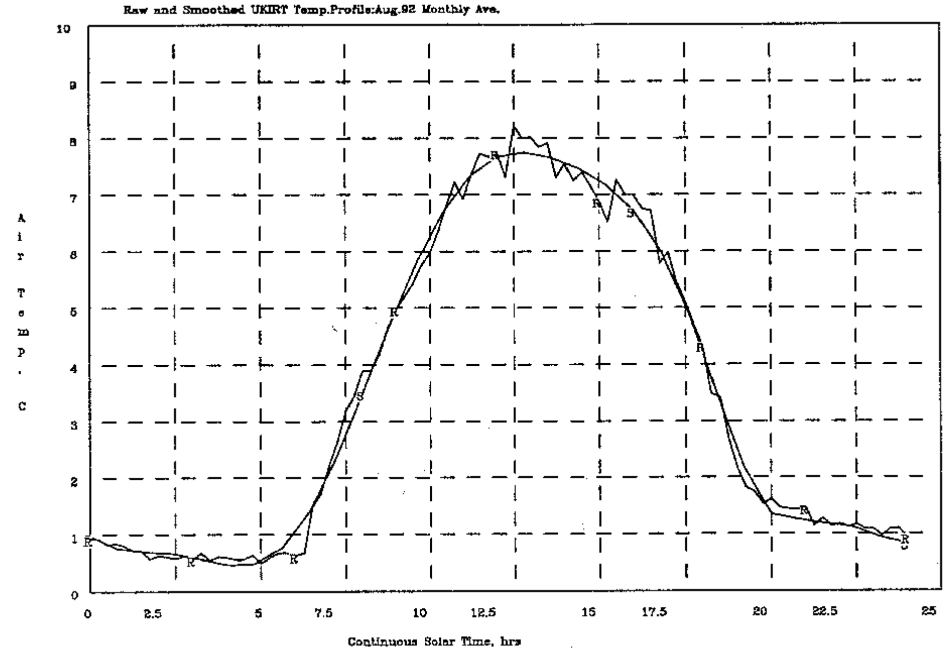

Figure 5a Raw and Smoothed UKIRT Aug. 1992 Monthly Average 24 Hr. Ambient Air Temperature Profiles

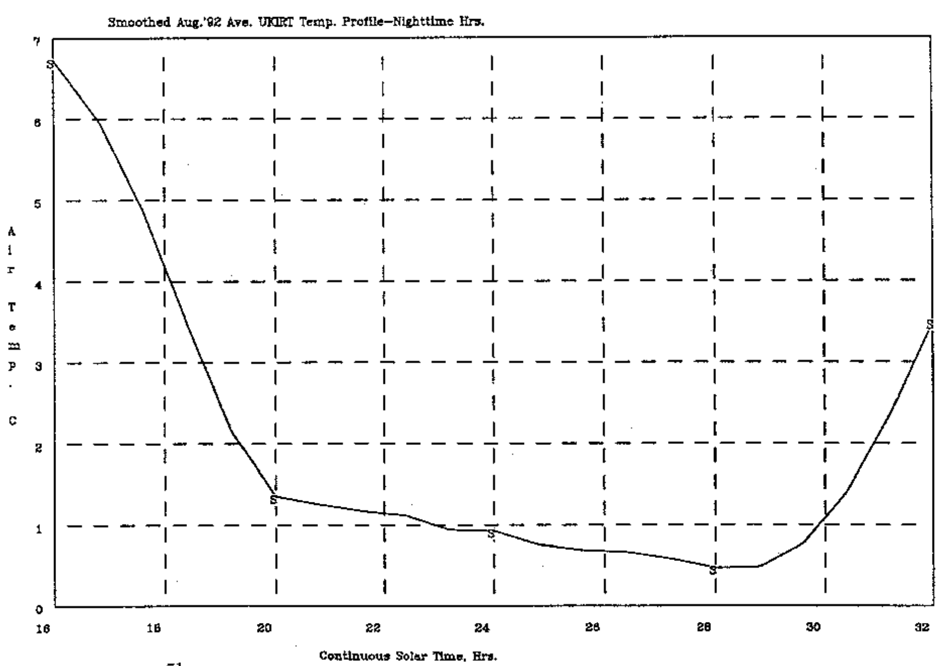

Figure 5b Smoothed UKIRT Aug. 1992 Monthly Average Nighttime Ambient Air Temperature Profile

Figures 5a and 5b.

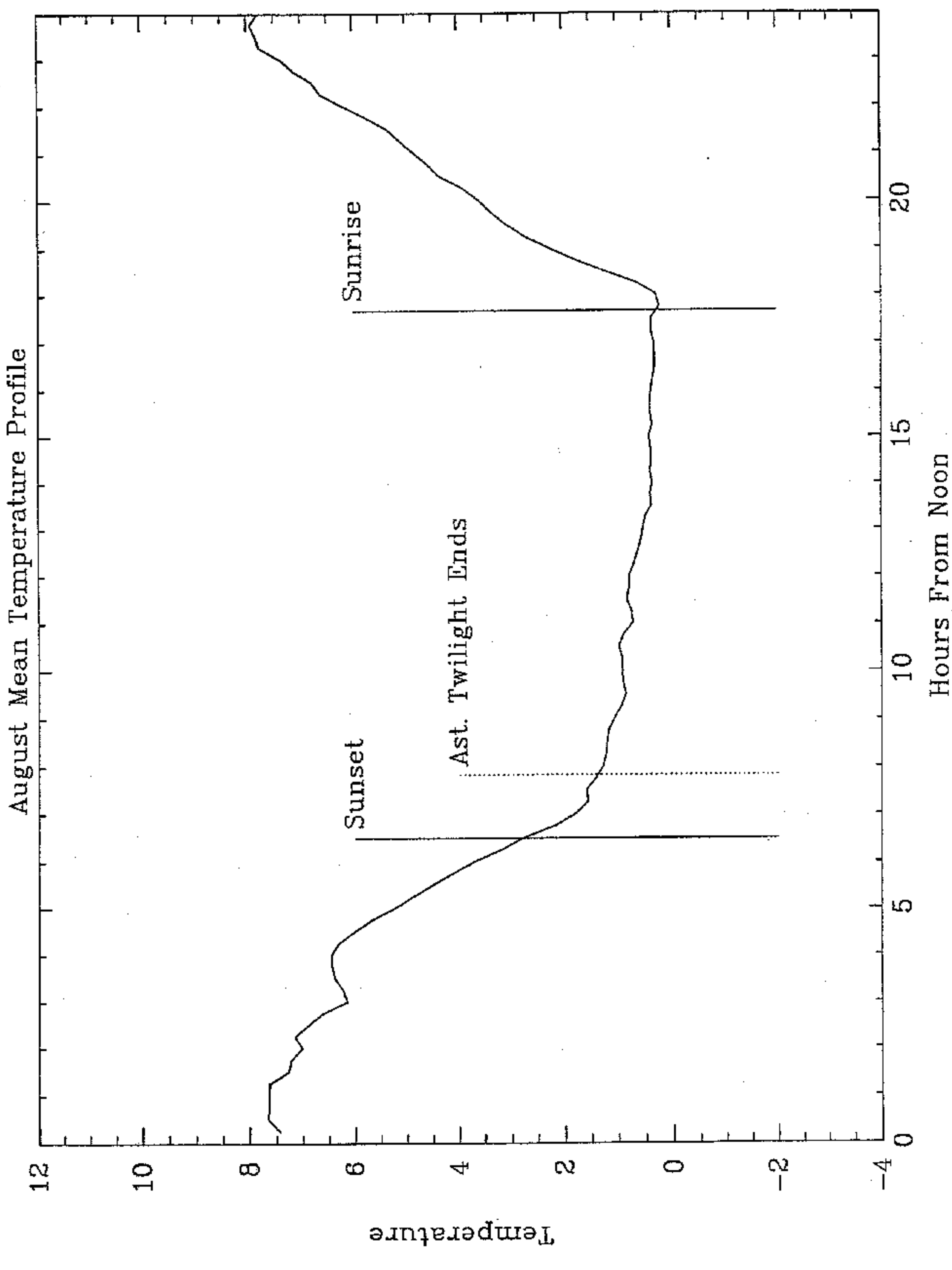
August Mean Temperature Profile
Sunrise
Ast. Twilight Ends
Sunset
Temperature
Hours From Noon
12
10
8
6
4
2
0
−2
−4
0
5
10
15
20

Figure 6.

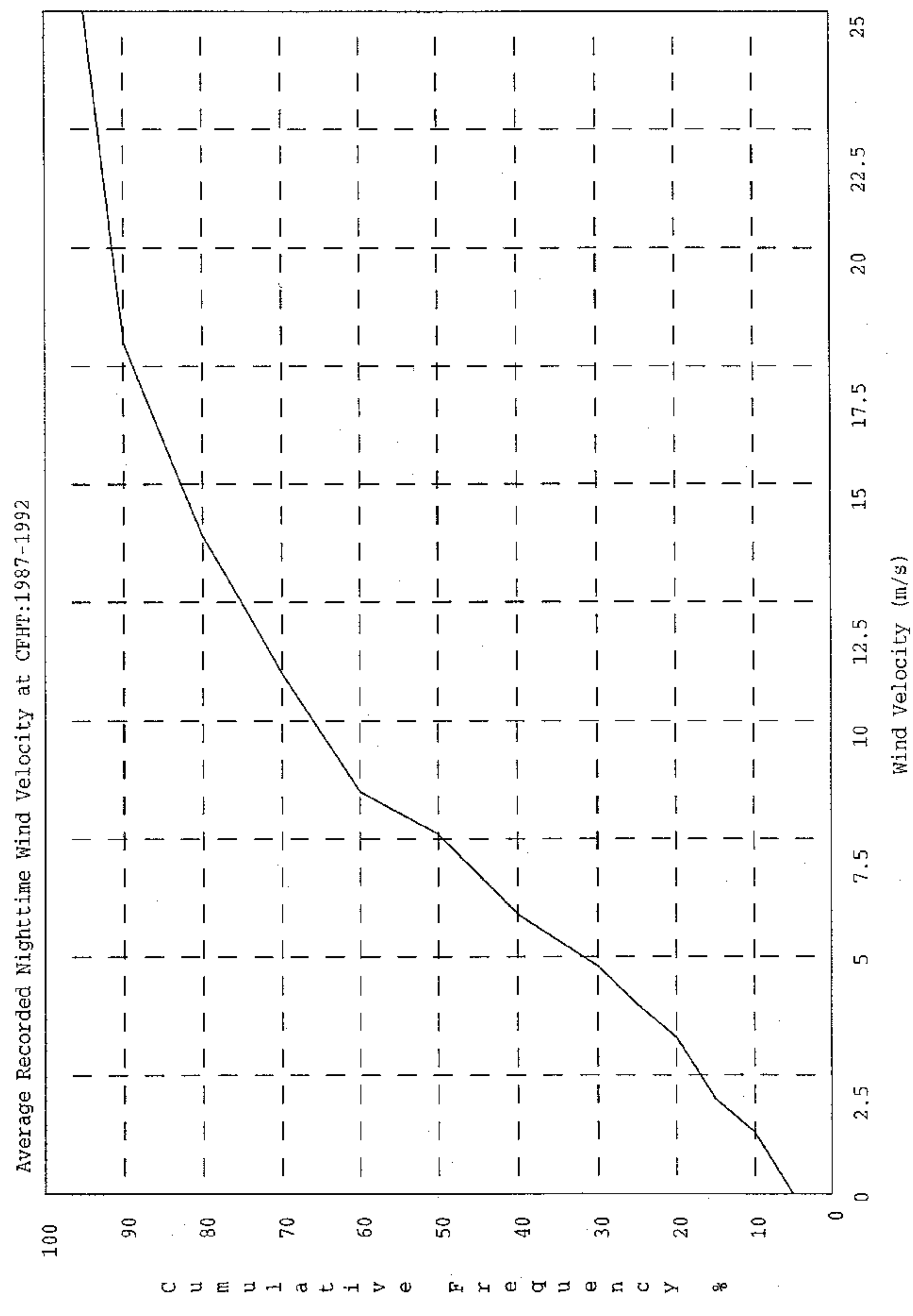
Average Recorded Nighttime Wind Velocity at CFHT:1987-1992
0
2.5
5
7.5
10
12.5
15
17.5
20
22.5
25
Wind Velocity (m/s)
0
10
20
30
40
50
60
70
80
90
100
Cumulative Frequency %

Figure 7

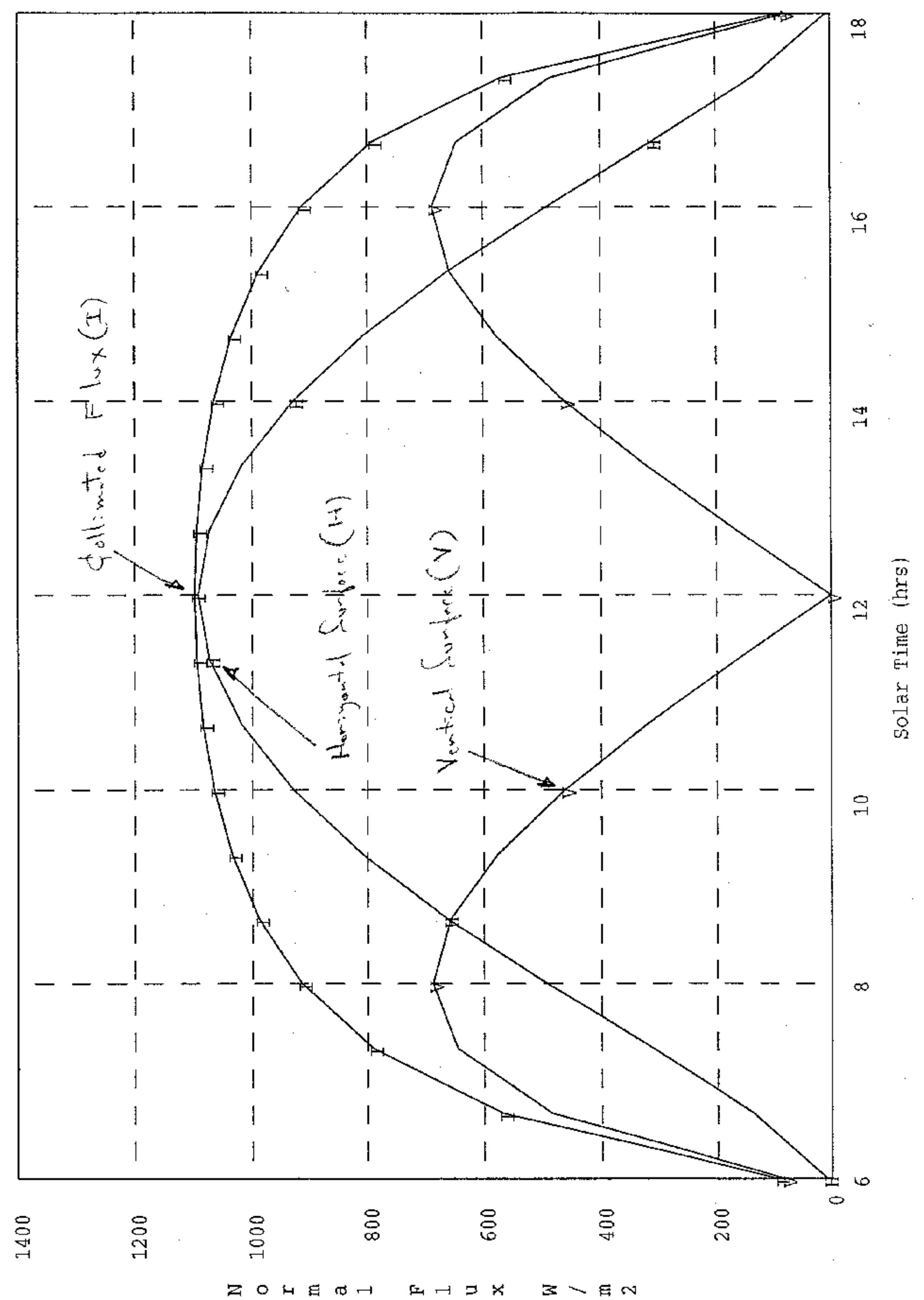
Collimated Flux (I)
Horizontal Surface (H)
Vertical Surface (V)
Normal Flux W/m2
1400
1200
1000
800
600
400
200
0
6
8
10
12
14
16
18
Solar Time (hrs)

Figure 8.

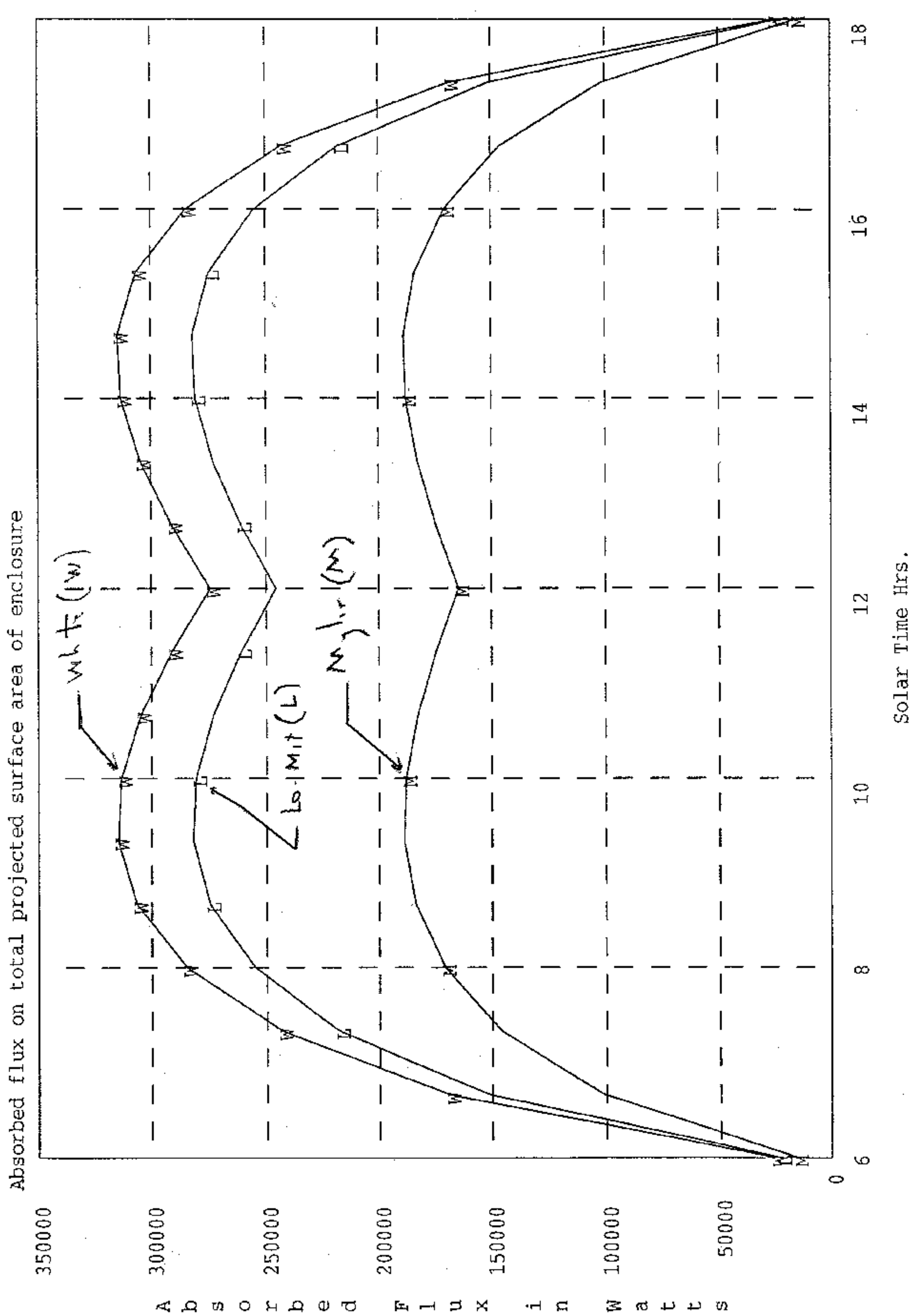
Absorbed flux on total projected surface area of enclosure
Absorbed Flux in Watts
350000
300000
250000
200000
150000
100000
50000
0
6
8
10
12
14
16
18
Solar Time Hrs.

Figure 9.

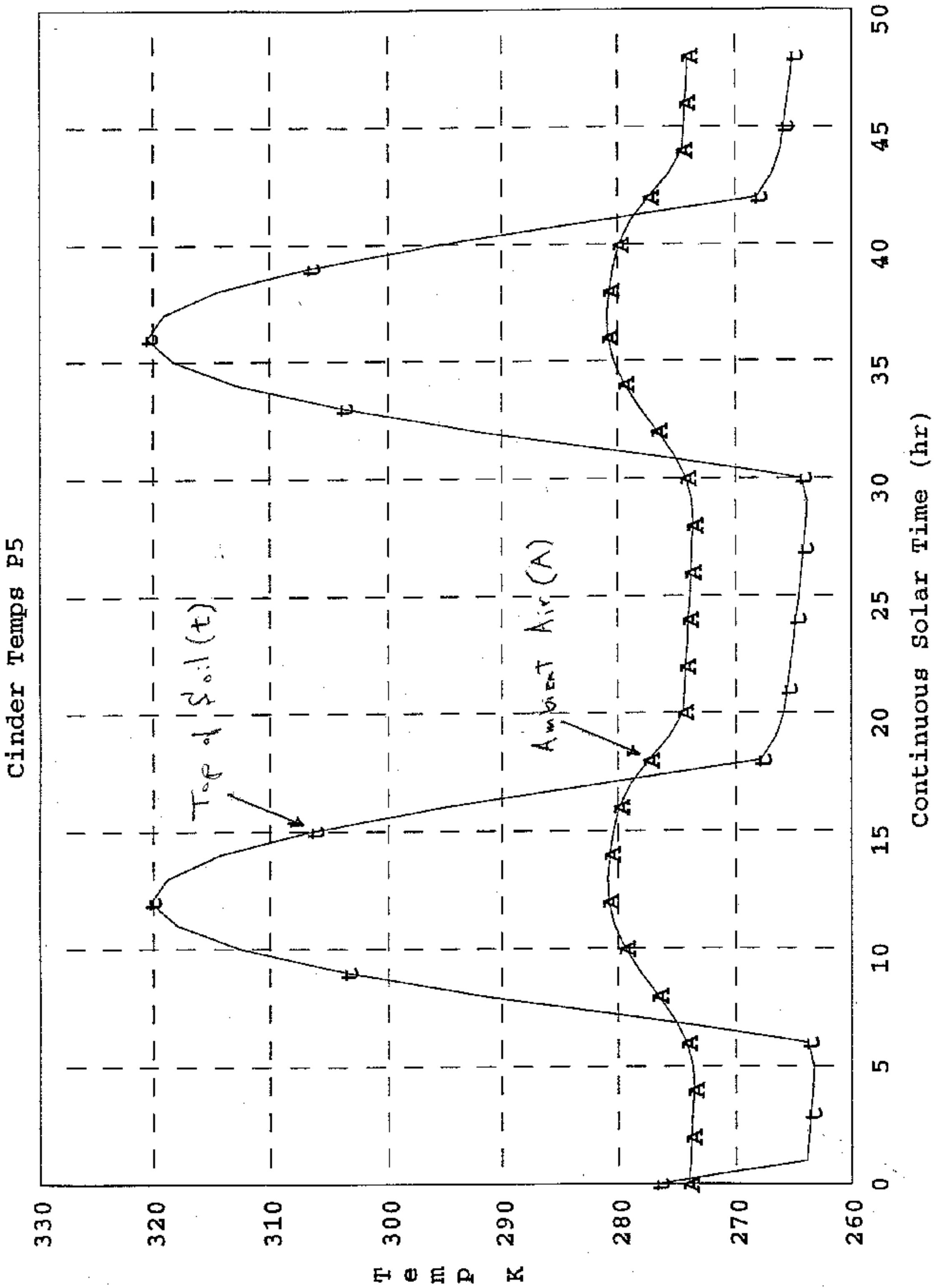
Cinder Temps P5
Top of Soil (t)
Ambient Air (A)
Temp K
330
320
310
300
290
280
270
260
0
5
10
15
20
25
30
35
40
45
50
Continuous Solar Time (hr)

Figure 10.

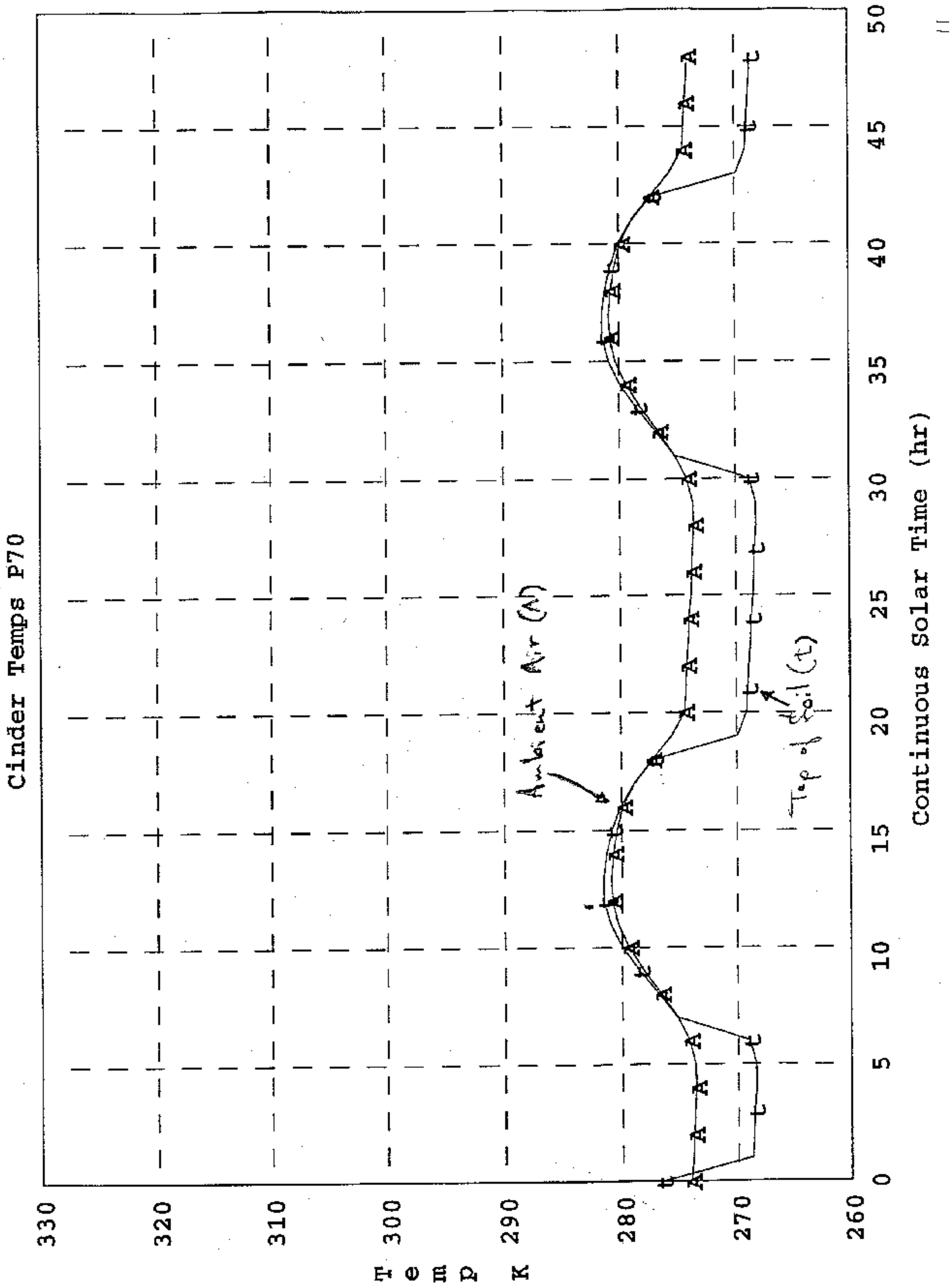
Cinder Temps P70
Temp K
330
320
310
300
290
280
270
260
0
5
10
15
20
25
30
35
40
45
50
Continuous Solar Time (hr)
Ambient Air (A)
Top of soil (t)

Figure 11.

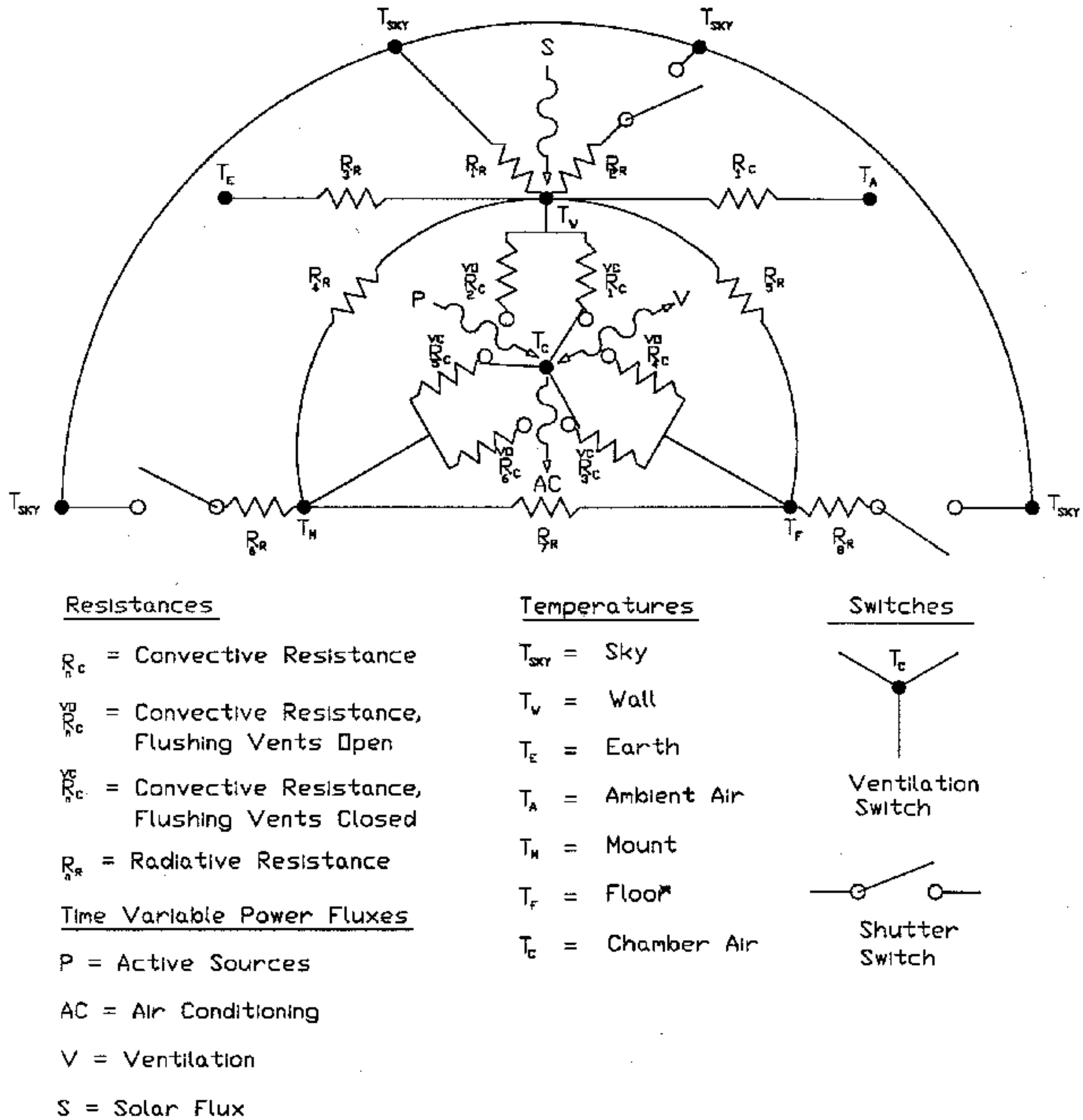

T_SKY
T_SKY
S
T_E
R_3R
R_1R
R_2R
R_1C
T_A
T_V
R_4R
R_5R
P
V
T_C
AC
T_SKY
T_SKY
T_M
T_F
R_6R
R_7R
R_8R
Resistances
R_nC = Convective Resistance
VO R_nC = Convective Resistance, Flushing Vents Open
VC R_nC = Convective Resistance, Flushing Vents Closed
R_nR = Radiative Resistance
Time Variable Power Fluxes
P = Active Sources
AC = Air Conditioning
V = Ventilation
S = Solar Flux
Temperatures
T_SKY = Sky
T_V = Wall
T_E = Earth
T_A = Ambient Air
T_M = Mount
T_F = Floor
T_C = Chamber Air
Switches
T_C
Ventilation Switch
Shutter Switch

Figure 12.

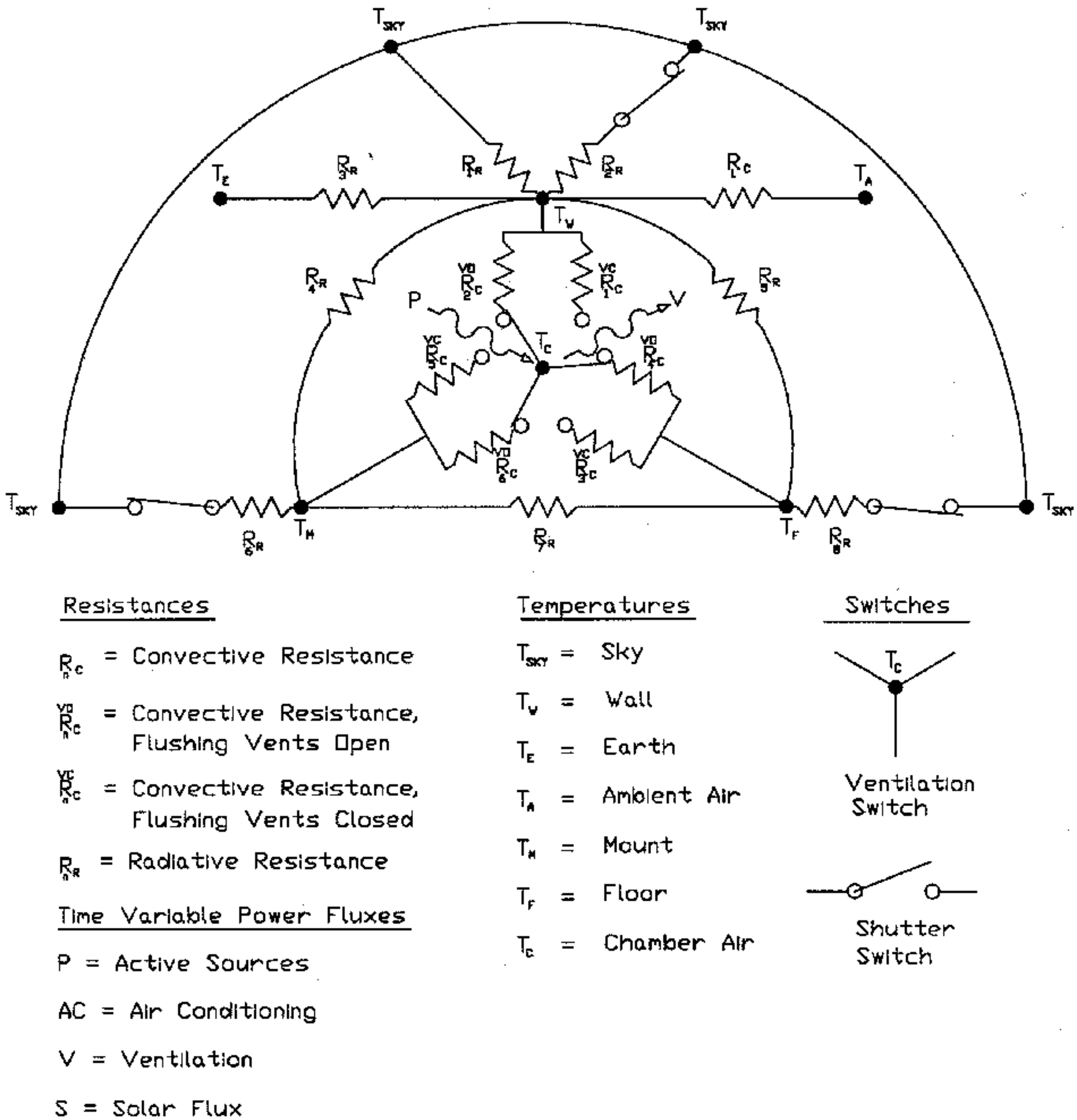
T_SKY
T_E
T_A
T_V
T_C
P
V
T_M
T_F
Resistances
R_C = Convective Resistance
VO R_C = Convective Resistance, Flushing Vents Open
VC R_C = Convective Resistance, Flushing Vents Closed
R_R = Radiative Resistance
Time Variable Power Fluxes
P = Active Sources
AC = Air Conditioning
V = Ventilation
S = Solar Flux
Temperatures
T_SKY = Sky
T_W = Wall
T_E = Earth
T_A = Ambient Air
T_M = Mount
T_F = Floor
T_C = Chamber Air
Switches
Ventilation Switch
Shutter Switch

Figure 13.

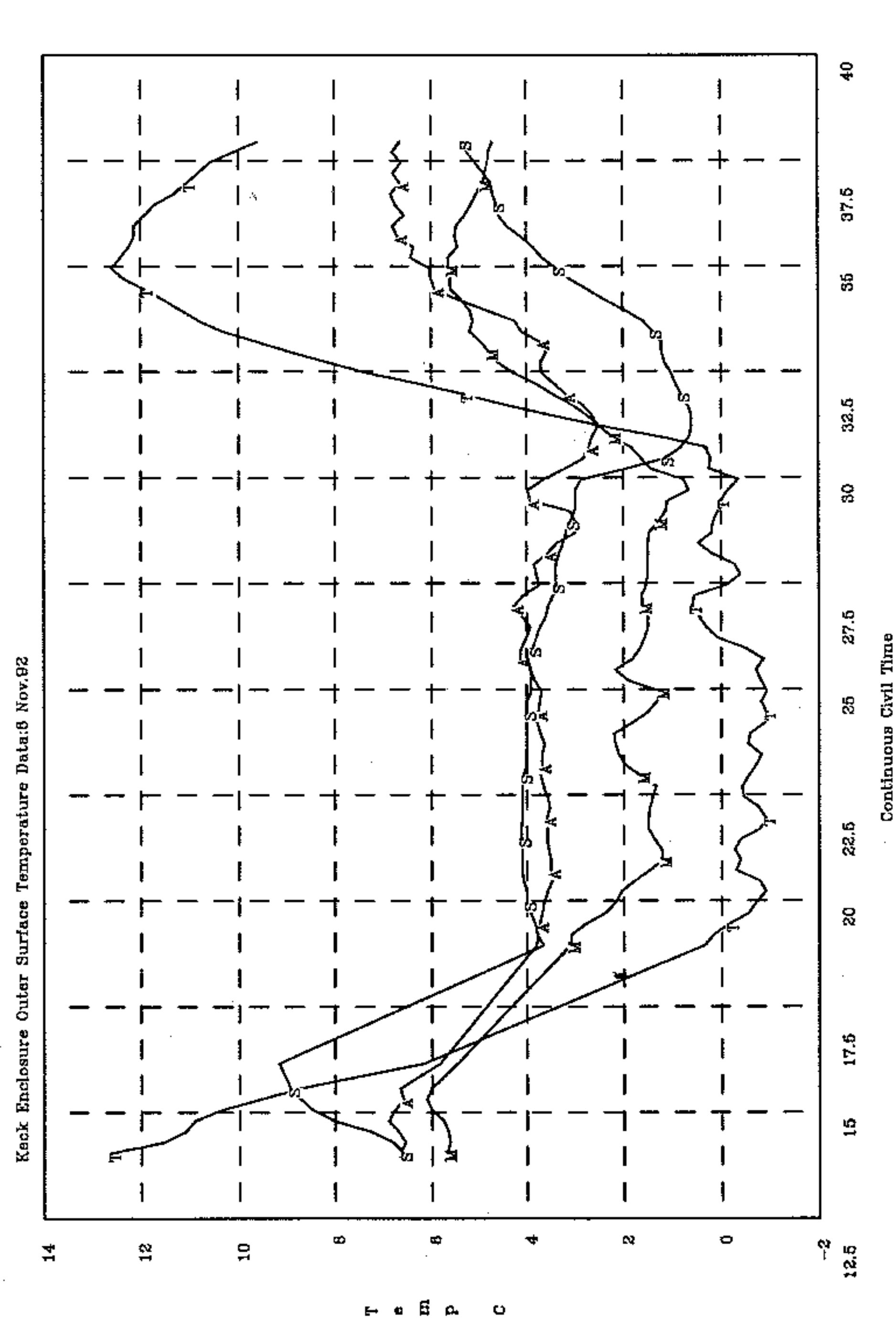

Figure 14   Keck Enclosure Outer Surface Temperature Data

Figure 14.

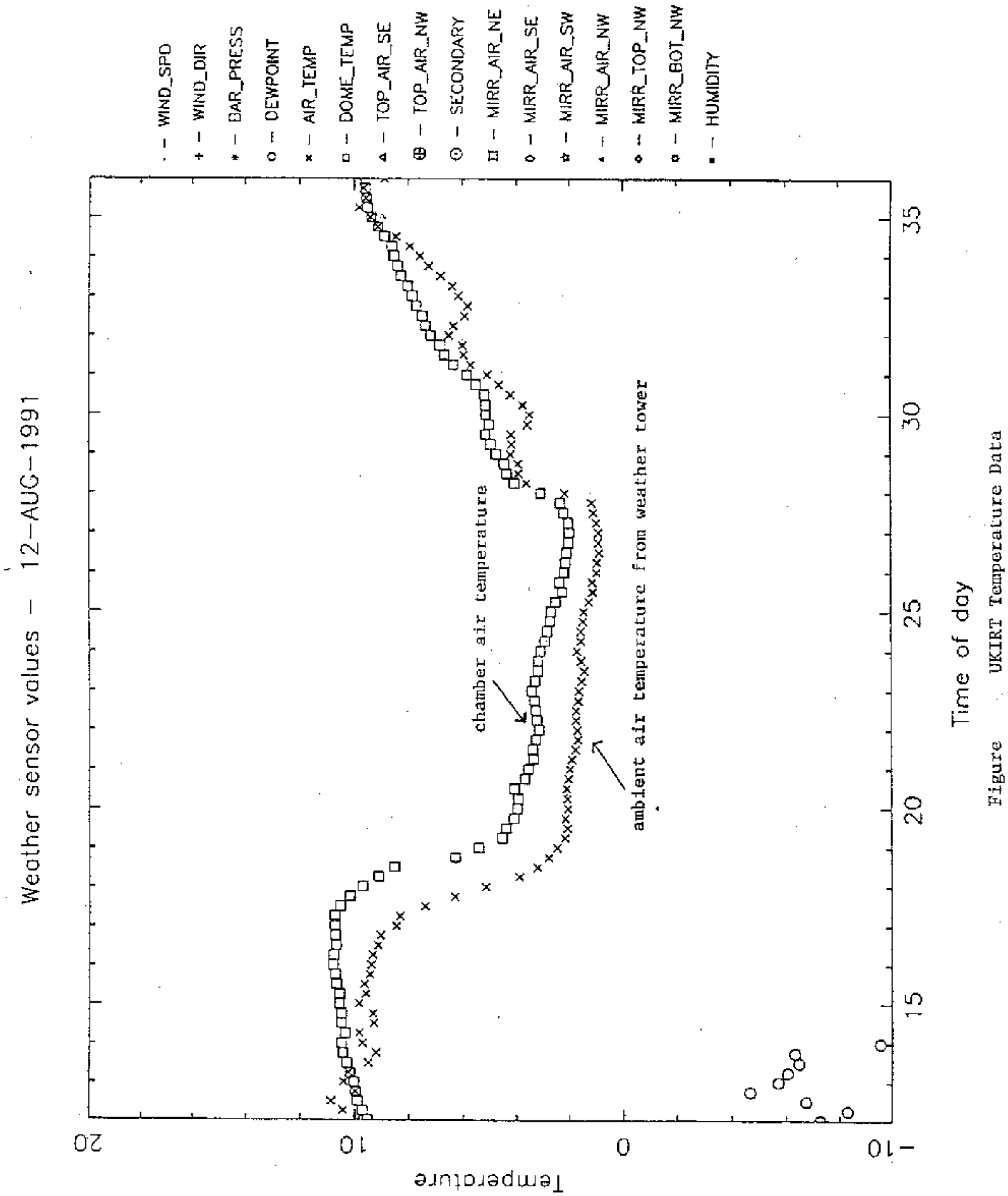
Weather sensor values - 12-AUG-1991
WIND_SPD
WIND_DIR
BAR_PRESS
DEWPOINT
AIR_TEMP
DOME_TEMP
TOP_AIR_SE
TOP_AIR_NW
SECONDARY
MIRR_AIR_NE
MIRR_AIR_SE
MIRR_AIR_SW
MIRR_AIR_NW
MIRR_TOP_NW
MIRR_BOT_NW
HUMIDITY
chamber air temperature
ambient air temperature from weather tower
Temperature
Time of day
Figure UKIRT Temperature Data

Figure 15.

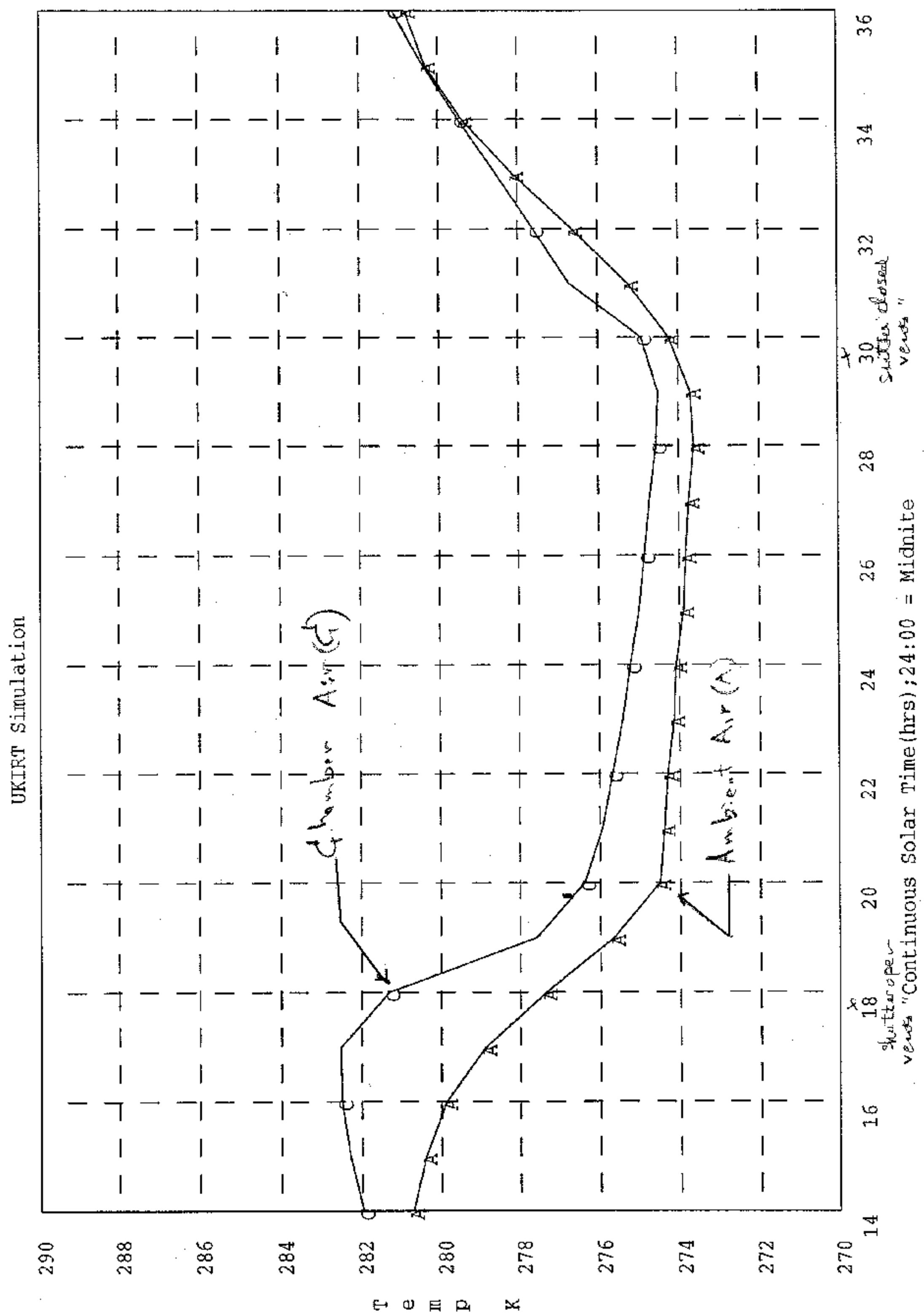
UKIRT Simulation
Continuous Solar Time(hrs);24:00 = Midnite
Temp K
Chamber Air (C)
Ambient Air (A)
shutter open vents
shutter closed vents

Figure 16.

GEMINI MODEL RUN NO. P5wnf

DESCRIPTION: White (TiO2) Coated shell @ 5th Percentile Wind

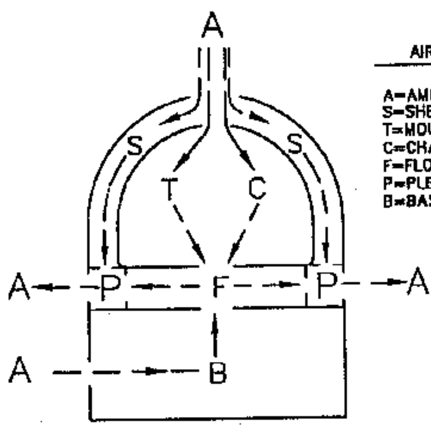

AIR VOLUMES

A=AMBIENT AIR
S=SHELL AIR
T=MOUNT AIR
C=CHAMBER AIR
F=FLOOR AIR
P=PLENUM AIR
B=BASEMENT AIR

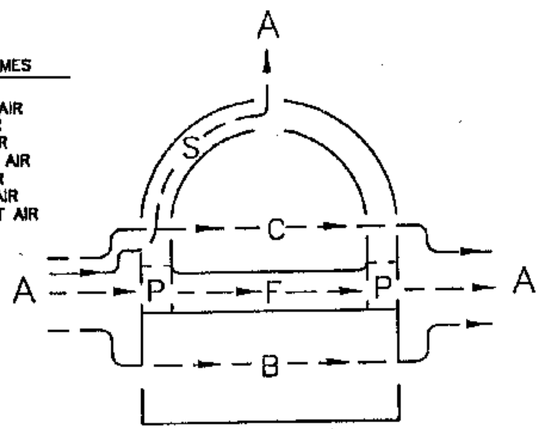

INSULATION TYPE AND THICKNESS

LOCATION	INSULATION TYPE	THICKNESS (m)
CHAMBER WALL	urethane	.080
BASEMENT WALL	urethane	.080
FLOOR BOTTOM	glass wool	.080

ACTIVE SOURCE POWER LOADS

Load location	Power (W)	Constant P=k	Time variable P=f(t)
SHELL AIR:	0		
MOUNT AIR:	0		
CHAMBER AIR:	8500	✓	
FLOOR AIR:	0		
PLENUM AIR:	0		
BASEMENT AIR:	0		

COATINGS

Location	Enamel	Lo-mit	Aluminum tape
Basement walls(out)	TiO2		
Shell (out)	TiO2		
Chamber wall (in)	✓		
Mount (out)	✓		
Floor top (out)	✓		

FAN FORCED FLOWS

Flow path	Flow rate (chamber vol/hr)	Start time (H.S.T.)	Finish time (H.S.T.)
ASP:	0		
ATF:	0.12	18:00	06:00
ACF:	10.	18:00	06:00
ABF:	0		
FP:	10.12	18:00	06:00
PA:	10.12	18:00	06:00

PASSIVE FLUSHING, INFILTRATION, AND BOUYANT FLOWS

Flow Path	Infiltration flow rate with vents closed (chamber vol/hr)	Flushing flow rate with vents open (chamber vol/hr)
ACA:	0	0
Flow Path	Flow rate (chamber vol/hr)	Flow type (Infiltration,bouyant)
ABA:	0	
ASA:	0.30	b
AFA:	0	

(H.S.T.=Hours Solar Time)

SHUTTER SIZE AND TIMING

Shutter size (m^2)	Shutter open (H.S.T.)	Shutter close (H.S.T.)
133	18:00	06:00

ENVIRONMENTAL BOUNDARY CONDITIONS

LOCATION: M. Kea

Ambient Air temp. profile (month)	Solar flux profile (month)	Wind speed (m/s)	Effective sky temp. (C)
AUG	AUG	0	-30

FLUSHING VENT SIZE AND TIMING

Vent projected size (m^2)	Vent open (H.S.T.)	Vent close (H.S.T.)
0		

CHAMBER AIR CONDITIONING

Sink Temp (°K)	Conductance to Sink (W)	Cond. On (H.S.T.)	Cond. Off (H.S.T.)
NONE			

Figure 17.

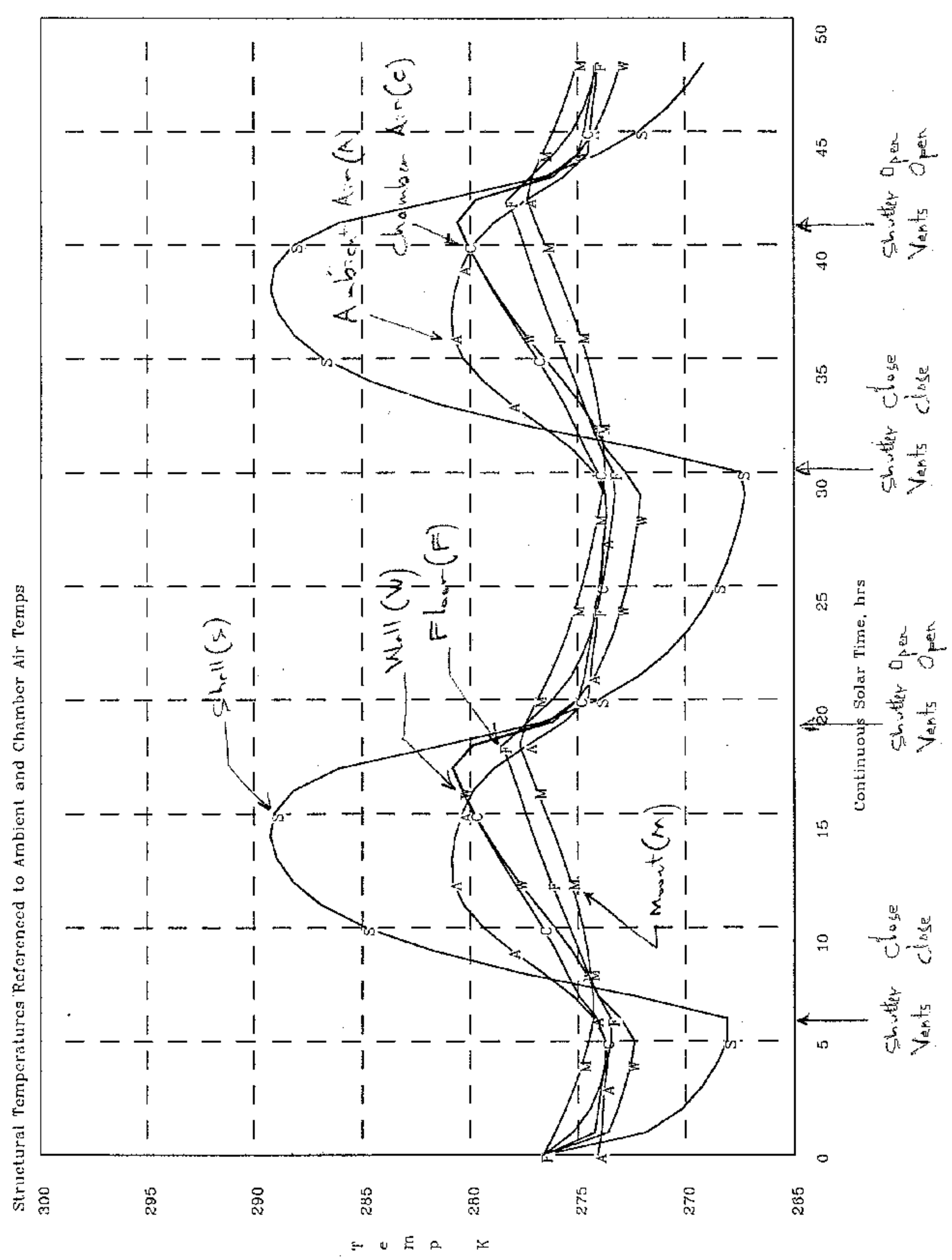
Structural Temperatures Referenced to Ambient and Chamber Air Temps
T e m p K
300
295
290
285
280
275
270
265
0
5
10
15
20
25
30
35
40
45
50
Continuous Solar Time, hrs
Shell (S)
Wall (W)
Floor (F)
Mount (M)
Ambient Air (A)
Chamber Air (C)
Shutter close
Vents close
Shutter Open
Vents Open

Figure 18.

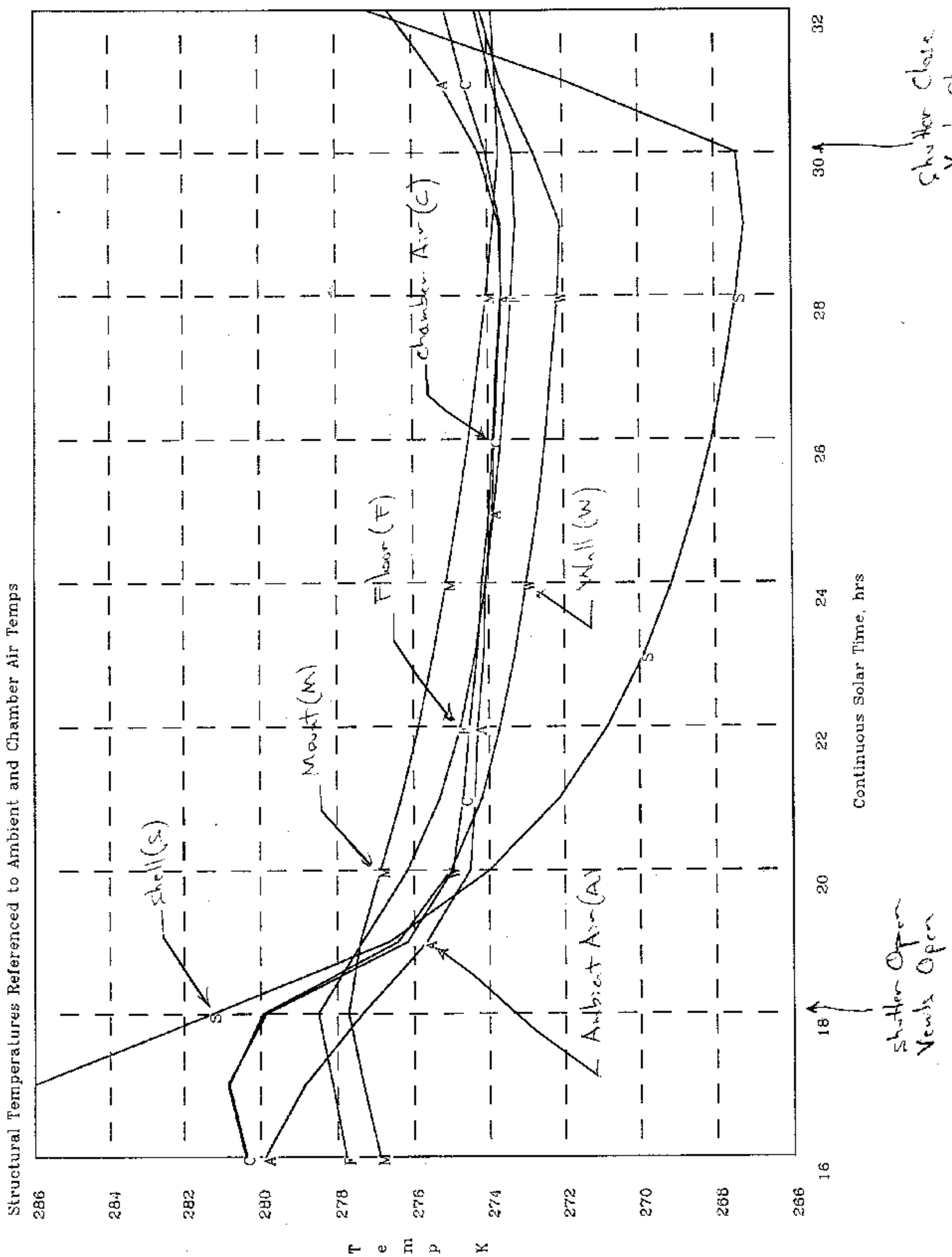
Structural Temperatures Referenced to Ambient and Chamber Air Temps
Continuous Solar Time, hrs
16
18
20
22
24
26
28
30
32
286
284
282
280
278
276
274
272
270
268
266
Temp K
Shell (S)
Mount (M)
Floor (F)
Chamber Air (C)
Wall (W)
Ambient Air (A)
Shutter Open
Vents Open
Shutter Close
Vents Close

Figure 19.

GEMINI MODEL RUN NO. P70W

DESCRIPTION: White (T-O2) Coated Shell @ 70th Percentile Wind

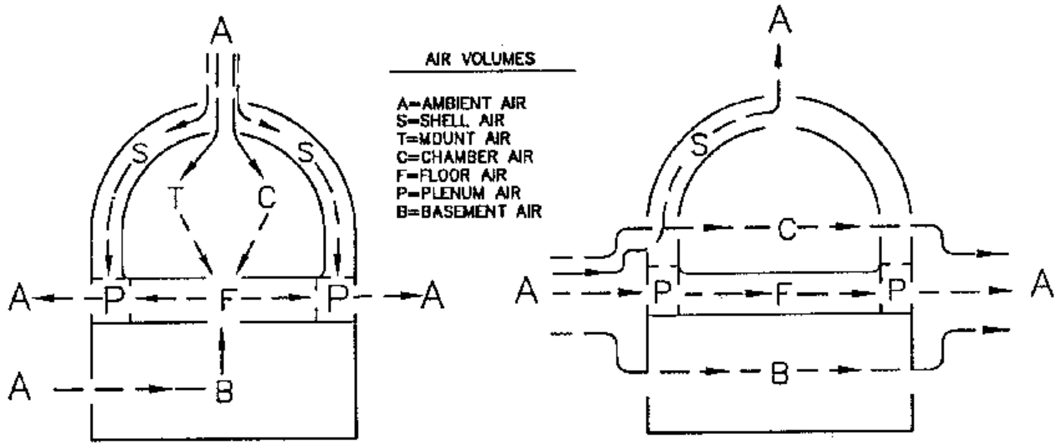

INSULATION TYPE AND THICKNESS		
LOCATION	INSULATION TYPE	THICKNESS (m)
CHAMBER WALL	urethane	.080
BASEMENT WALL	urethane	.080
FLOOR BOTTOM	Glass Wool	.080

ACTIVE SOURCE POWER LOADS			
Load location	Power (W)	Constant P=k	Time variable P=f(t)
SHELL AIR:	0		
MOUNT AIR:	0		
CHAMBER AIR:	8500	✓	
FLOOR AIR:	0		
PLENUM AIR:	0		
BASEMENT AIR:	0		

COATINGS			
Location	Enamel	Lo-mit	Aluminum tape
Basement walls(out)	T-O2		
Shell (out)	T-O2		
Chamber wall (in)	✓		
Mount (out)	✓		
Floor top (out)	✓		

FAN FORCED FLOWS			
Flow path	Flow rate (chamber vol/hr)	Start time (H.S.T.)	Finish time (H.S.T.)
ASP:	0		
ATF:	0.12	18:00	06:00
ACF:	10	18:00	06:00
ABF:	0		
FP:	10.12	18:00	06:00
PA:	10.12	18:00	06:00

PASSIVE FLUSHING, INFILTRATION, AND BOUYANT FLOWS		
Flow Path	Infiltration flow rate with vents closed (chamber vol/hr)	Flushing flow rate with vents open (chamber vol/hr)
ACA:	1	60
Flow Path	Flow rate (chamber vol/hr)	Flow type (infiltration,bouyant)
ABA:	0.6	i
ASA:	0.3	b
AFA:	0.1	i

(H.S.T.=Hours Solar Time)

SHUTTER SIZE AND TIMING		
Shutter size (m^2)	Shutter open (H.S.T.)	Shutter close (H.S.T.)
133	18:00	06:00

ENVIRONMENTAL BOUNDARY CONDITIONS			
LOCATION:			
Ambient Air temp. profile (month)	Solar flux profile (month)	Wind speed (m/s)	Effective sky temp. (C)
AUG	AUG	11	-30

FLUSHING VENT SIZE AND TIMING		
Vent projected size (m^2)	Vent open (H.S.T.)	Vent close (H.S.T.)
200	18:00	06:00

CHAMBER AIR CONDITIONING			
Sink Temp (°K)	Conductance to Sink (W)	Cond. On (H.S.T.)	Cond. Off (H.S.T.)
NONE			

Figure 20.

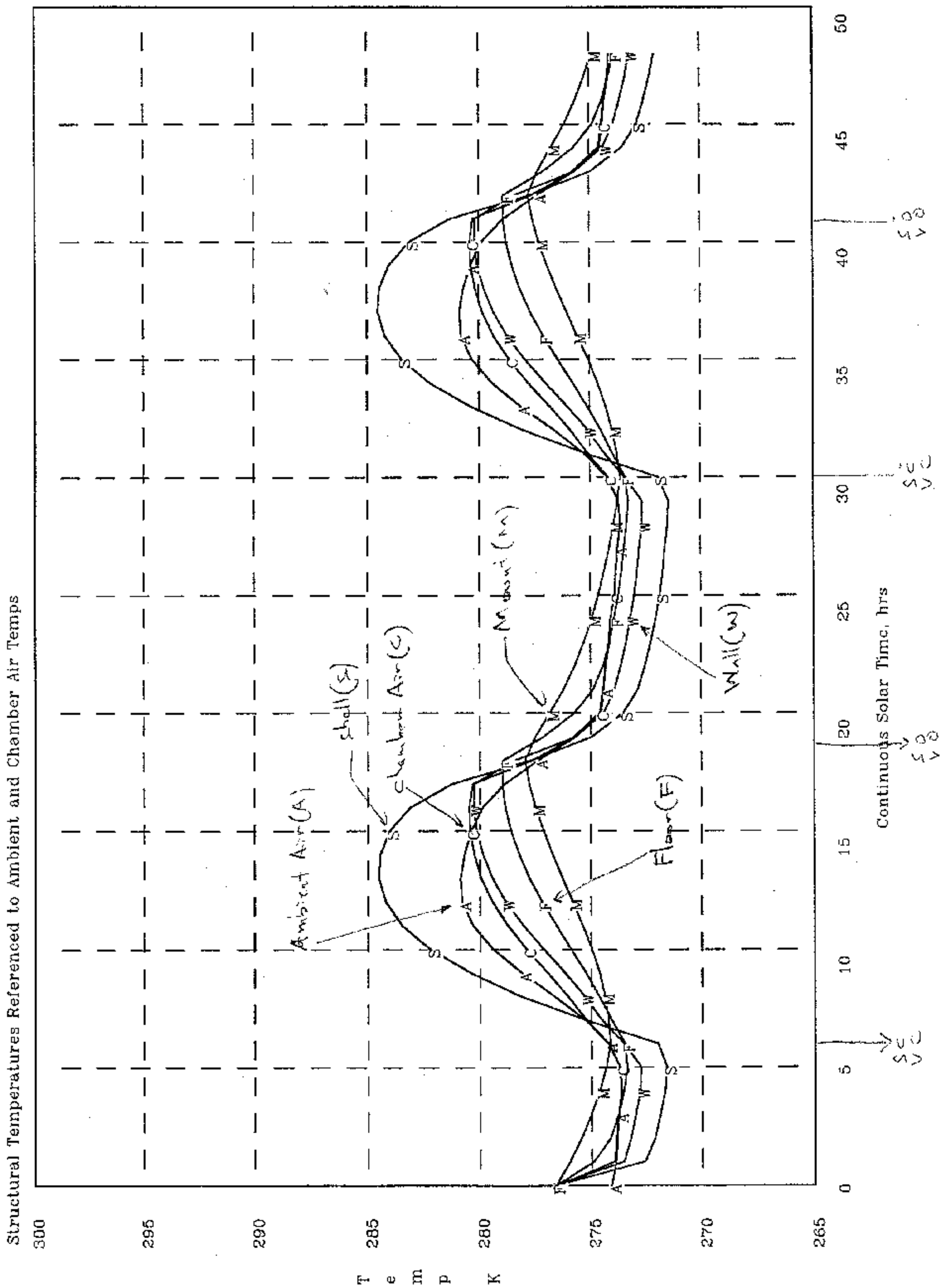
Structural Temperatures Referenced to Ambient and Chamber Air Temps
Continuous Solar Time, hrs
T e m p K
300
295
290
285
280
275
270
265
0
5
10
15
20
25
30
35
40
45
50
Ambient Air(A)
Shell(S)
Chamber Air(C)
Mount (M)
Wall(W)
Floor(F)

Figure 21.

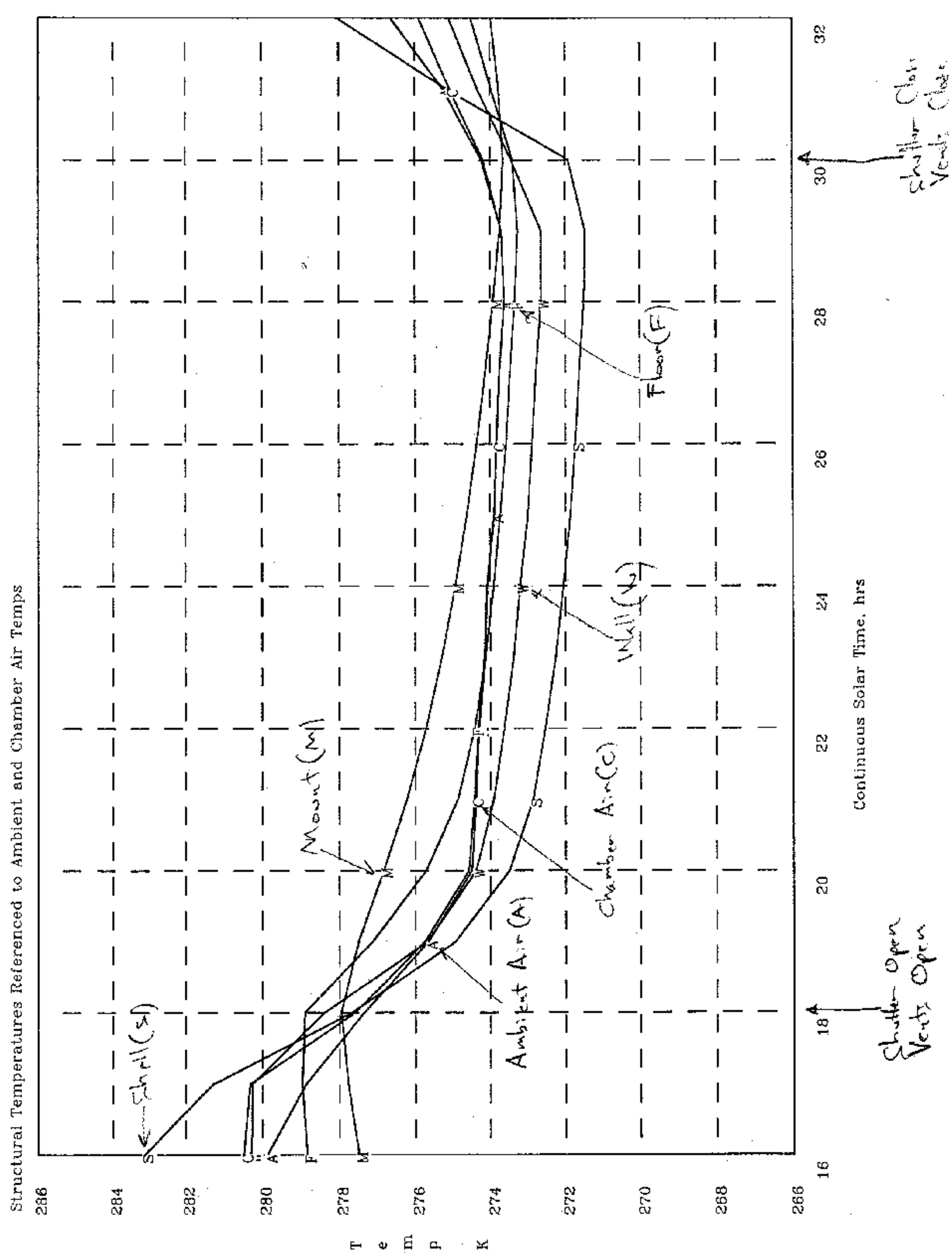
Structural Temperatures Referenced to Ambient and Chamber Air Temps
Continuous Solar Time, hrs
Temp K
Shell (S)
Mount (M)
Ambient Air (A)
Chamber Air (C)
Wall (W)
Floor (F)
Shutter Open Vents Open

Figure 22.

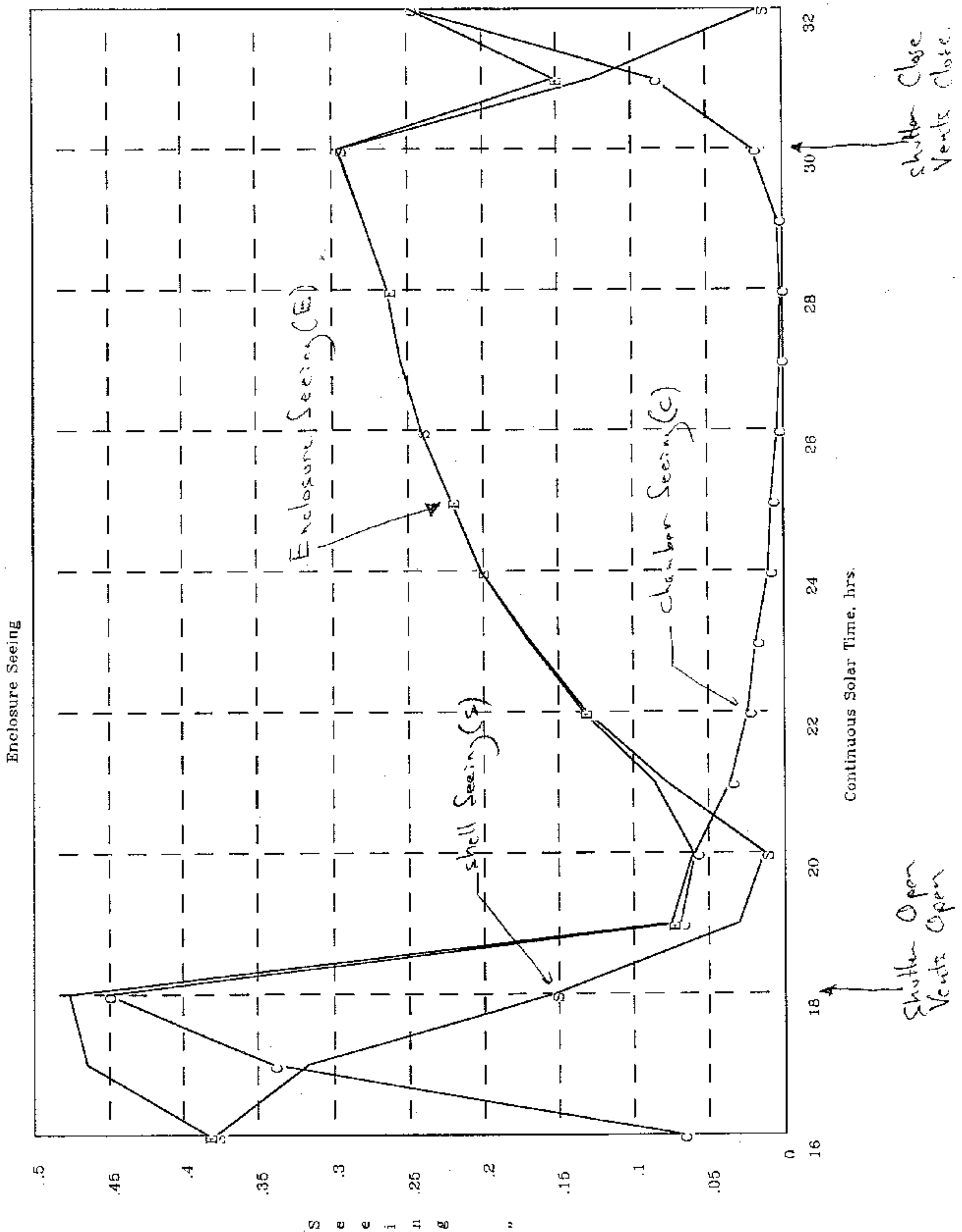
Enclosure Seeing
Continuous Solar Time, hrs.
Seeing, "
0
.05
.1
.15
.2
.25
.3
.35
.4
.45
.5
16
18
20
22
24
26
28
30
32
Enclosure Seeing (E)
Shell Seeing (S)
Chamber Seeing (C)
Shutter Open
Vents Open
Shutter Close
Vents close.

Figure 23.

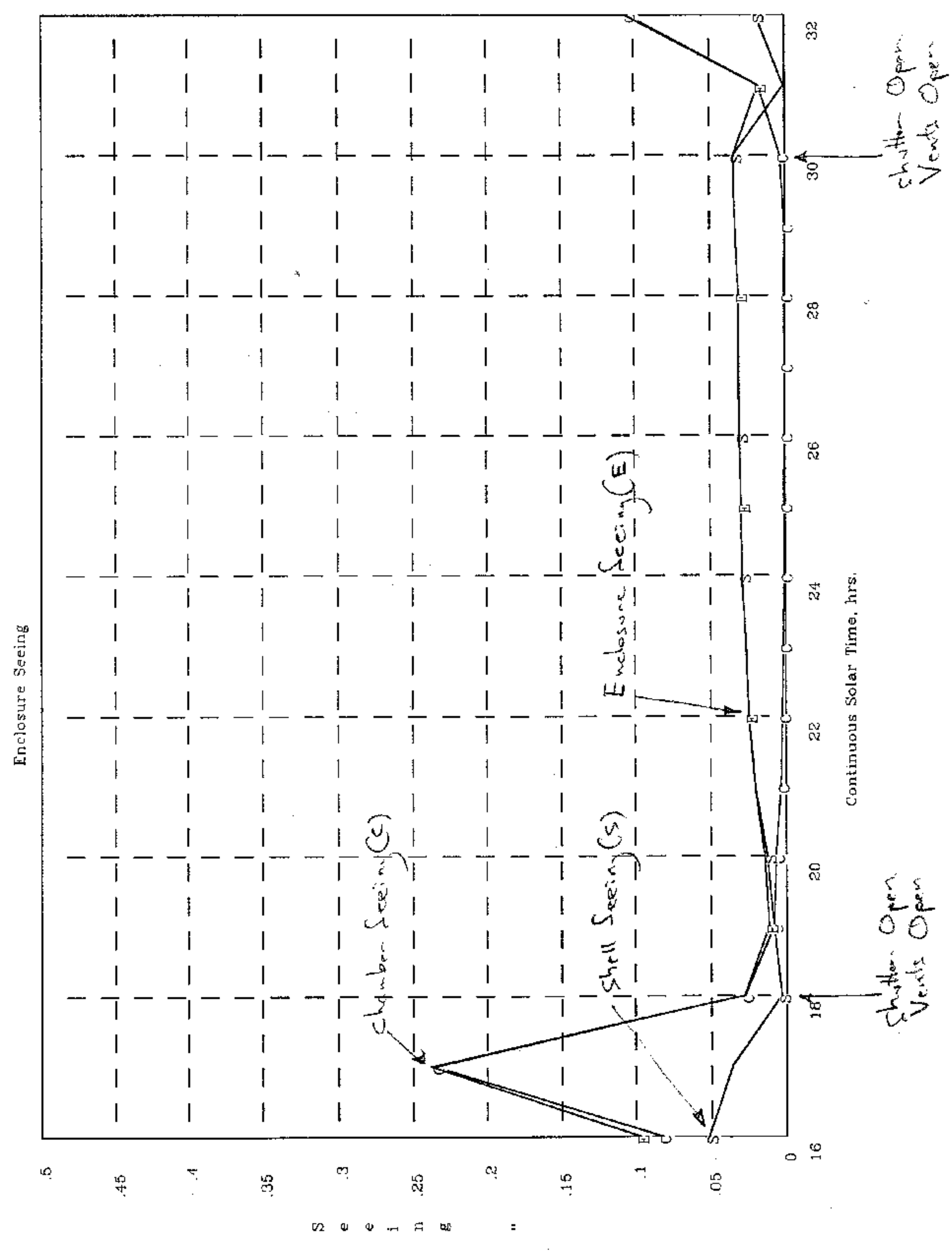
Enclosure Seeing
Continuous Solar Time, hrs.
16
18
20
22
24
26
28
30
32
0
.05
.1
.15
.2
.25
.3
.35
.4
.45
.5
Chamber Seeing (C)
Shell Seeing (S)
Enclosure Seeing (E)
Shutter Open
Vents Open
Shutter Open
Vents Open

Figure 24.

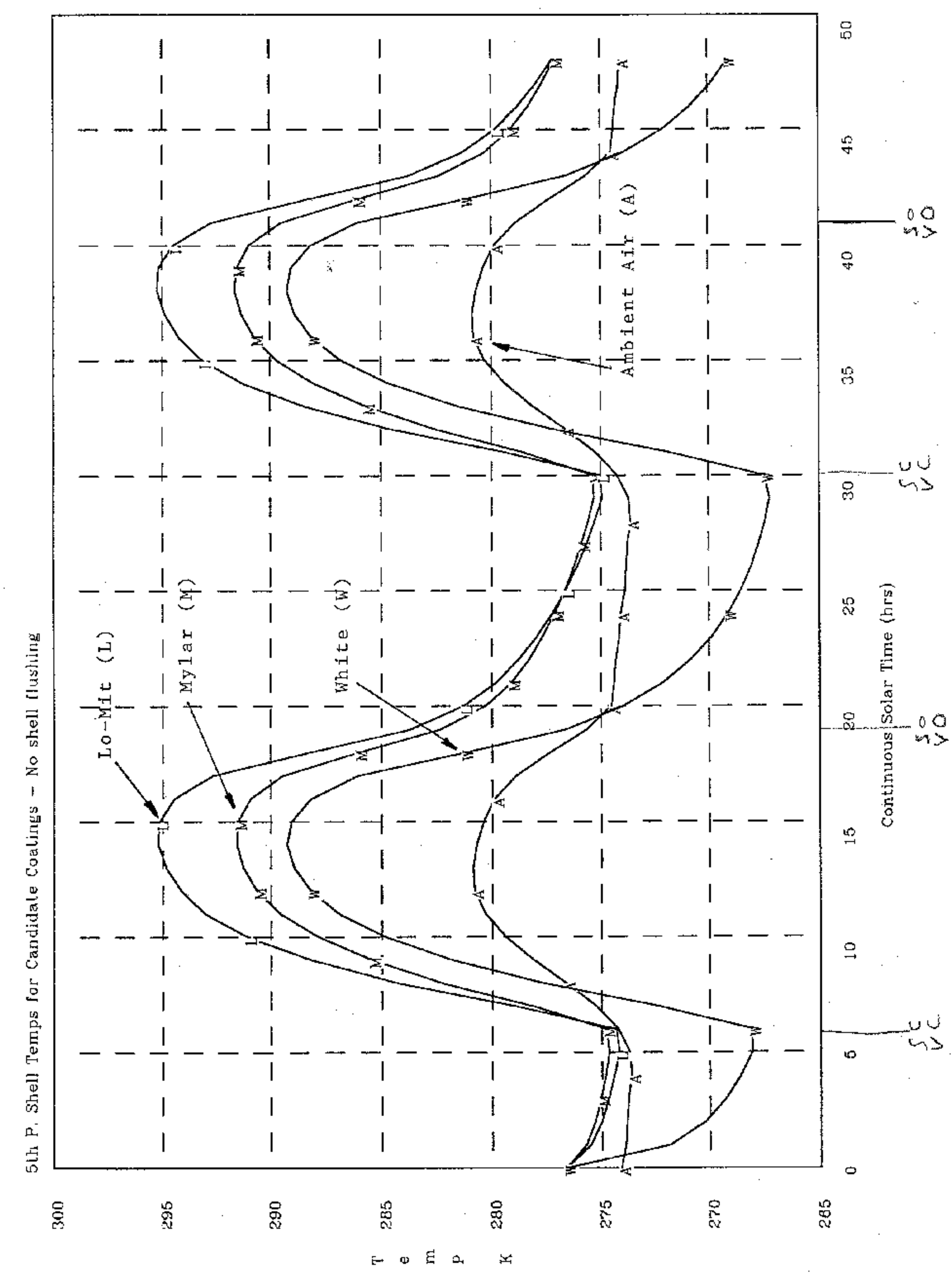
5th P. Shell Temps for Candidate Coatings -- No shell flushing
Lo-Mit (L)
Mylar (M)
White (W)
Ambient Air (A)
Continuous Solar Time (hrs)
Temp K
300
295
290
285
280
275
270
265
0
5
10
15
20
25
30
35
40
45
50

Figure 25.

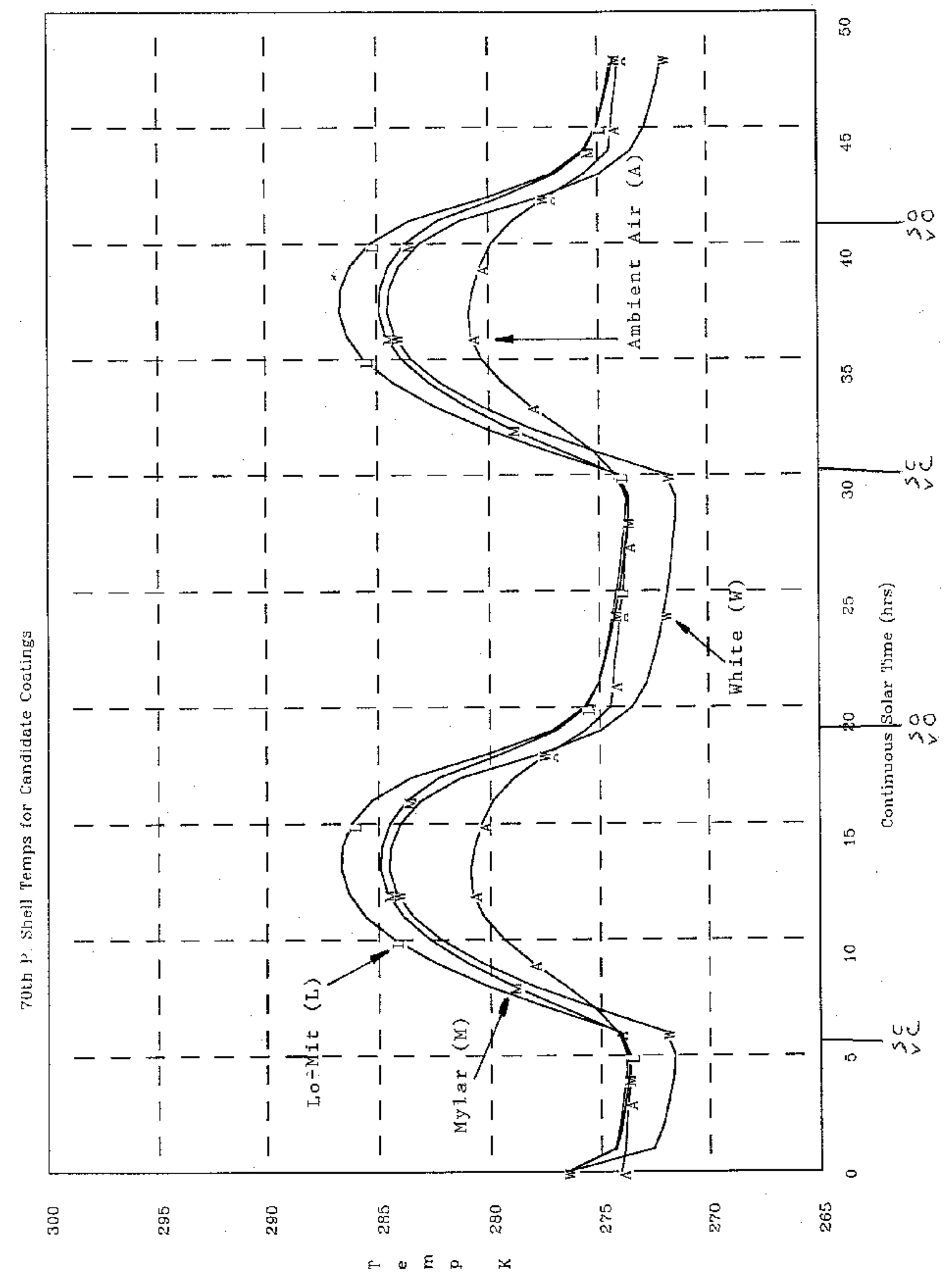
70th P. Shell Temps for Candidate Coatings
Lo-Mit (L)
Mylar (M)
White (W)
Ambient Air (A)
Continuous Solar Time (hrs)
Temp K

Figure 26.

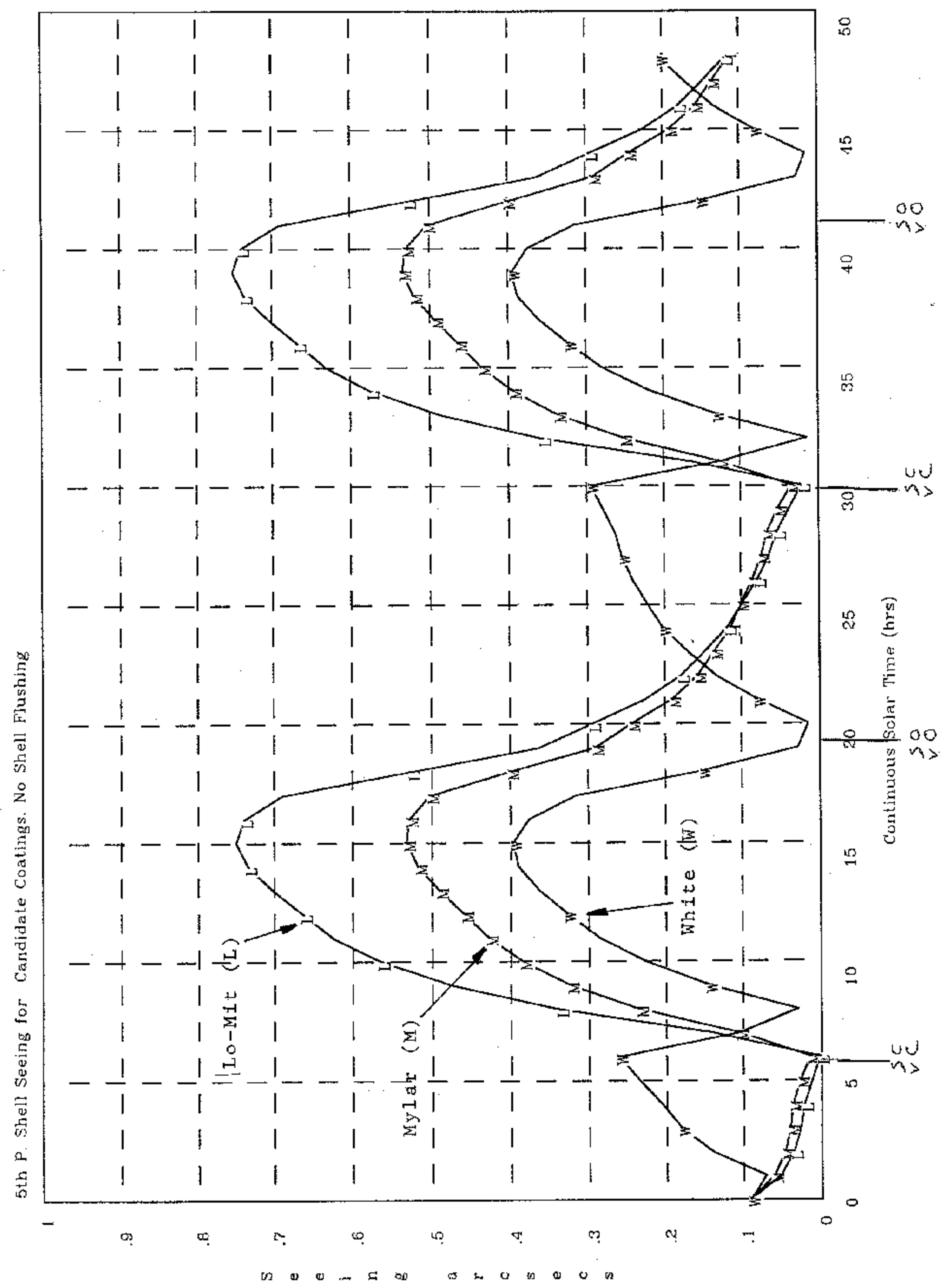
5th P. Shell Seeing for Candidate Coatings. No Shell Flushing
Lo-Mit (L)
Mylar (M)
White (W)
Continuous Solar Time (hrs)
Seeing arcsecs

Figure 27.

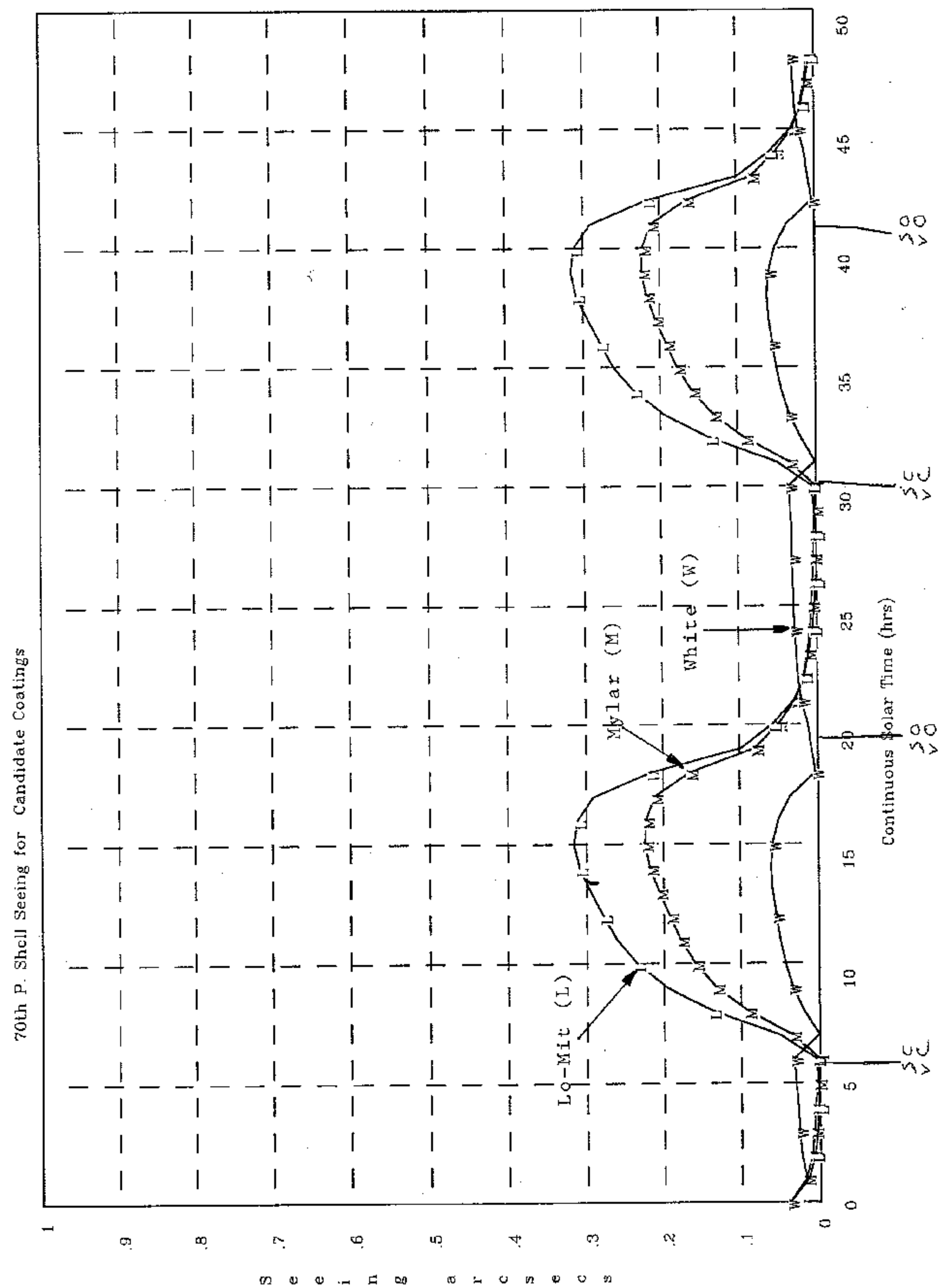
70th P. Shell Seeing for Candidate Coatings
Continuous Solar Time (hrs)
Seeing arcsecs
Lo-Mit (L)
Mylar (M)
White (W)
0
5
10
15
20
25
30
35
40
45
50
.1
.2
.3
.4
.5
.6
.7
.8
.9
1

Figure 28.

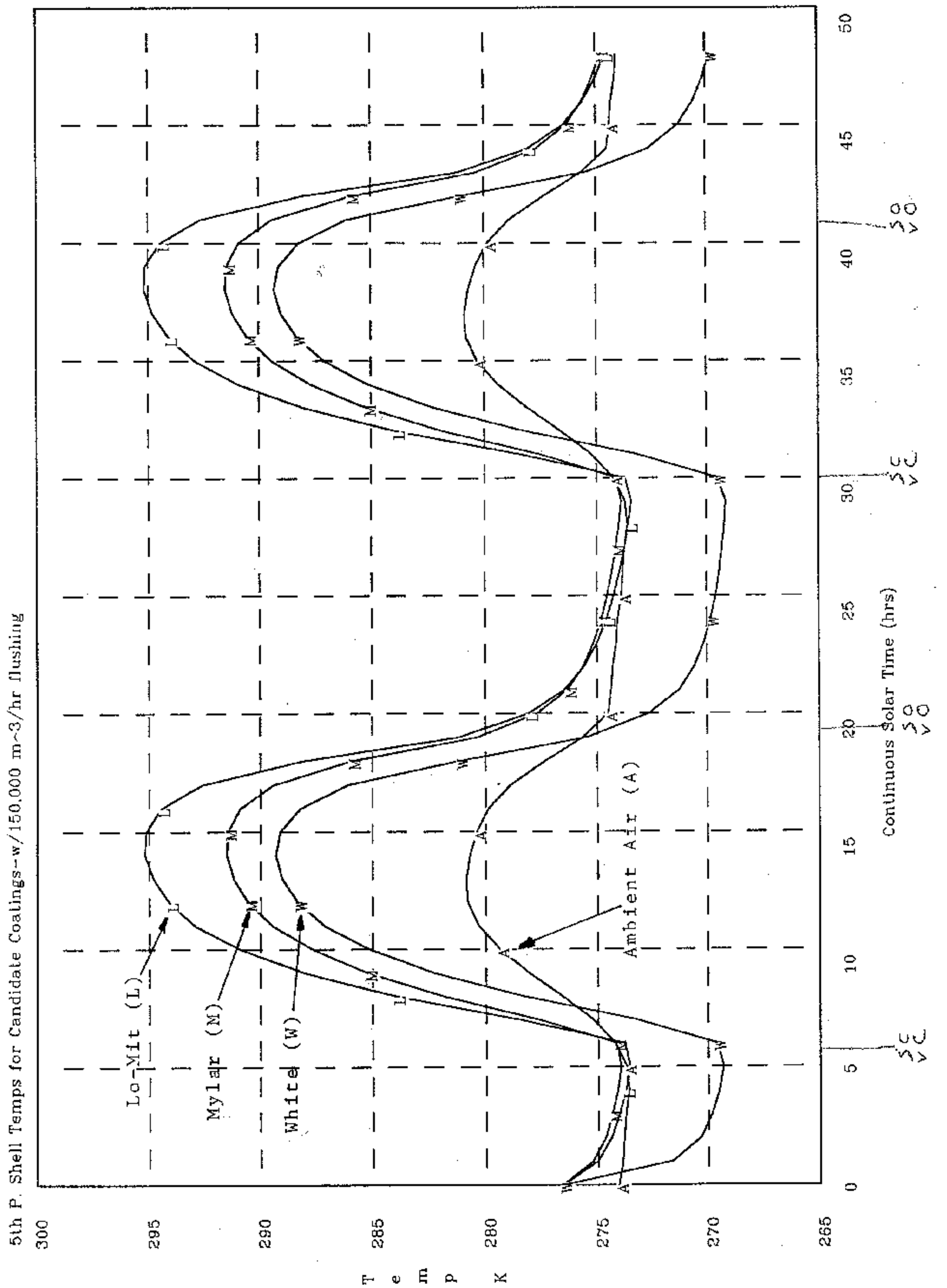
5th P. Shell Temps for Candidate Coatings-w/150,000 m^3/hr flushing
Lo-Mit (L)
Mylar (M)
White (W)
Ambient Air (A)
Temp K
Continuous Solar Time (hrs)
300
295
290
285
280
275
270
265
0
5
10
15
20
25
30
35
40
45
50

Figure 29.

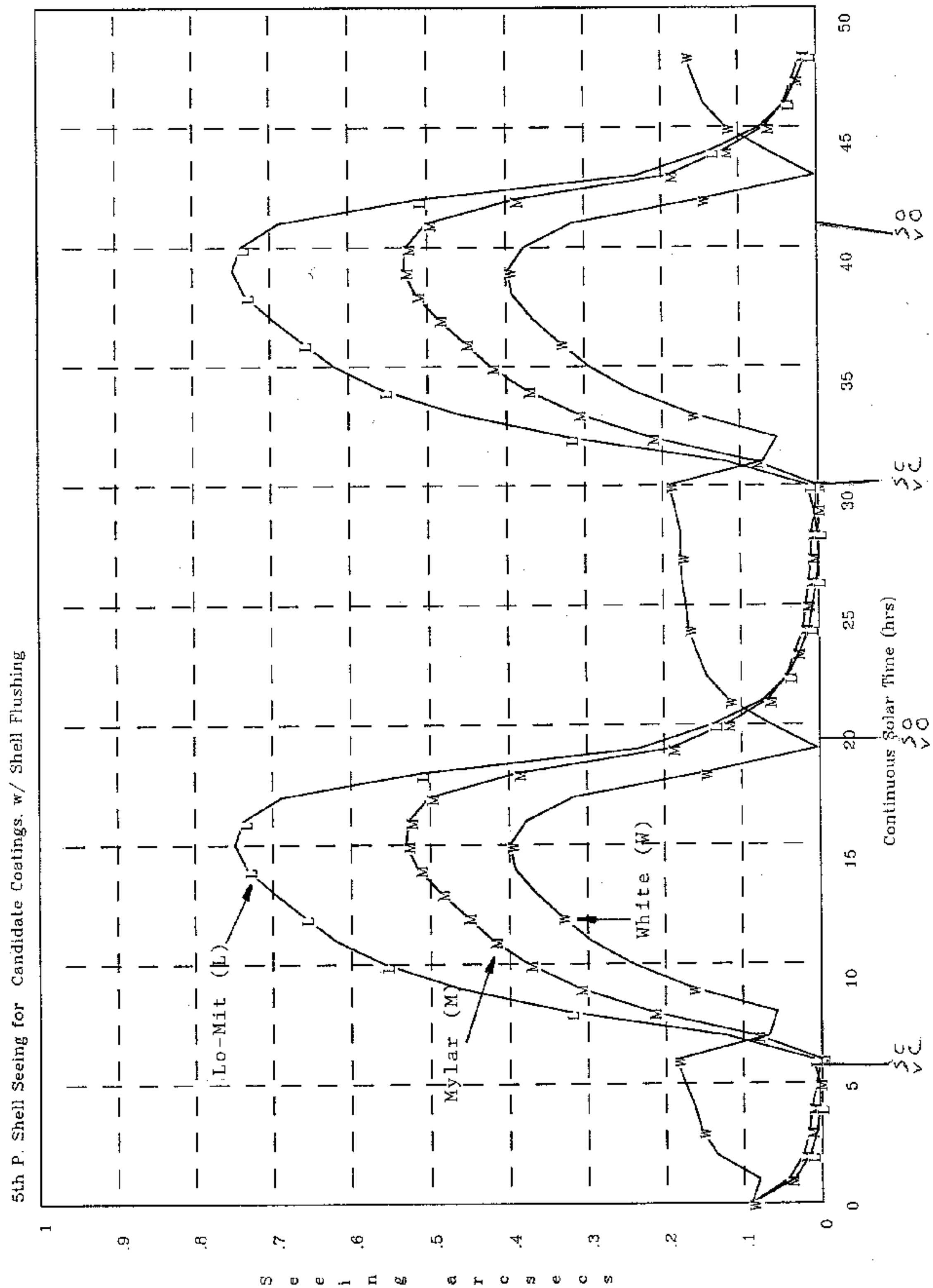
5th P. Shell Seeing for Candidate Coatings. w/ Shell Flushing
Lo-Mit (L)
Mylar (M)
White (W)
Continuous Solar Time (hrs)
Seeing arcsecs
SC
SO

Figure 30.

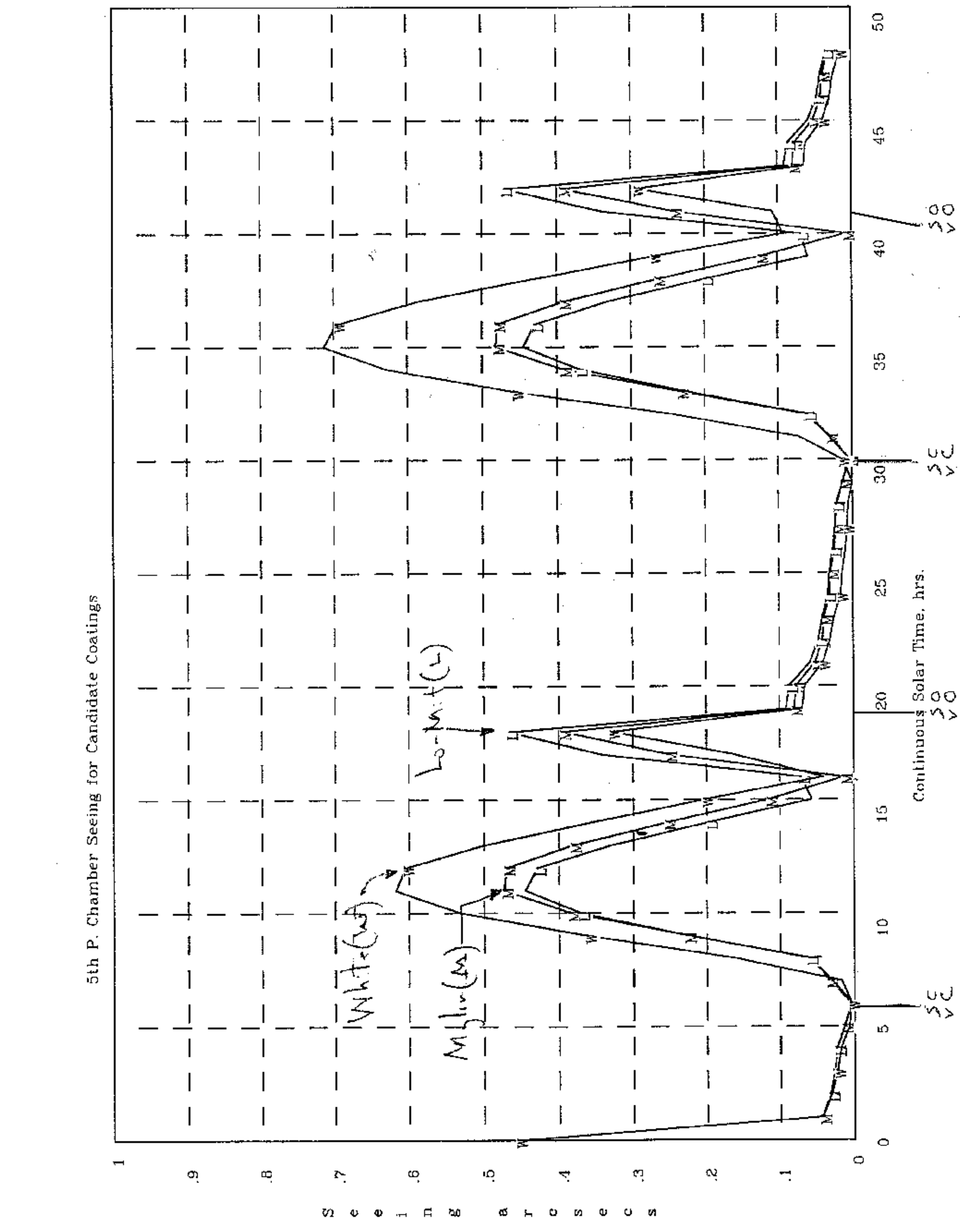
5th P. Chamber Seeing for Candidate Coatings
Seeing arcsecs
Continuous Solar Time, hrs.
White (W)
Mylar (M)
Lo-Mit (L)

Figure 31.

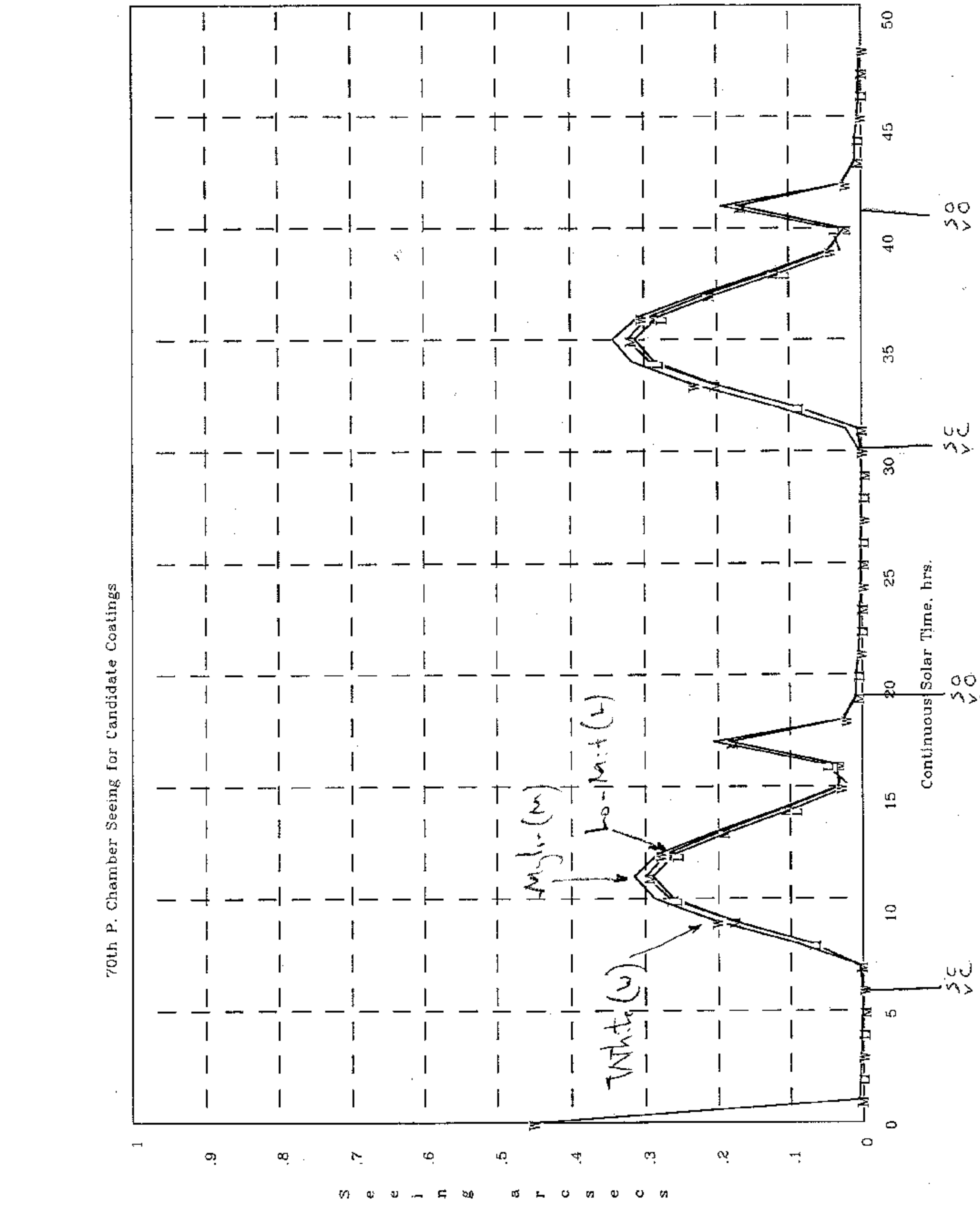
70th P. Chamber Seeing for Candidate Coatings
Continuous Solar Time, hrs.
Seeing arcsecs

Figure 32.

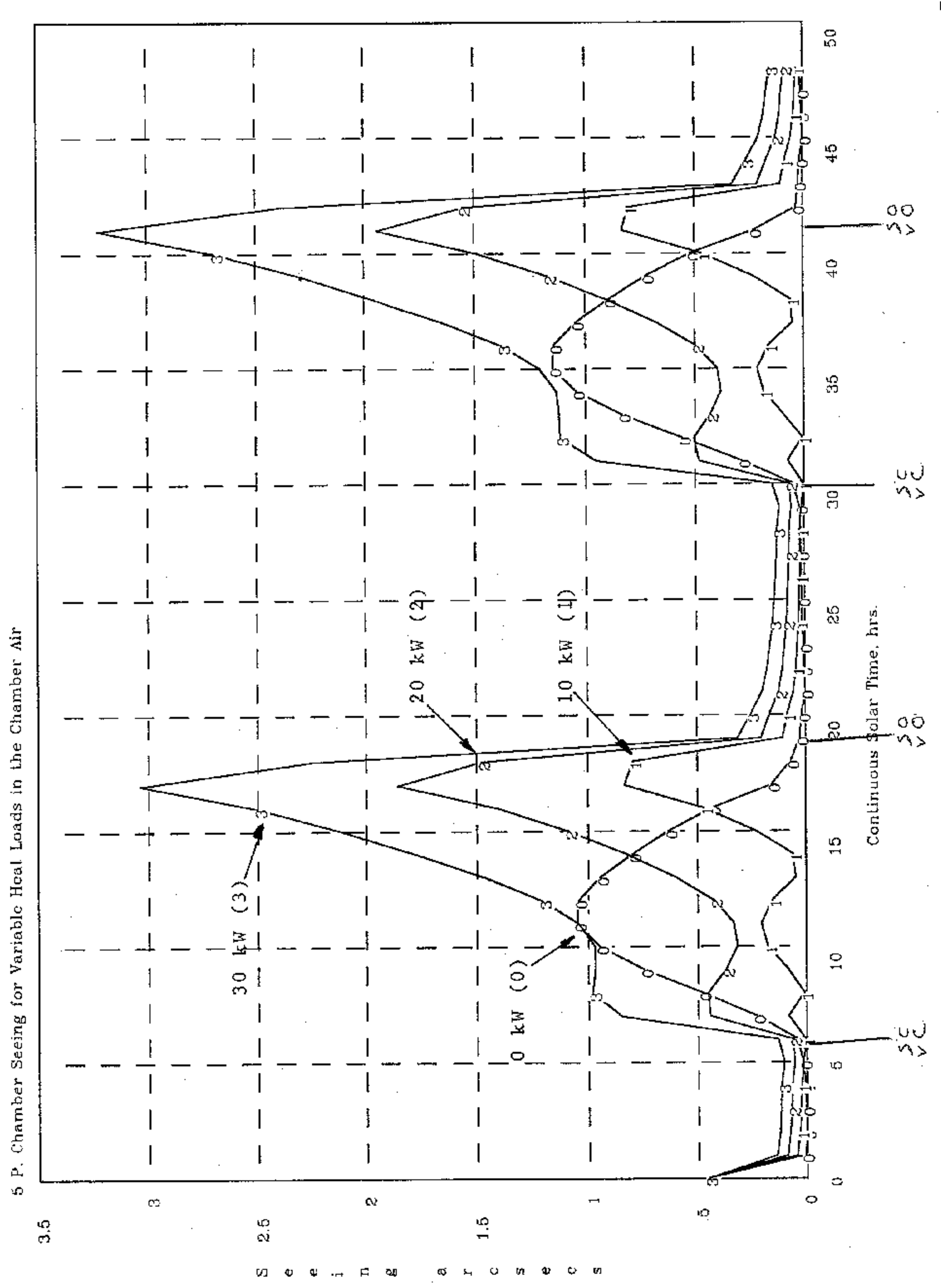
5 P. Chamber Seeing for Variable Heal Loads in the Chamber Air
Seeing arcsecs
Continuous Solar Time, hrs.
30 kW (3)
20 kW (2)
10 kW (1)
0 kW (0)

Figure 33,

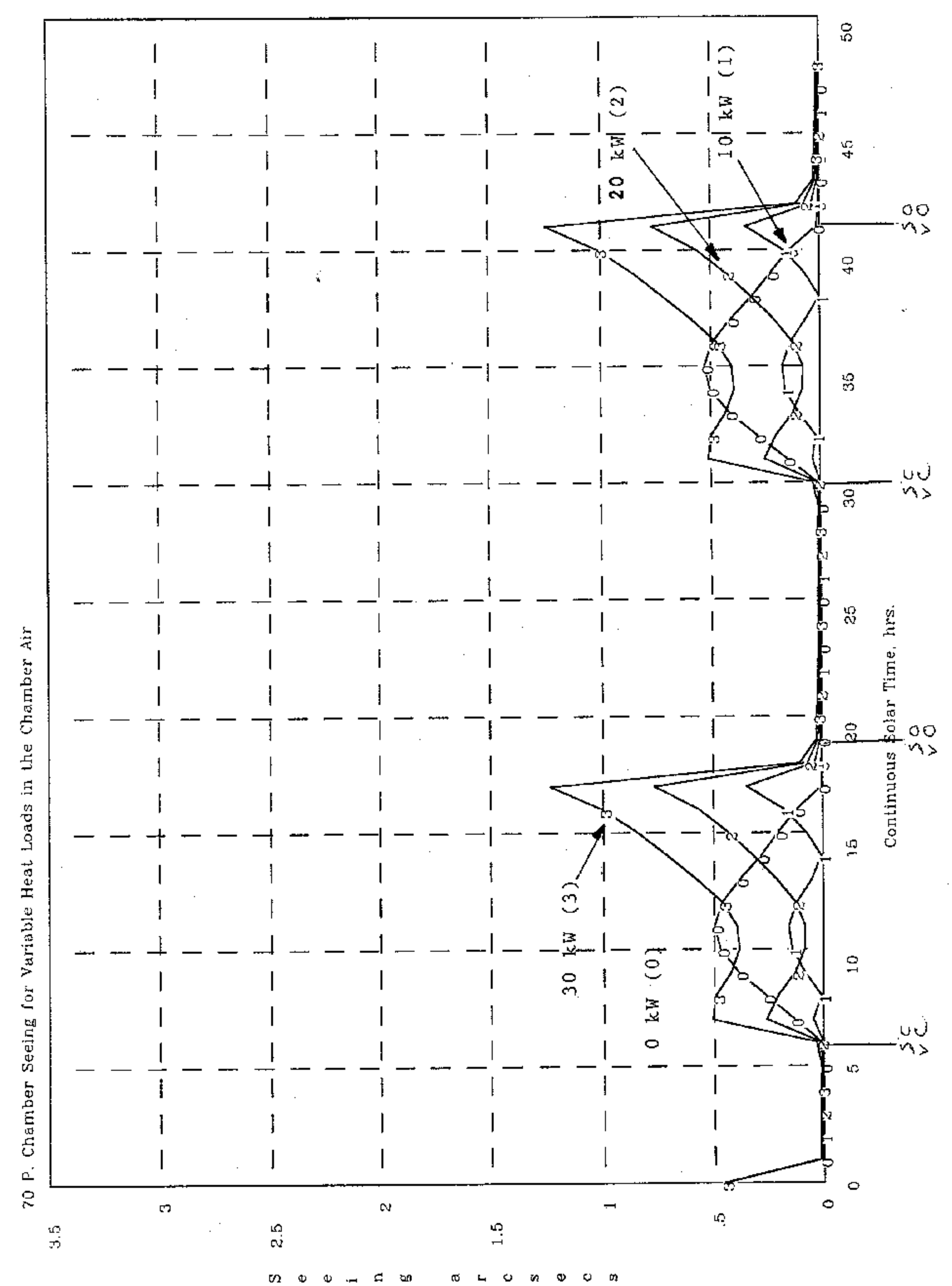
70 P. Chamber Seeing for Variable Heat Loads in the Chamber Air
Seeing arcsecs
Continuous Solar Time, hrs.
30 kW (3)
20 kW (2)
10 kW (1)
0 kW (0)

Figure 34.

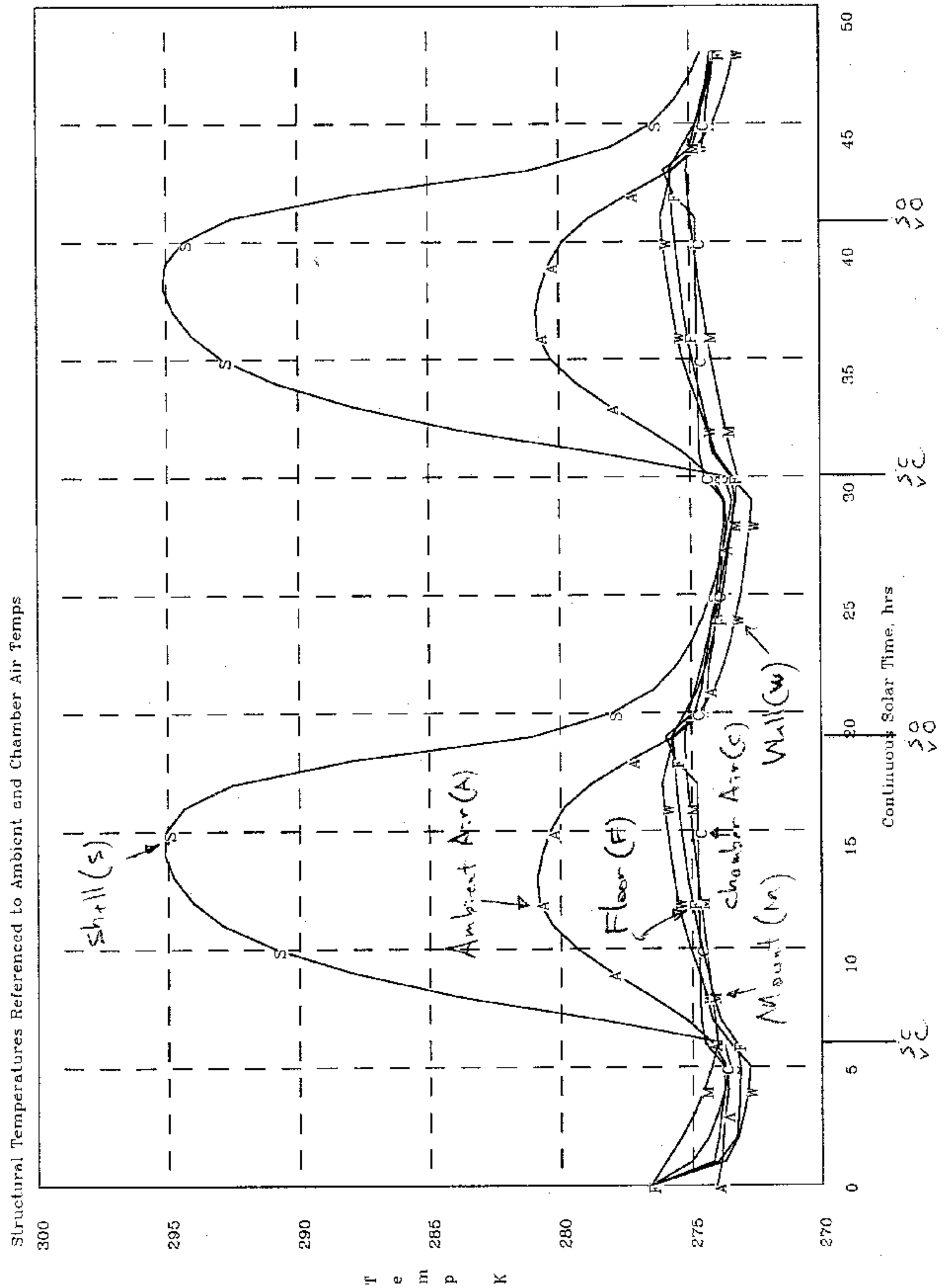
Structural Temperatures Referenced to Ambient and Chamber Air Temps
Temp K
300
295
290
285
280
275
270
Continuous Solar Time, hrs
0
5
10
15
20
25
30
35
40
45
50
Shell (S)
Ambient Air (A)
Floor (F)
Chamber Air (C)
Mount (M)
Wall (W)

Figure 35.

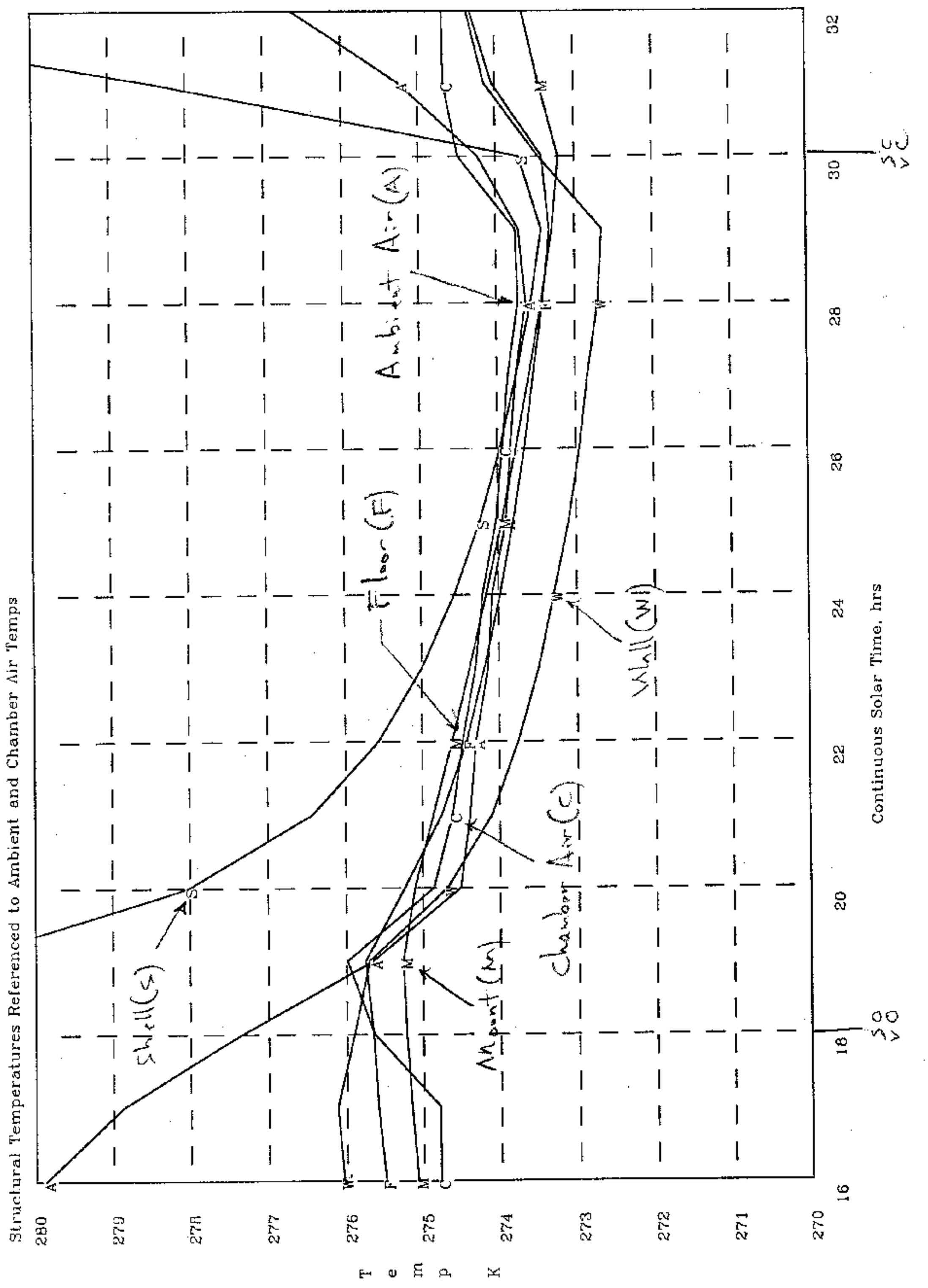
Structural Temperatures Referenced to Ambient and Chamber Air Temps
Continuous Solar Time, hrs
Temp K
280
279
278
277
276
275
274
273
272
271
270
16
18
20
22
24
26
28
30
32
Shell (S)
Mount (M)
Chamber Air (C)
Wall (W)
Floor (F)
Ambient Air (A)

Figure 36.

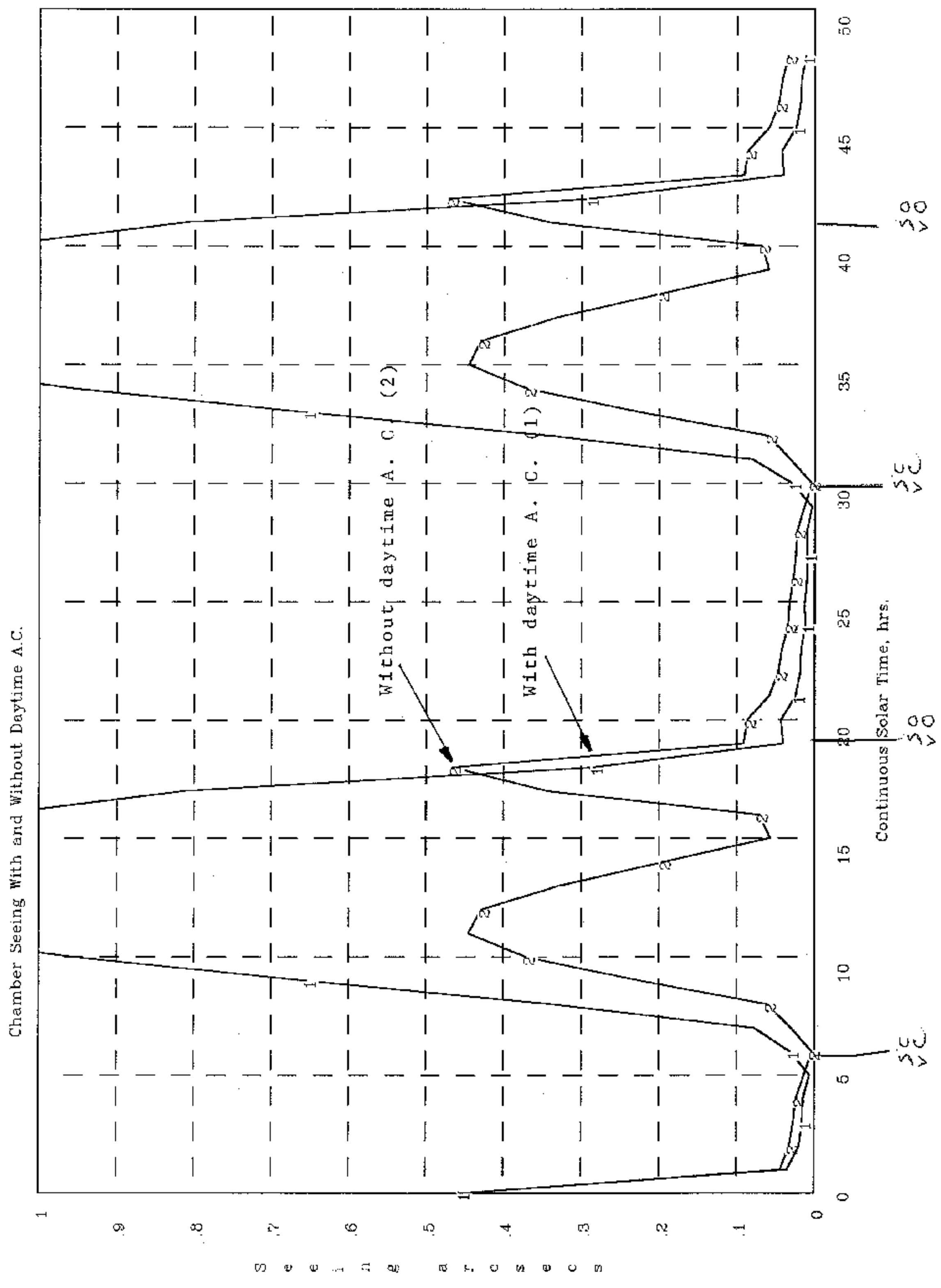
Chamber Seeing With and Without Daytime A.C.
Without daytime A. C. (2)
With daytime A. C. (1)
Continuous Solar Time, hrs.
0
5
10
15
20
25
30
35
40
45
50
0
.1
.2
.3
.4
.5
.6
.7
.8
.9
1

Figure 37.

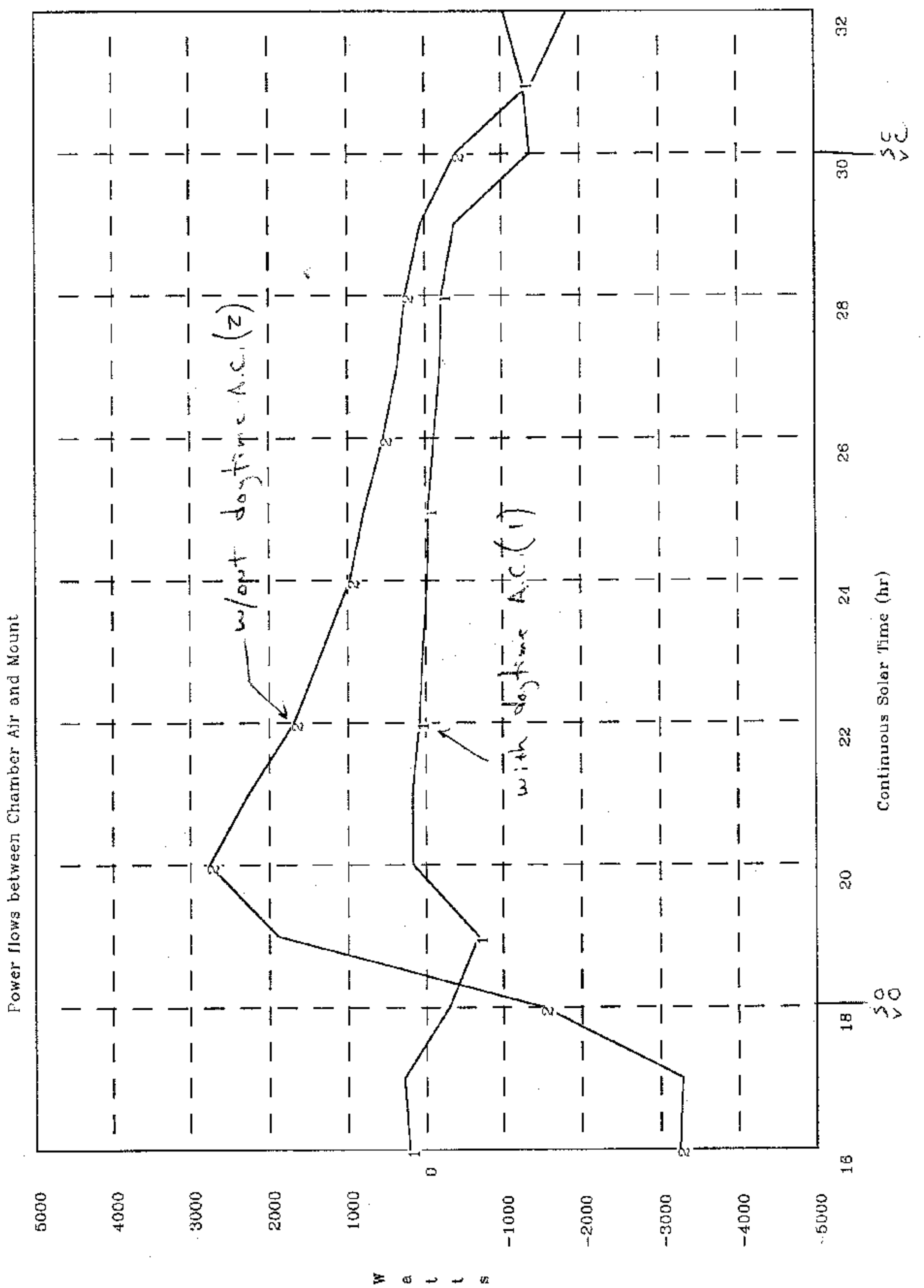
Power flows between Chamber Air and Mount
Continuous Solar Time (hr)
Watts
5000
4000
3000
2000
1000
0
-1000
-2000
-3000
-4000
-5000
16
18
20
22
24
26
28
30
32
w/opt daytime A.C. (2)
with daytime A.C. (1)

Figure 38.

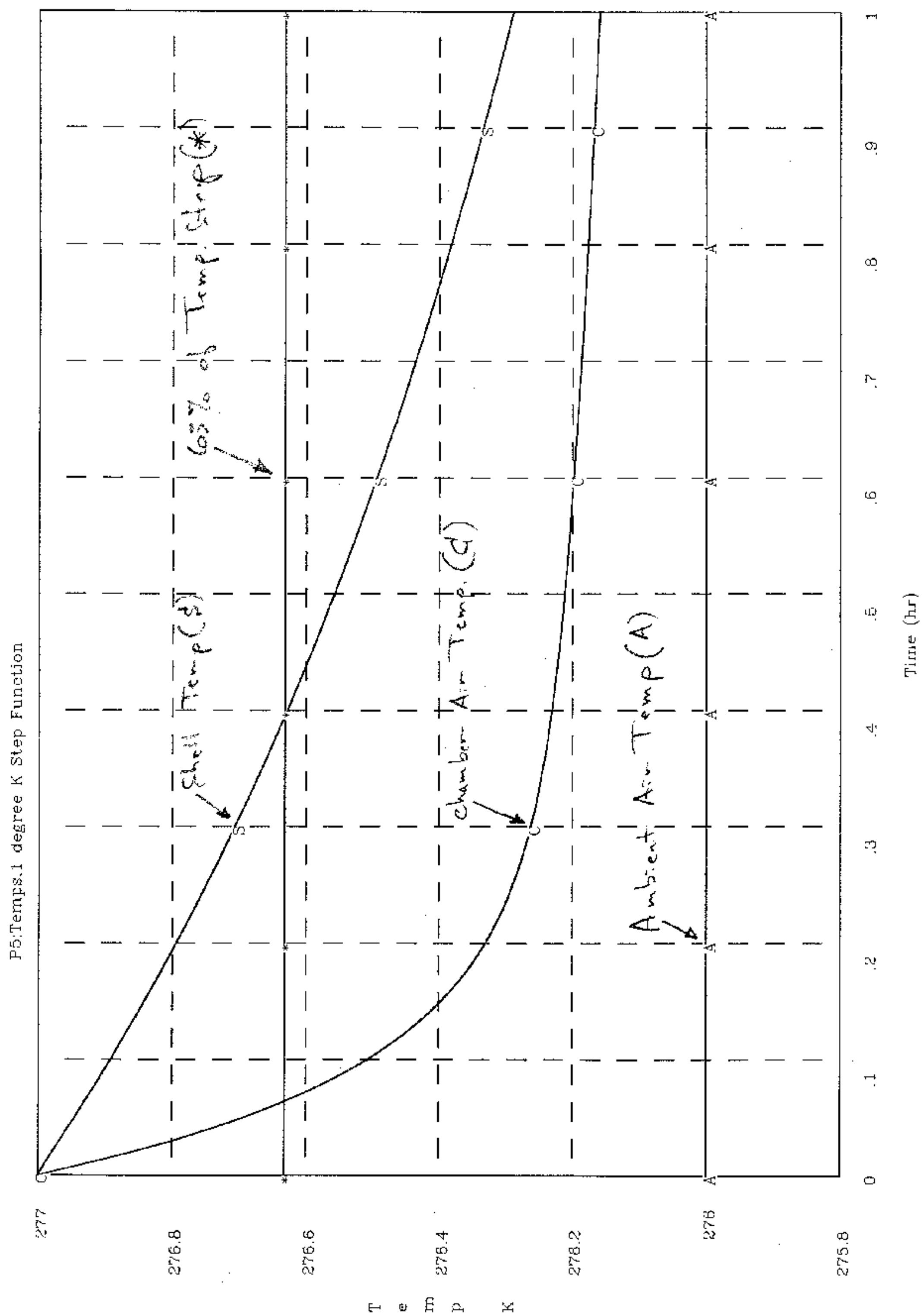
P5:Temps.1 degree K Step Function
Shell Temp (S)
Chamber Air Temp (C)
Ambient Air Temp (A)
63% of Temp. Step (*)
Time (hr)
Temp K
277
276.8
276.6
276.4
276.2
276
275.8
0
.1
.2
.3
.4
.5
.6
.7
.8
.9
1

Figure 39.

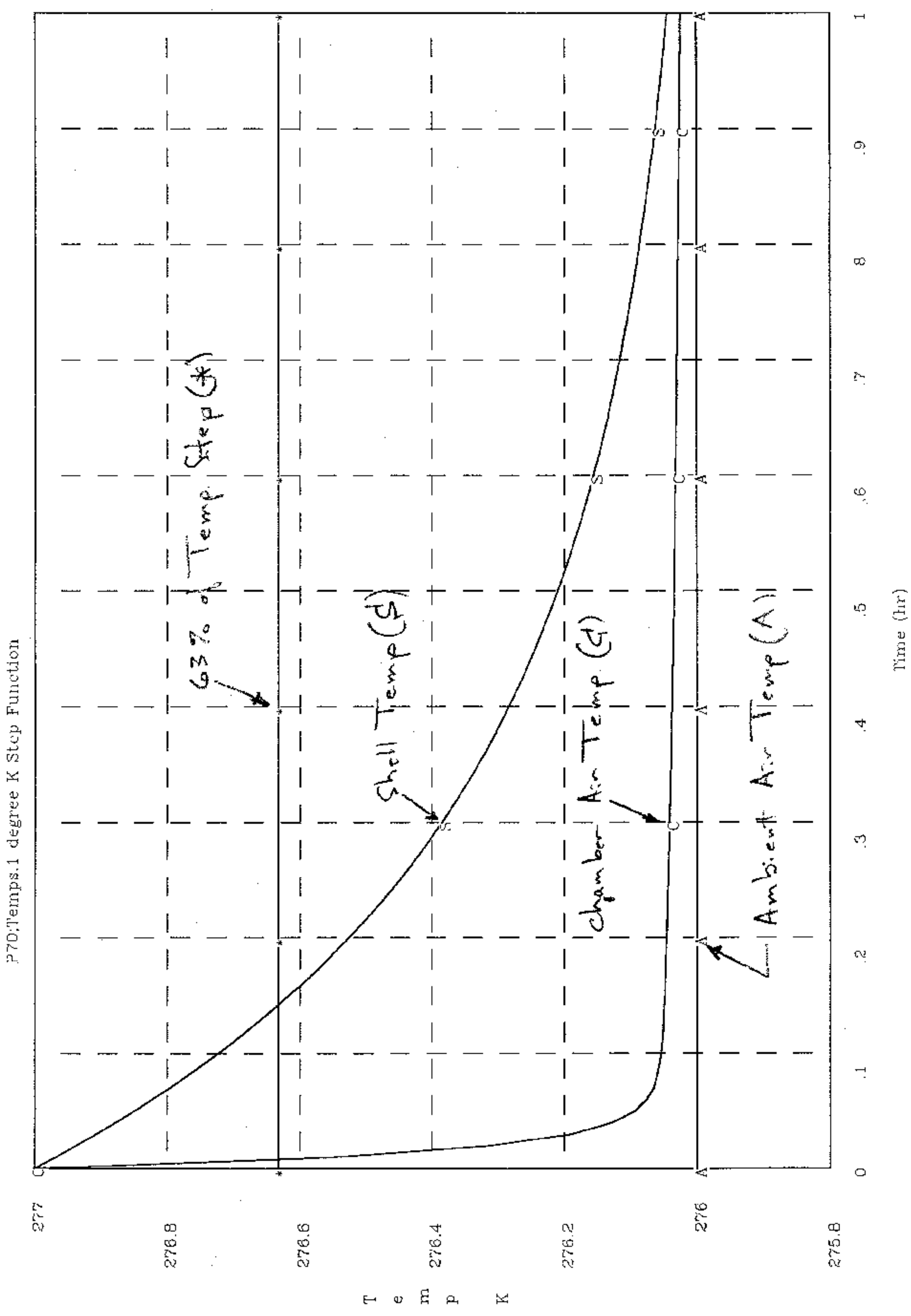
P70:Temps.1 degree K Step Function
63% of Temp Step (*)
Shell Temp (S)
Chamber Air Temp (C)
Ambient Air Temp (A)
277
276.8
276.6
276.4
276.2
276
275.8
T e m p K
0
.1
.2
.3
.4
.5
.6
.7
.8
.9
1
Time (hr)

Figure 40.

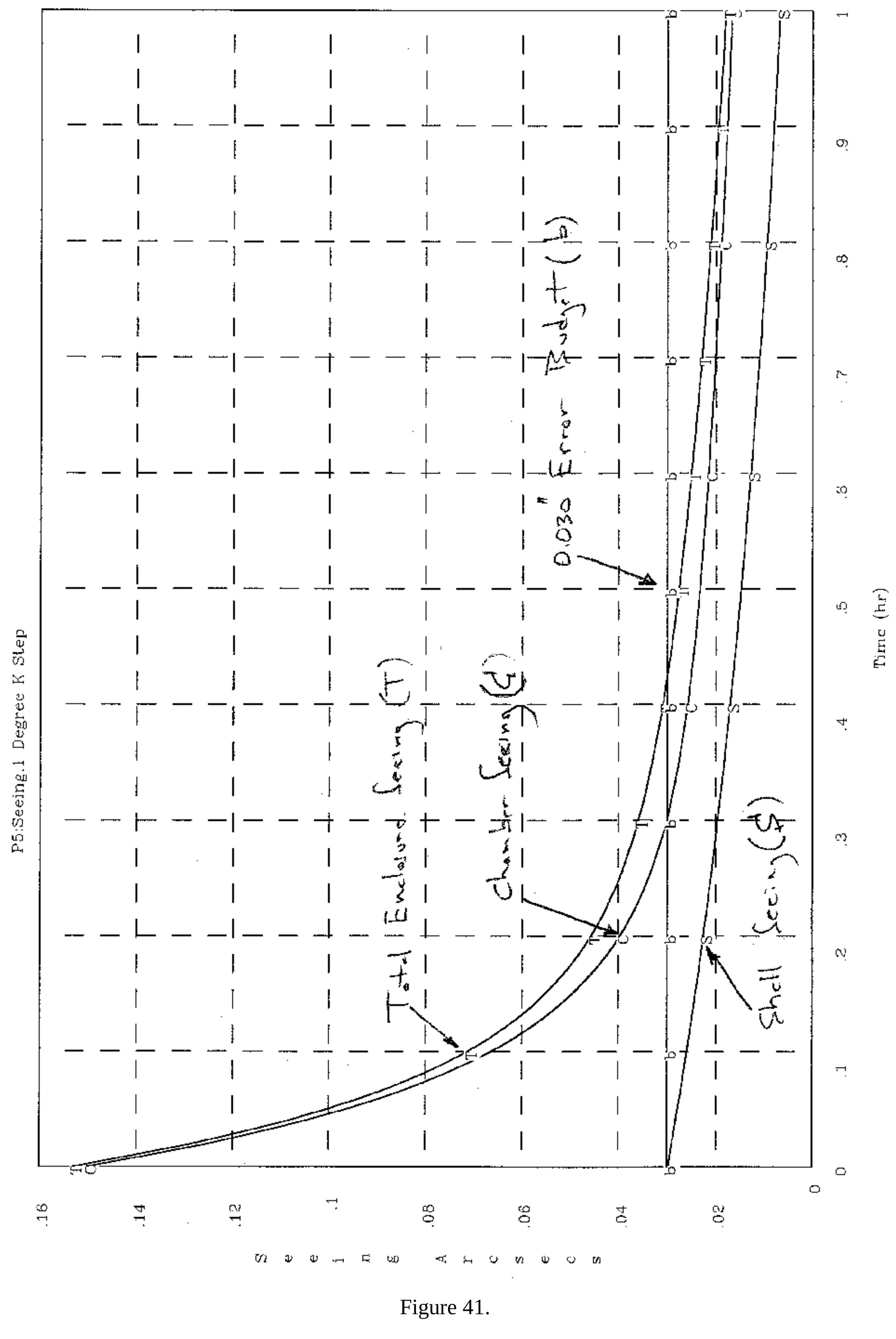
P5:Seeing.1 Degree K Step
Total Enclosed Seeing (T)
Chamber Seeing (C)
Shell Seeing (S)
0.030" Error Budget (b)
Time (hr)
Seeing Arcsecs

Figure 41.

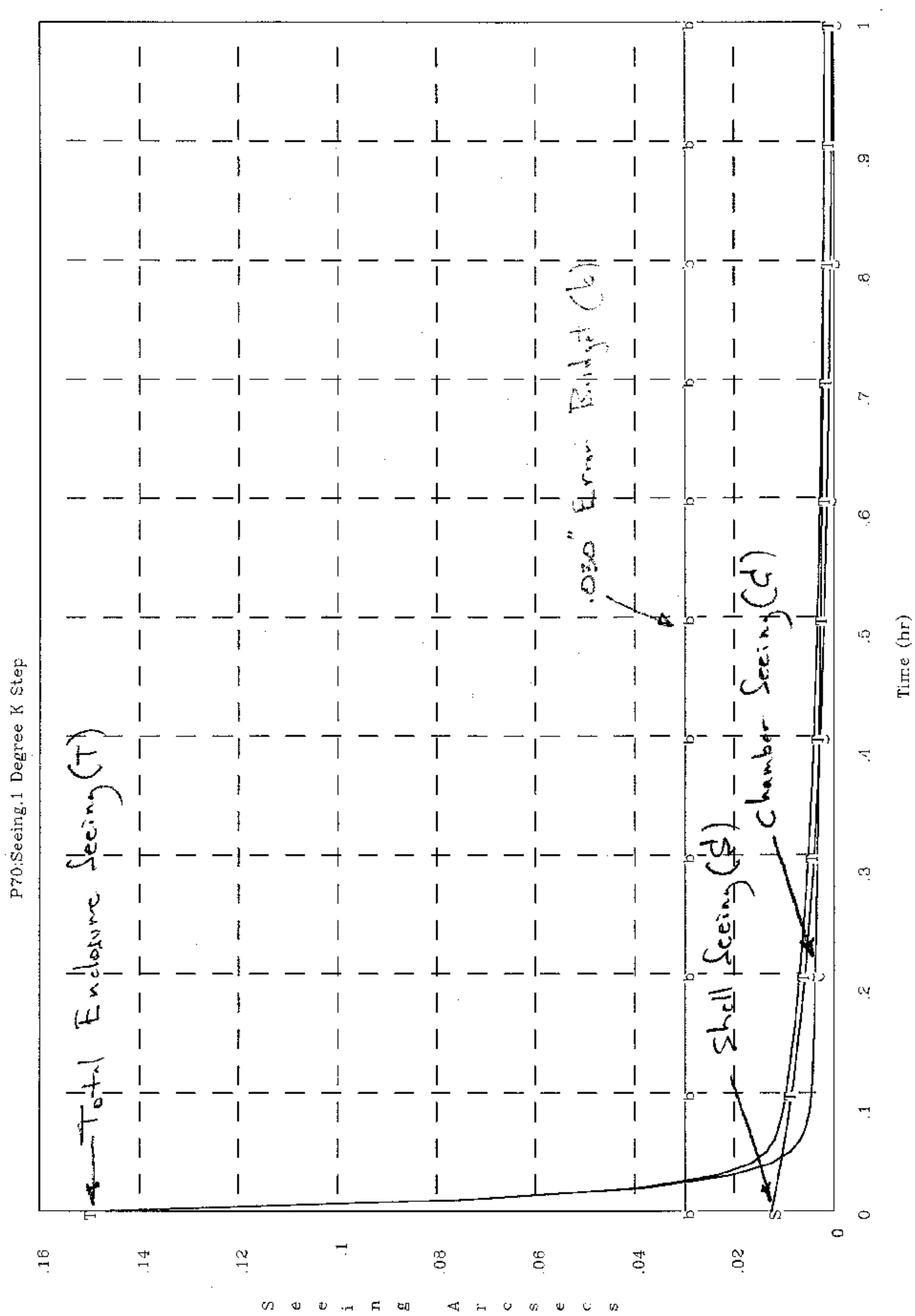

P70:Seeing.1 Degree K Step
Time (hr)
Seeing Arcsecs
Total Enclosure Seeing (T)
Shell Seeing (S)
Chamber Seeing (C)
.030" Error Budget (b)
0
.02
.04
.06
.08
.1
.12
.14
.16
0
.1
.2
.3
.4
.5
.6
.7
.8
.9
1

Figure 42.